ISSN: 1040-8398 (Print) 1549-7852 (Online) Journal homepage: <http://www.tandfonline.com/loi/bfsn20>

Thermodynamics, Transport Phenomena and Electrochemistry of External Field Assisted Non-thermal Food Technologies

N.N. Misra, Alex Martynenko, Farid Chemat, Larysa Paniwnyk, Francisco J. Barba & Anet Režek Jambrak

To cite this article: N.N. Misra, Alex Martynenko, Farid Chemat, Larysa Paniwnyk, Francisco J. Barba & Anet Režek Jambrak (2017): Thermodynamics, Transport Phenomena and Electrochemistry of External Field Assisted Non-thermal Food Technologies, Critical Reviews in Food Science and Nutrition, DOI: [10.1080/10408398.2017.1287660](https://doi.org/10.1080/10408398.2017.1287660)

To link to this article: <http://dx.doi.org/10.1080/10408398.2017.1287660>



Accepted author version posted online: 31 Mar 2017.



Submit your article to this journal



Article views: 59



View related articles



View Crossmark data

Full Terms & Conditions of access and use can be found at
<http://www.tandfonline.com/action/journalInformation?journalCode=bfsn20>

Thermodynamics, Transport Phenomena and Electrochemistry of External Field Assisted Non-thermal Food Technologies

N.N. Misra^{*1}, Alex Martynenko², Farid Chemat³, Larysa Paniwnyk⁴, Francisco J. Barba⁵, and Anet Režek Jambrak⁶

¹GTECH, Research & Development, General Mills India Private Limited, Mumbai, India

²Department of Engineering, Faculty of Agriculture, Dalhousie University, Canada

³Avignon University, INRA, Green Extraction Team, Avignon, France

⁴Faculty of Health and Life Sciences, Coventry University, U.K.

⁵Faculty of Pharmacy, Preventive Medicine & Public Health, Food Science, Toxicology & Forensic Medicine Department, University of València, València, Spain

⁶Faculty of Food Technology & Biotechnology, University of Zagreb, Zagreb, Croatia

March 9, 2017

Abstract

Interest in the development and adoption of nonthermal technologies is burgeoning within the food and bioprocess industry, the associated research community, and among the consumers. This is evident from not only the success of some innovative nonthermal technologies at industrial scale, but also from the increasing number of publications dealing with these topics, a growing demand for foods processed by nonthermal technologies and use of natural ingredients. A notable feature of the nonthermal technologies such as cold plasma, electrohydrodynamic processing, pulsed electric fields, and ultrasound is the involvement of external fields, either electric or sound. Therefore, it merits to study the fundamentals of these technologies and the associated phenomenon with a unified approach. In this review we revisit the fundamental physical and chemical phenomena governing the selected technologies, highlight similarities and contrasts, describe few successful applications, and finally, identify the gaps in research.

Keywords: nonthermal; cold plasma; PEF; Electrohydrodynamic; ultrasound; hydrodynamics

Contents

1	Introduction	2
2	Cold plasma technology	4
2.1	Elementary thermodynamics of cold plasma	4
2.2	Plasma sources	4
2.2.1	Dielectric barrier discharge (DBD)	5
2.2.2	Corona Discharge	5
2.2.3	Microwave discharges	5
2.3	Transport phenomena	6
2.4	Electrochemistry	8

*Corresponding author; misra.cftri@gmail.com

3 Electrohydrodynamic (EHD) processing	11
3.1 EHD Applications in Food Processing	11
3.1.1 Shelf-life extension and food quality retention	13
3.1.2 Electrofreezing and EHD assisted thawing	14
3.1.3 EHD effects on macromolecules	14
3.1.4 EHD Drying - Heat and mass transfer enhancement	14
3.2 Charge Transport	15
3.3 Mass Transport	17
3.4 Heat Transport	19
3.5 Correlations Between Transport Processes	20
4 Pulsed Electric Fields	21
4.1 Transport Phenomena in PEF	21
4.2 The Physics of Electroporation	23
4.3 PEF Assisted Extraction of Intracellular Compounds	25
4.4 Radical Formation	25
5 Ultrasound Processing	26
5.1 Principles and applications of ultrasound to food systems	26
5.2 Thermodynamics in ultrasound processing	28
5.3 Transport Phenomena in ultrasound processing	29
5.4 Radical chemistry in ultrasound processing	30
6 Final Remarks	32
7 Appendices	33
7.1 Quasineutrality of plasma	33
7.2 Knudsen Number	33
7.3 Gas heating in plasma	33
7.4 Reactions leading to formation of hydrogen peroxide	33
7.5 Dimensionless Numbers of Transport Processes	34
7.6 The Stretched Exponential Model	34
7.7 Radical production during ultrasound application	35

1 Introduction

Within recent years, there have been many excellent books and reviews dealing with the nonthermal technologies and their applications in food processing (Zhang et al., 2011a; Rastogi et al., 2007; O'Donnell et al., 2012). However, with some exceptions, a coverage of the fundamental physics and chemistry governing these technologies has been largely missing in literature. It is essential that the fundamental physical principles underlying these technologies be well-understood for accelerating innovations. Therefore, in this review we provide an overview of the fundamental aspects related to selected nonthermal food processing technologies which rely on application of external fields, viz. electric fields, ultrasound, and plasma fields. Specifically, we focus on the emerging research topic of cold plasma, the conceptually mature yet industrially unexplored electrohydrodynamic (EHD) processing, and the recently commercialized ultrasound and pulsed electric field (PEF) processing technologies. One can intuitively find that there exists a commonality between these technologies- all of them rely on external fields (electromagnetic in case of cold plasma, EHD and PEF, and acoustic force field in case of ultrasound processing) at a fundamental

level. Furthermore, EHD phenomenon in gases is a manifestation of the plasma state, while many PEF systems at a micro-scale are ‘hot plasmas’.

Another interesting fact lies in the history of these technologies; all were initially explored in the pre-world war era, and remained un-noticed for several years. In fact, the idea of using electricity for food processing is more than a century old, when investigations into bactericidal effect of electric field were conducted ([Prochownick and Spaeth, 1890](#)). Likewise, the modern concept of plasma discharges inside sealed containers ([Misra et al., 2015b](#)) and corona fields are perhaps, modern avatars of JJ Thomson and William Crookes seminal works on cathode ray tubes dating back to late 1800s.

Cold plasma technology has gained increased attention for food and bio-decontamination purposes ([Misra et al., 2011](#)), and more recently for food property modification ([Segat et al., 2015](#); [Pal et al., 2015](#); [Misra et al., 2014b, 2015a](#)). The increasing number of papers and conference contributions on cold plasma for food processing published during the last few years accentuates the rising importance of this field. In parallel to this trend, several research studies have demonstrated the advantages of electrohydrodynamic (EHD) processes for heat and mass transfer enhancement in unit operations, in general, and drying of food materials in particular ([Martynenko and Zheng, 2016](#)). While electric field induced hydrodynamic effects in fluids are well documented, EHD drying of foods is attracting the interests of food industry only recently, because it is also a nonthermal technology, thereby presenting opportunities in perfect alignment with the market needs and consumer trends.

In environmental science, chemical engineering and chemistry, the term “advanced oxidation processes” (AOP) typically refer to those processes that are employed to degrade pollutants or contaminants by their oxidation. Therefore, the term AOP is one of the typical hallmarks of these fields and is less used in other contexts. However, in recent times, AOPs have been increasingly researched for food processing operations and are topics of active research in food engineering, as these are mostly near-ambient temperature treatment processes based on highly reactive chemical species ([Misra, 2015](#)). Among the topics discussed in our review, cold plasma and ultrasound are often considered within the framework of AOPs, with both the technologies exploiting the power of hydroxyl radicals, when it comes to processing of fluid foods.

It is interesting to note that the introduction of cold plasma, PEF and ultrasound had as their original goal, the inactivation of micro-organisms in foods. In the course of such investigations, it was found that some of the effects for PEF and ultrasound on eukaryotic cells were useful on their own, and have evolved into mass transfer processes; however this is of more recent origin. The first report of mass transfer enhancement using cold plasma has also appeared very recently [Kodama et al. \(2014\)](#). On the other hand, the focus of EHD research has remained on heat and mass transfer since its inception and adoption by food engineers.

There is a great contrast between the electric fields and sound fields, with the former being transverse waves capable of transmitting in vacuum, while the latter being longitudinal waves transmitting in presence of material media. However, the similar nature of food and biological applications of these ‘external fields’ makes them attractive topics for discussion via an unified and analogy driven approach. We also wish to point that the radical production during ultrasound processing is not an outcome of electrochemical effect, i.e. chemical effects resulting from the application of electric field. These changes in the medium are due to sonochemical effects. However, for consistency and in the spirit of involvement of electrons in radical chemistry, we are not attempting to capture this in the title of our review.

We target this review at graduate students and researchers in food engineering to give them a good exposure to the fundamental physical and chemical principles governing the selected non-thermal technologies. We expect this review to be useful for experienced researchers as well, considering that we also critically unfold some epistemological aspects. We have ensured ample coverage of the fundamentals by including many classic references, as well as contemporary papers describing the advances in technologies. For reasons of completeness and brevity, we have relegated some useful notes to the appendices, besides being selective in discussed food applications. The choice of discussed applications for each technology is

propelled by the personal experience of the authors, as well as their industrial relevance.

2 Cold plasma technology

Reactive oxygen species (ROS) have historically been viewed as purely harmful metabolic by-products that cause oxidative damage to lipids, proteins, and nucleic acids. However, recent research studies have been successfully exploiting ROS for new roles including microbiological pathogen inactivation, treatment of waste streams and food property modification. Ozonation is one such technology which relies on the use of ozone, a powerful ROS, and has been researched well-over three decades for food applications. One can think of cold plasma as a successor to ozone technology, where ozone happens to be only one component of the reactive system. In fact, ozone is as generated for biological applications under laboratory and industrial conditions is oxygen plasma. Therefore, for readers familiar with ozone technology, what follows here forthwith may sound somewhat familiar.

2.1 Elementary thermodynamics of cold plasma

Plasma is an ensemble of several excited atomic, molecular, ionic, and radical species, co-existing with numerous reactive species, including electrons, positive and negative ions, free radicals, gas atoms, molecules in the ground or excited state, quanta of electromagnetic radiation (UV photons and visible light) ([Misra et al., 2015c](#)). Plasma is often referred to as the fourth state of matter in compliance with the increasing order of energy from solid, to liquid, to gas, ultimately to the ionised state- plasma. In the plasma state, the free electric charges *viz.* electrons and ions, make plasma electrically conductive, internally interactive, and strongly responsive to electromagnetic fields ([Fridman, 2008](#)). The energy required to ionise a given gas can be fed from any source; either by heating or subjecting to electromagnetic field (electric field or high energy light). It should be noted that a background density of free electrons in the order of $\approx 10^6 \text{ m}^{-3}$ is present naturally in the ambient environment due to ionisation from background radiation, and these serve as precursors for breakdown in presence of external fields.

On recalling the fundamental laws of mechanics, we find that when two bodies with different masses (say, m_1 and m_2) collide, the extent to which they exchange energy depends on the ratio of their masses (m_1/m_2). In the context of gas plasma, one can approximate ions and neutral particles to possess similar order of masses (i.e. $m_1/m_2 \approx 1$), which suggests that the energy sharing is nearly complete. Furthermore, the ion essentially stops after every collision. We also note that because electrons are much lighter than ions and neutral (i.e. $m_1/m_2 \ll 1$), only a minor fraction of the total energy is exchanged. As a consequence, when an electric field is applied to a gas, the electrons' temperature (T_e) tends to be much higher than that of the ions, neutrals and global gas (T_g) temperature ($T_e \gg T_g$), while the electrons collide further to generate reactive radicals. Thanks to this thermodynamic non-equilibrium condition which allows to generate and sustain reactive chemical species under ambient gas temperature and atmospheric pressure conditions. We refer such thermodynamically unstable, low temperature, electrical gas discharges as *non-equilibrium* or *cold* plasma. Contrary to cold plasma, in a thermal plasma, the electrons, ions and neutrals have the same average temperature.

The properties of a plasma, such as the density of charged particles (electrons and ions) and their energy distribution, generally depend on the power, type of power (e.g. AC, DC, pulsed, frequency, etc.), type of gas, etc.

2.2 Plasma sources

The configuration of a physical set-up for technological applications of plasma is very commonly referred to as the plasma source. A discussion of the various plasma sources and their characterisation could

render itself into separate reviews. However, we will briefly touch up on the plasma sources commonly employed for food applications. The discussion that follows is somewhat biased towards the dielectric barrier discharges (DBD), being the most popular among the research community.

2.2.1 Dielectric barrier discharge (DBD)

The DBD set-up consists of two dielectric plates, the gap in between which is filled with the working gas. A sinusoidal voltage is applied in the order of several thousand kilovolts at frequencies ranging from line frequency (50 Hz) to radio-frequency (RF) on the high voltage side, while the other electrode is grounded (however, it could occasionally be left at floating potential). As the high voltage electrode experiences the increase in voltage, so does the gas in the gap between the electrodes. As a consequence, any free electrons in the gap are accelerated, thus acquiring enough energy to cause ionization. This results in a cascade effect, which exponentially increases the number of electrons in the gap. Electrons created via electron impact ionization rush toward one of the dielectric plates, in the opposite direction to the electric field. An equal number of ions are also generated during electron impact ionization (see appendix 7.1). The ions rush toward the opposite dielectric plate in the same direction as the electric field. As a result, surface charge with opposite sign accumulates on both dielectric plates. This causes the electric field to become shielded from the gas filled gap. In fact, the electric field across the gap cannot exceed the breakdown electric field, which is highly dependent on the gas and background pressure. The breakdown electric field is also a function of the surface properties of the dielectric material. Surface charge accumulation temporarily terminates the discharge until the field reverses direction and the process repeats in the opposing direction. The barrier discharge phenomena could operate in different regimes, typically, homogeneous glow or filamentary regimes (see Figure 1). The duration of an individual plasma filament in the DBD is relatively short- from a few to tens of ns (Tian and Kushner, 2014).

For practical applications, DBDs can be used in various configurations. The concentric electrode scheme with gas flowing through the discharge region is common for plasma jets (Schutze et al., 1998). The flat electrode configuration has been leveraged for in-package plasma treatments. In another similar design, the flexible electrodes on the package have also been employed for encapsulated plasma treatment of foods (Yong et al., 2015).

2.2.2 Corona Discharge

Electrical discharges generated at atmospheric pressure near sharp points, edges, or thin wires under the action of large electric fields are usually weakly luminous, and referred to as *Corona*. Corona discharges are typically self-sustaining, with the plasma generated being stable and in steady condition for long periods. The underlying reason for the ease of corona generation and its stability can be understood as follows; the sharp edges promote the formation of high intensity local electric fields, which results in a decreased breakdown voltage (V_b) and helps stabilize the discharge uniformly over the electrode surfaces (Bárdos and Baránková, 2010). That said, it is also important to note that corona discharges are spatially non-uniform, which is why the geometry of the set-up becomes important for their analysis.

2.2.3 Microwave discharges

Microwave power (typically operating at 915 MHz and 2.45 GHz) is often used to generate volumetric non-equilibrium plasma. At the microwave frequencies, the mobilities of electrons and ions are very different. Therefore, the alternating current (AC) fields enable “pumping” of the power selectively to electrons, thus enabling a non-equilibrium cold plasma at high gas pressures (Bárdos and Baránková, 2010). In addition, the use of microwave radiation enables generating *electrodeless* plasma.

2.3 Transport phenomena

Knowledge of the number densities, and fluxes of plasma species is of paramount importance for explaining and harnessing the effects of plasma on micro-organisms and foods. Physico-mathematical models provide a goal-oriented representation of the plasma, thereby helping to understand the spatio-temporal chemical dynamics and the transport phenomena in discharges. A complete understanding of the plasma chemistry and transport phenomena, in general, is a highly complex task involving a tight coupling between electromagnetics, physical and chemical kinetics, heat transfer, mass transfer, and fluid dynamics. To capture all these physical phenomena in a model demands computational solutions to a highly non-linear coupled set of space and/or time dependent partial differential equations. Furthermore, non-equilibrium cold plasma is characterised by multi-scale processes occurring over a wide range of time and length scales. The time scales involved in DBDs, for example, span over several orders of magnitude; the very fast time scales associated with streamer formation and propagation, to the very slow associated with ion recombination, chemical kinetics of neutral species and diffusion (Barni et al., 2005b).

Physicist's almost always tend to simplify things (of course, without losing the elegance and universality); they model the individual plasma particles as *hard-spheres*, within the general class of particle-in-cell simulations. However, plasma can be described not just as an ensemble of discrete particles under the *kinetic* approach, but also using a relatively simpler, *fluid* approach (discussed later) (Zhu and Kong, 2005). The former is governed by the famous *Boltzmann equation* (1), yielding a fully kinetic description of the particle velocity and position

$$\frac{\partial f_s(x, y, z, t)}{\partial t} + v \cdot \nabla f_s(x, y, z, t) + a_s \nabla_v f_s(x, y, z, t) = I_{col} \underbrace{\left(\frac{\partial f_s(x, y, z, t)}{\partial t} \right)}_{\text{elastic, inelastic and non-conservative collisions}} \quad (1)$$

Herein, $f_s(x, y, z, t)$ is the distribution function in (x, y, z) space of particle positions and velocities for species 's' at time t (here velocity variables v_x , v_y , and v_z are omitted for brevity). Furthermore, for an ensemble of electrons in an ionised gas, $a_s = -\frac{e}{m}E$, with e being the elementary charge, E , the electric field, \mathbf{m} , the electron mass. The term ∇_v stands for the gradient in velocity space. The right hand side (RHS) represents the rate of change in $f_s(x, y, z, t)$ due to collisions. This collision integral describes the pairwise collisions of charged particles with neutral molecules, accounting for elastic, inelastic, and non-conservative (e.g. ionizing or attaching) collisions (Dujko et al., 2013). The collision operator, I_{col} , allows to include a statistical account of the random interactions (typically two-body collisions) of particle species in the plasma with other particles. The two most commonly used collision operators are Boltzmann collision operator and Fokker-Planck collision operator, which allow to conserve the particles, their momentum, and energy at each calculation step. Under most practical circumstances, evaluating the distribution functions via solving the integrodifferential Boltzmann equation is challenging and computationally expensive. In addition, speaking practically, the large amount information contained in the distribution function may not translate into any direct (biological) application.

Fortunately, to model cold plasma processes for effective food and biological applications, it is not an absolute necessity to solve the Boltzmann equations for obtaining the distribution function, which could provide information about the macroscopic variables of physical interest, e.g. number density, mean velocity (momentum), electron mean energy, temperature etc. The differential equations ruling the space-time variations of the macroscopic properties can be derived directly from the Boltzmann equation by approximating few moments of the equation. Alternatively, one could also derive them from first principles using physical arguments. This is referred to as the plasma fluid approach, that we mentioned of earlier. The mathematical derivation of the (velocity) moments has been covered in great detail in several books (Bittencourt, 2004; Lieberman and Lichtenberg, 2005; Smirnov, 2008). It is worth noting that a continuum approach is applicable when the *Knudsen Number* (K_n) of the gas discharge under consideration is low

(Gogolides and Sawin, 1992) (refer appendix 7.2). We will now discuss some important mathematical results which are of high significance to simulation of technological plasma sources.

In principle, one could obtain infinite moments of the Boltzmann equation, and for practical reasons one has to truncate after a certain moment equation. Moreover, the physical meaning of higher moments remains a topic of debate. Multiplying the Boltzmannn equation (1) by m_s (i.e. m_sv^0 ; zeroth order moment related to mass) and m_sv^1 (first order moment related to velocity), followed by integration over all velocities, results in the first two moments of the Boltzmann equation, which are the equations for conservation of mass (2) and momentum (3) respectively-

$$\frac{\partial n_s(x, y, z, t)}{\partial t} + \underbrace{\nabla \cdot \Phi_s(x, y, z, t)}_{\text{convective drift}} + \underbrace{u \cdot \nabla n_s(x, y, z, t)}_{\text{Source}} = Q_s = \sum_{i,j} k_{ijk} n_i n_j n_k \quad (2)$$

$$\Phi_s(x, y, z, t) = \underbrace{\mu_s n_s(x, y, z, t) E}_{\text{Drift by electric field}} - \underbrace{D_s \nabla n_s(x, y, z, t)}_{\substack{\text{Diffusion by} \\ \text{conc}^n \text{ gradient}}} \quad (3)$$

Herein, $\Phi_s(x, y, z, t)$ represents the flux of particles $n_s(x, y, z, t)$, the subscript ‘s’ being the particle species. The source term, Q_s for the electron/ion/neutral plasma particles given by the summation on RHS of equation (2) representing the product of species density $n_{i,j,k}$ and reaction rate coefficients k_{ijk} for collisions between the species i , j , and k . Equation (3) is deduced after several simplifications such as ignoring the effects of inertial, viscous and magnetic effects, ultimately resulting in the *drift-diffusion approximation*, meaning the charged particles are drifted by the electric field and all species diffuse due to concentration gradient. The convective drift term in equation (2) signifies the effect of convective fluid flow which is governed by the Navier-Stokes equations (discussed later within this section). Plasma being composed of more than one particle species (electrons, ions and neutrals), one has to solve a system of transport equations for each species to estimate the macroscopic variables.

Similar to the approach employed for equation (2) and (3), on multiplying equation (1) by $\frac{m_s v^2}{2}$ (second order moment related to kinetic energy), and integrating over the velocity space, we obtain the equations for conservation of energy (also referred to as the *electron energy density* equation)-

$$\frac{\partial n_\varepsilon(x, y, z, t)}{\partial t} + \nabla \cdot \Phi_\varepsilon(x, y, z, t) + \underbrace{E \cdot \Phi_e(x, y, z, t)}_{\text{convective drift}} + \underbrace{u \cdot \nabla n_\varepsilon(x, y, z, t)}_{\text{source coefficients}} = Q_\varepsilon \quad (4)$$

$$\underbrace{\Phi_\varepsilon(x, y, z, t)}_{\text{electron energy flux}} = \underbrace{n_\varepsilon(x, y, z, t) \frac{5}{3} \mu_e E}_{\text{electron drift}} - \underbrace{\frac{5}{3} D_e \nabla n_\varepsilon(x, y, z, t)}_{\text{electron diffusion}} \quad (5)$$

$$Q_\varepsilon = \underbrace{-e \Phi_e(x, y, z, t) \cdot E}_{\text{Joule Heating}} - \underbrace{\sum_j k_{ej} n_e n_j \Delta \varepsilon_j}_{\text{Collisional losses}} \quad (6)$$

In equations (4), (5) and (6), we solve for only the electron temperatures, as the ions and neutrals are assumed in thermal equilibrium with the background gas for cold plasma, the temperature of which is generally known. The terms n_e and ε refer to electron density and mean electron energy, respectively, and $\Delta \varepsilon_j$ is the reaction energy loss for electron collision of j . Thus, we have the electron energy density, $n_\varepsilon(x, y, z, t) = n_e(x, y, z, t) \bar{\varepsilon}(x, y, z, t)$.

Another important consideration is the input of transport coefficients (D_s) and rate coefficients (k_{ijk}), which are functions of electron energy distribution function. These are generally calculated from collision cross section data available in literature (Pitchford et al., 2017) using a Boltzmann equation solver such

as the BOLSIG+ code (Hagelaar and Pitchford, 2005). These calculations also provide the values for μ_s , which in turn aids in calculating the diffusion coefficient (D_s) via the Einstein's relation, $D_s = \mu_s \frac{k_B T_s}{q_s}$, where k_B is the Boltzmann constant and T_s the particle species temperature. For equation (5) a lookup table is built with the electron and electron energy mobility as function of the mean electron energy, which is used for obtaining D_e , from the Einstein relation. The mobilities and diffusion coefficients for ionic and neutral species can be obtained from literature (Bird et al., 2007; Viehland and Mason, 1995; Ellis et al., 1976, 1978, 1984).

The electric field in all the equations above is calculated by solving the Poisson's equation which involves the gradient of the potential-

$$\nabla \cdot \epsilon_0 \epsilon_r E = -\nabla^2 \epsilon_0 \epsilon_r \mathbf{V} = -\sum_p q_p n_p \quad (7)$$

where ϵ_0 is the permittivity of free space, ϵ_r , the dielectric constant of the material, q_p is the charge of the particle, and \mathbf{V} , the applied voltage. It may well be appreciated that while plasma is *quasineutral* (see appendix 7.1), the charged species are in free motion, creating spontaneous regions of net charge density; therefore, there exists an electric field within the plasma. Equation (7) allows to account for the modification of electric field due to such space-charge re-distribution within gas.

The effect of the bulk gas flow, such as those arising in plasma jets and corona discharges is described by the Navier-Stokes equations, which couples with the plasma dynamics via the velocity term \mathbf{u} in equations (2) and (4). Equation (8)-(9) describe the compressible form of the Navier-Stokes equations with a volume force term for capturing the convection due to mixing of plasma plume with ambient gas and/or density differences arising from heating.

$$\rho \frac{\partial \mathbf{u}}{\partial t} + \rho(\mathbf{u} \cdot \nabla \mathbf{u}) = \nabla \cdot [-pI + \tau] + \underbrace{\mathbf{F}}_{\text{Volume force } = g(\Delta\rho)} \quad (8)$$

$$\tau = \mu(\nabla \mathbf{u} + (\nabla \mathbf{u})^T) - \frac{2}{3}\mu(\nabla \cdot \mathbf{u})I \quad (9)$$

$$\frac{\partial \rho}{\partial t} + \rho(\nabla \cdot \mathbf{u}) = 0 \quad (10)$$

where ρ is the density, \mathbf{u} the velocity vector, p the pressure, and τ the viscous stress tensor. The volume force F can be dropped out when such effects are not significant; e.g. for trapped gas cold plasma sources or situations where indirect treatments are to be simulated. Equation (10) is the equation for mass continuity. Finally, the gas heating effects of cold plasma although small (typically $\approx 20\text{-}30$ °C above ambient), could also be captured using the transient heat equation (see appendix 7.3).

The space-charge re-distribution and convective fluid motion due to temperature/density gradients in plasma reveal an important aspect that is related to in-package plasma treatment of foods. These phenomena promote the homogeneous exposure of the food surface. This overcomes problems that are encountered with other comparable techniques such as ultraviolet light decontamination; e.g. shadowing effects. In conclusion, within a *continuum/fluid* modelling framework, a complete profile of the spatio-temporal plasma dynamics and plasma-food interactions can be obtained using computational models solving equations for the electric field, dynamics of charged and neutral species, the electron energy, and fluid flow of the neutral gas (via Navier-Stokes equations). While detailed physico-chemical models of plasma are being leveraged for plasma medicine field (Norberg et al., 2015; Chen et al., 2014), for food systems it remains unexplored.

2.4 Electrochemistry

The simultaneous formation of several reactive chemical species confers non-equilibrium plasma a winning antimicrobial intervention and an effective chemical method for modulating chemistry of food materials.

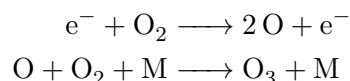
An array of reactions in plasma discharge result in the production of reactive metastables and radicals: (i) the electron impact reactions (vibration, excitation, dissociation, attachment and ionization), (ii) ion-ion recombination to form neutrals, (iii) interactions between ions and molecule, (iv) Penning ionization, (v) quenching processes, (vi) recombination of neutrals via three body reaction schemes, and (vii) photoemission, photoabsorption and photoionization (Norberg, 2015; Bhoj, 2006).

The concentration of plasma chemical species is a function of their formation and loss rates. The formation rate is dependent on the electron density and the temperature, while the loss rate is decided by the discharge configuration and the material being treated (Mozetič et al., 2015). Barni et al. (2005b,a) have performed computer simulation of the plasma kinetics in a DBD streamer to obtain the time evolution profiles of charged as well as neutral species densities. They noted that the dynamics of charged particles is seemingly quicker than neutrals, and attributed it to the faster rates of ion-ion recombination and electron attachment. As can be observed in Figure 2 (a), initially a roughly exponential rise in charged particles happens, where after electrons are rapidly eliminated and a molecular ion plasma appears, evanescing due to recombination and diffusion in ~ 5 ms. The neutral gas-phase, on the other hand, appears over longer time-scales and ozone dominantly emerges within a few ms (Figure 2 (b)).

N_2 and O_2 molecules when present in feed gas, they participate in collision reactions with electrons resulting in a series of reactions and the production of NO_x species. Kossyi et al. (1992) modelled the kinetics of plasma chemistry in a microwave discharge in N_2/O_2 mixture taking into consideration ≈ 450 reactions to describe the active species including excited states and the reaction products. Figure 3 shows the time evolution of reactive oxygen species (ROS) and reactive nitrogen species (RNS) produced over time scales ranging from $1\ \mu s$ to $1\ ks$.

Firstly, we note from Figure 3 that the underlying mechanism for the species formation involves a complex set of simultaneous competing and sequential reactions. Secondly, we can see that the O, N appear at early stages whereas NO_x species appear later. RNS of particular importance are the NO_2 , NO_3 , N_2O_3 , and N_2O_5 (Sakiyama et al., 2012). The dominant ionisation mechanisms in a plasma are governed by the process parameters. For example, it is known that at the current range 0.01-0.1 A, a transition in the dominant ionization mechanism is onset, from electron mediated ionization at low currents to associative ionization in atomic collisions at high currents (Benilov and Naidis, 2003). Via reaction with superoxide in a plasma, nitric oxide could also yield peroxy nitrite, which is a potent oxidant responsible for oxidation of sulphydryl groups and nitration of tyrosine residues in cellular proteins of micro-organisms. Literature reveals that nitric oxide treatments lead to the inactivation of enzymes in fruits (Deng et al., 2013). Recent literature also shows that considerable amounts of nitrogen oxides (NO_x) are produced in air plasma, as monitored through UV-Vis optical absorption spectroscopy (Moiseev et al., 2014). Therefore, plasma led inactivation of enzymes can partly be summed as the action of not only reactive oxygen species (ROS) like ozone or singlet oxygen, but also NO_x .

Finally, from Figure 3 we also note that ozone is formed at high concentrations and persists for longer durations. The long-lived nature of ozone makes it an important species of action in bio-chemical-decontamination processes (Misra et al., 2015b), and therefore, deserves a special mention. In a discharge, the collision of electrons (e^-) with molecular O_2 results in a lone O atom within the discharge zone, which subsequently attacks molecular O_2 by a three body reaction to yield ozone (O_3)- a powerful oxidant with a redox potential of 2.07 (Misra et al., 2015b).



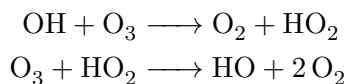
where, M = O, O_2 or O_3 . The ozone and singlet oxygen are primarily responsible for the oxidation of lipid in membranes of bacterial cells (via attack on the double bonds of unsaturated groups), which results in an increased membrane permeability, decreased fluidity and consequently, the secondary products released

act up on DNA (Khadre et al., 2001). When nucleotides react directly with O₃, the carbohydrate and phosphate ions are released. Ozone also possesses a tendency to attack polysaccharides, causing breakage of glycosidic bonds to form aliphatic acids and aldehydes (Bablon et al., 1991). An oxidation of the sulphydryl groups of membrane proteins and microbial enzymes effected by ozone is another route for antimicrobial action.

The effects of water molecules (or humidity) on the plasma chemistry in air has been comprehensively studied using experimental as well as computational modelling tools (Moiseev et al., 2014; Ardelyan et al., 2013). It has been recognised that the humid air plasmas are more effective than dry air in terms of their anti-microbial and sporicidal efficacy (Patil et al., 2014). The presence of water in the gas promote the formation of OH and H species, which could potentially quell the O₃ produced.

An important plasma species formed in air plasma, particularly in the presence of humidity, is hydrogen peroxide (H₂O₂). It should be noted that H₂O₂ could also be the key species in when using atmospheric plasma sources in noble gases or gas mixtures without hydrogen containing species. The H₂O₂ originates from the humidity in the air to which the plasma comes in contact. For completeness the reactions leading to the formation of H₂O₂ are summarised in appendix 7.4. The importance of H₂O₂ and free hydroxyl radicals (resulting from its degradation) for sporicidal action was elucidated decades ago by Russell (1982) and later by Setlow and Setlow (1993). The enhanced sporicidal action of plasma in presence of humidity has been attributed to hydrogen peroxide, hydroxyl radicals and atomic oxygen.

When discharges are introduced into water or liquid foods, O₃ acts on organic matter either via direct oxidation route or indirectly by conversion into OH radicals, which in subsequent steps oxidises matter.



Note that, both solvated H₂O₂ and O₃ can persist in the water for up to days, and such longer time-scale of activities is now being exploited in plasma activated water (PAW) for washing of fresh produce Kamgang-Youbi et al. (2009); Ma et al. (2015); Tian et al. (2014). One should also recall that most fresh foods often have a layer of liquid water at their surface ranging over length scales of at least a few micrometers.

The charged particles in plasma are characterised by small lifetimes (<10⁻⁶ s), which prevents them from diffusing to significant distances in aqueous solution. However, ozone, nitrogen oxides, and nitric acid, which are characterized by higher lifetimes do participate in chemistry at the gas-liquid interface. Via a global chemical kinetic model, Hamaguchi (2013) investigated the electrochemistry in water resulting from exposure to plasma. The time evolution of the simulated densities for reactive species are shown in Figure 4, assuming hydroxyl radicals (OH), nitric oxide (NO) molecules, and N₂ and O₂ of air, all dissolve into water.

The dissolved nitrogen oxides react irreversibly with water molecules to form nitric and nitrous acid. In addition, a variety of species such as nitrate ion (NO₃⁻), peroxy nitrous acid (ONOOH), and superoxide radical anion (O₂⁻) also form in water. Depending on the gas composition, discharge gap and gas flow rates, there could be spatial gradients in the reaction progression and the resulting concentration of ROS and RNS, as simulated by Tian and Kushner (2014); c.f. Figure 5 and caption for details.

Nitrous acid and N-nitroso compounds formed in liquid phase can diazotise and deaminate amino groups in, for example, nucleotides of bacterial cells (Cammack et al., 1999). Furthermore, the inhibition of respiration in aerobic bacteria has long been associated with the bacterial growth inhibiting activity of nitrite (Misra et al., 2014a). Besides the antimicrobial activity, the nitrite produced in the liquid phase on exposure to cold plasma also offers a new route to meat curing, which imparts distinct colour and flavour to meat products, while allowing to control spoilage micro-organisms. Recently, Jung et al. (2015) demonstrated that the nitrite and nitrate rich plasma treated water acts as an effective curing agent in emulsion type pork sausages.

An array of novel applications and industrial innovations are expected to emerge in near future, as more and more researchers from multiple disciplines get involved and/or collaborate in the plasma research. A key point worthwhile noting is that the ability to control plasma decontamination processes is very challenging, and perhaps, limiting its adoption by the industry. This requires focused research actions to match with (or exceed) the consistent, and effective performance of chemical disinfectants currently in use (e.g. chlorine).

3 Electrohydrodynamic (EHD) processing

Electrohydrodynamic (EHD) processing is considered as an energy efficient non-thermal technology, suitable for the treatment of heat-sensitive foods and food ingredients, such as high-value bioactive components of fruits and medicinal plants (oligomeric procyanidins, polyphenols, flavonoids, dietary fiber, etc.), living cells (bacteria, yeasts and viruses), organic substances of biological origin (blood plasma, serum, hormones, antibiotics, prebiotics, nutraceuticals, etc.) ([Alemrajabi et al., 2012](#); [Bajgai et al., 2006b](#); [Singh et al., 2012](#); [Zhang et al., 2015a](#)).

EHD phenomenon is based on the high-voltage ionic discharge between electrodes with substantially different radii of curvature, for example sharp pin-plate or thin wire-plate ([Robinson, 1961](#)). Unlike DBDs intended for food treatments or PEF processes, EHD relies on direct current (DC) to initiate glow discharge. The ionic discharge from the electrode could be observed in dark conditions as purple “glowing” light due to a recombination of high-energy ions, as can be observed in Figure 6. Herein, the visible bright spots at the free ends of the pins indicate the ionization region. Notably, on further increasing the electric field strength an expansion of the ionization region will follow into a transition to spark-type discharge. This effect is not desirable, because high energy sparks could damage the food/biological material under processing.

Extending the discussions in section 2.2.2, the type of corona generally used in EHD processes is a self-sustaining, non-luminous discharge produced at the electrodes of small characteristic dimensions, e.g. needles or slender wires ([Kulacki, 1982](#)). The hallmark of a corona type discharge is the presence of a low field drift zone, connecting the zone of ionization with the electrode at ground potential (Figure 7).

The surface $\alpha' = 0$ in Figure 7 represents the outer limit of ionization zone, where the production of electrons by ionization just balances the loss by attachment. In unipolar discharge, the drifting ions/electrons is always of corona polarity. Within the drift region, charged particles collide with neutrals, but their energy is not sufficient for causing ionization and their density is too low for the chemical reactions to occur ([Goldman et al., 1985](#)). The spatial distribution of charge within this zone determines the current density and overall energy transfer.

3.1 EHD Applications in Food Processing

In Table 1 a summary of the up-to-date applications of EHD in food processing are summarized. Before delving into a discussion of these applications we wish to point that the effects of EHD on food quality described in Table 1 were studied on the lab scale for most cases.

Table 1: EHD applications in food processing. *Point/wire-to-plate discharge electrode

Application	Material	Electric field intensity, kV/cm	Performance Indicators	Reference
Potato slabs		5.25 DC*	2-2.5 times faster	Chen and Barthakur (1991)
Apple slices		2.0 - 5.5 AC*	4-6	Hashinaga et al. (1999)
Agar gel		2.0 - 10 DC*	8-280	Isobe et al. (1999)
Okara		3.0-5.7 DC*	1.4	Li et al. (2000)

	Spinach	4.3 AC*	4.15	Bajgai and Hashinaga (2001b)
	Japanese radish	4.3 AC*	3.3	Bajgai and Hashinaga (2001a)
	Wheat	0.2 - 10 DC*	1.5-1.9	Cao et al. (2004)
	Okara cake	n/a*	1.7-3.2	Li et al. (2005)
	Rapeseed	6.0-10 DC*	1.78-2.47	Basiry and Esehaghbeygi (2010)
	Tomato slices	3.0-5.0 DC*	1.3-2.0	Esehaghbeygi and Basiry (2011)
	Tofu	5.6 DC*	8-9	Bai et al. (2010)
	Fish	5.0 DC*	4.5	Bai et al. (2011a)
	Scallop	5.0 DC*	8.0	Bai et al. (2012)
	Carrot slices	3.3-6.5 DC*	3-5	Alemrajabi et al. (2012)
	Rice	5.0 DC*	1.23-1.59	Esehaghbeygi (2012)
	Sea cucumber	5.0 DC*	3.6	Bai et al. (2013)
	Kiwi slices	4.5 DC*	n/a	Dalvand et al. (2013)
	Banana slices	6.0-10 DC*	n/a	Esehaghbeygi et al. (2014)
	Mushroom slices	2.4-4.2 DC*	1.4-1.78	Dinani et al. (2014)
	Meat	0-3.2 DC*	n/a	Ding et al. (2014)
	Carrot slices	n/a*	up to 2.33	Ding et al. (2015)
	Apple slices	0-5.0 DC*	3-4	Martynenko and Zheng (2016)
Refrigeration	Carrot juice	Point-to-plate*	Better color, stability, retention of phenols and carotenoids	Hsieh and Ko (2008)
	Tilapia	Point-to-plate*, 1.0 kV/cm	Delayed deterioration	Hsieh et al. (2011)
	Tilapia	Parallel plates, 3,6, 9 kV/cm	Delayed ATP and protein degradation, lipid oxidation and bacterial growth	Ko et al. (2016a)
	Tilapia		Extended shelf-life	Ko et al. (2016b)
Freezing	Water	Parallel plates, 10-60 kV/cm	Facilitated phase transition due to increase of ice nucleation temperature, reduced size of ice crystals	Wei et al. (2008)
	Water		Controlled ice nucleation	Orlowska et al. (2009)
	Pork meat		Reduced size of ice crystals and cell damage	Xanthakis et al. (2013)
	Lamb meat		Good retention of color and texture	Dalvi-Isfahan et al. (2016)
Thawing	Ice	Point-to-plate, 5.625 kV/cm	Accelerated thawing rate	Bai et al. (2011b)
	Ice	Point-to-plate* vs. parallel plates, 2.9-4.8 kV/cm	Ionic, wind is more efficient than electric field	He et al. (2016)
	Tuna fish	Point-to-plate, 1.25-3.5 kV/cm	Accelerated thawing, but negatively affect color, texture and protein solubility	Mousakhani-Ganjeh et al. (2015)
	Chicken meat	Point-to-plate, 1 kV/cm	Accelerated thawing (30%), reduced cooking loss and increased water holding capacity	Hsieh et al. (2010)

	Pork meat	Point-to-plate, 0.8-2 kV/cm	Accelerated thawing and decreased drip loss by 20%	He et al. (2013)
	Pear, plum, banana	Wire-to-plate AC, 1.05 kV/cm for 1hr	Suppressed respiration rate during storage Delayed chlorophyll and flavonoids degradation	Kharel et al. (1996)
Shelf-life extension	Mandarin			Zhang and Hashinaga (1997)
	Mangoes	Point-to-plate, 1.5 kV/cm for 45 min	Suppressed respiration rate and antioxidant capacity	Shivashankara et al. (2004)
	Apples	Point-to-plate vs. parallel plates, 2 kV/cm	Suppressed respiration rate during storage	Atungulu et al. (2003, 2004b, 2005b)
	Plum	Parallel plates, 2 kV/cm	Suppressed putrefaction and mold growth	Atungulu et al. (2005a)
	Embllic fruit	Parallel plates AC and DC 4.3 kV/cm for 2 h	AC treatment improved quality	Bajgai et al. (2006a)
	Tomato	Point-to-plate vs. parallel plates, 2 kV/cm	Point-to-plate accelerated weight loss, whereas parallel plate suppressed weight loss	Atungulu et al. (2005a)
	Cranberries	Parallel plates 2, 5, 8 kV/cm for 0.5-2 h	Suppressed respiration rate during storage	Palanimuthu et al. (2009)

As a general guiding principle, when considering EHD treatment of food materials, three closely related effects should be taken into account:

1. Direct effect of electric field in the range from 2 to 10 kV/cm.
2. Physical electro-convective effect of ionic wind.
3. Chemical effect of cold plasma, containing air ions N_2^+ , O_2^+ , N^+ , O^+ and ozone.

A careful modulation of the process parameters (as we will see next) could enable obtaining distinct effects in foods, thus enabling potentially different applications.

3.1.1 Shelf-life extension and food quality retention

Most of the food applications highlighted in Table 1 consider positive DC discharge because of better stability and less production of ozone. However, in some applications, for example extending the shelf life of fresh foods, ozone production is desirable due to the antimicrobial effect of ozone (Misra et al., 2011). Effects of ionic wind and cold plasma are dominantly surface phenomena, affecting boundary layer at the gas-material interface.

Positive effect of EHD on the shelf stability of fresh foods was reported for onions (Song et al., 2000), apples (Atungulu et al., 2003, 2004a, 2005a,b), emblic fruit (Bajgai et al., 2006a), cranberry (Palanimuthu et al., 2009), and tilapia (Ko et al., 2016b). This effect, accompanied with significant decrease of oxidation rate and weight loss, was explained by direct effect of electric field and antimicrobial action of cold plasma (Misra et al., 2011). It is important to recognise that this effect is observed only in parallel-plate electrode

system with uniform electric field, while ionic wind generated by point-to-plate electrode system, has been found to accelerate the weight loss in fresh apples ([Atungulu, 2007](#)).

Different electrode configurations (parallel plates, pin/wire-to-plate or multiple pin/wire-to-plate) determine the effect of EHD on the food quality. For example, pin/wire-to-plate configuration results in a remarkably uneven ionization and spatial distribution of electric field. This highly non-uniform nature of EHD treatment creates some problems in consistency of product quality [Chen and Mujumdar \(2002\)](#). Chemical effects in the treated food products, such as intensive surface oxidation due to ozone, should also be considered when applying EHD processes.

3.1.2 Electrofreezing and EHD assisted thawing

Several papers have reported the beneficial effects of high voltage treatment on the food quality during refrigeration ([Hsieh et al., 2011](#); [Ko et al., 2016a,b](#); [Hsieh and Ko, 2008](#)), freezing ([Orlowska et al., 2009](#); [Dalvi-Isfahan et al., 2016](#)), and thawing of frozen foods ([Hsieh et al., 2010](#); [Mousakhani-Ganjeh et al., 2015](#); [He et al., 2013, 2016](#)). The major findings are related to the effect of high-intensity electric field on the water phase transition, in particular ice nucleation ([Orlowska et al., 2009](#)). These effects can be explained by realising that an external electric field of sufficient strength could significantly increase the nucleation temperature and decreased the ice crystal size ([Xanthakis et al., 2013](#)), resulting in improvement of overall quality of frozen foods ([Dalvi-Isfahan et al., 2016](#)). In fact, Experiments with electrofreezing have demonstrated the direct effect of electric field on thermodynamic changes of the state of water within food material ([Wei et al., 2008](#); [Carpenter and Bahadur, 2015](#)). [Orlowska et al. \(2009\)](#) showed that electric field E changes the free energy of ice nucleation ΔG , proportionally to the dipole polarization P of the water molecules:

$$\Delta G = 4\pi r^2 [\gamma - 0.33 (\Delta G_v - P \cdot E)] \quad (11)$$

where r is the radius of the water molecule, γ is the surface free energy of the crystal fluid interface.

Similar to electrofreezing, EHD-assisted thawing has been found to significantly improve the food quality, such as color, texture, protein solubility in fish products ([Mousakhani-Ganjeh et al., 2015](#)) and reduced thawing loss of meat products ([He et al., 2016](#); [Hsieh et al., 2010](#)). It was demonstrated that significant enhancement (~twice) of thawing rate is due to EHD effect on thermodynamics of ice-liquid water phase transition [He et al. \(2016\)](#); [Bai et al. \(2011a\)](#).

3.1.3 EHD effects on macromolecules

The effects of EHD processing on macromolecular structures have been studied by [Xue et al. \(1999\)](#), [\(Singh et al., 2013\)](#), and [Vanga et al. \(2015a\)](#). In general, for electric fields in the order of 5 to 6 kV/cm, no changes in structure of proteins has been observed; for e.g. whey proteins ([Xue et al., 1999](#)). However, stronger electric fields in the order of 30 kV/cm could significantly affect the protein conformation and solvent accessible surface area ([Singh et al., 2013](#)). The significant effects of strong electric fields on the protein activity emerge from conformational changes in the protein structure ([Singh et al., 2013](#)), specifically the helical secondary structure ([Vanga et al., 2015b](#)). Research studies to fully elucidate the mechanism underlying EHD-macromolecule interactions are under way.

3.1.4 EHD Drying - Heat and mass transfer enhancement

The heat transfer enhancement resulting from an electric field as such was reported long ago by [Asakawa \(1976\)](#). Such distinct effects, which we will elaborate a little later, have been successfully leveraged for water evaporation ([Barthakur, 1990](#)) and drying of solids including, food and biological materials ([Singh et al., 2012](#)). EHD has been successfully leveraged for improving the heat transfer in an array of industrial

processes (Owsenek and Seyed-Yagoobi, 1997). Boosting of heat transfer coefficients for single and two-phase flows via exploitation of EHD phenomenon (Thornton and Porter, 1973) has been demonstrated. Several gaps in explaining the mechanisms underlying energy, mass and momentum transfer in EHD technology still persist. The mechanism of mass transfer in the drift region remains partially explained. Analogy amongst mass exchange processes in gases and liquid electrolyte were laid by (Weber et al., 2014); however, a comprehensive theory for mass transfer in charged gases is yet to be established.

Examples of foods subjected to EHD drying largely include plant foods; however, positive effects of EHD drying on animal origin foods has also been reported (Table 1). The schematic of a laboratory scale EHD drying set-up is presented in Figure 8.

Most of the EHD applications for food drying reported in literature rely on direct current (DC) high voltage in the range of 5-30 kV; however alternative current (AC) also facilitate water removal. It is well recognized that EHD enhances evaporation rate of wet foods from 1.4 to 4 times as compared to control. The best performance of EHD was observed in case of free water surface, increasing with voltage and decreasing with receding front of evaporation.

Well-documented positive effect of EHD on the food drying is often explained by the prevailing action of the ionic wind (Bajgai et al., 2006b; Martynenko and Kudra, 2016). EHD drying positively affects the food quality, for example by lowering shrinkage (Singh et al., 2012; Bajgai and Hashinaga, 2001b), increasing rehydration ratio (Bajgai and Hashinaga, 2001a), preserving colour (Bajgai and Hashinaga, 2001a; Alemrajabi et al., 2012; Esehaghbeygi and Basiry, 2011) and vitamin C content (Bajgai and Hashinaga, 2001b). Both EHD and high voltage electric field, used for pre-treatment of foods, decreased shrinkage and thermomechanical stresses in food materials during thermal drying (Singh et al., 2013; Bai et al., 2012; Dutta et al., 2012). This residual effect of electric field indicates that irreversible changes in foods could be related to thermodynamic state of water molecules and decreased entropy of vaporization.

Energy consumption in EHD drying is typically much lower than that in hot air drying, likely because of a targeted supply of energy for moisture evaporation and practically no heat lost with exhaust air. The energy efficiency in EHD drying of foods is at least ca. three times higher than that of conventional heat assisted drying (Lai and Lai, 2002). The energy-related issues in EHD drying have been reviewed by Kudra and Martynenko (2015).

There is a consensus about negligibly small share of momentum transport in overall energy balance. Calculations have shown that only 0.6% of the discharge energy is translated into direct momentum of the drifting ions, while 1.4% is transferred into kinetic energy of ionic wind (Goldman et al., 1985). Apparently, the rest of the energy is used for electrical excitation of neutrals, thus, raising their electrochemical potential. Such phenomenon, mostly pronounced at the interface between the media and metal electrode, is used for electrostatic coating (Bailey, 1998). Unfortunately, the amount of thermal energy dissipated in corona discharge, is still unknown, which limits analysis of overall energy balance. This topic requires careful experimental investigation.

The mass and energy transport intensification resulting from corona wind could be attributed to many underlying processes. A few of these, including electric field, ion acceleration, mechanical effect on the surface, polarization, charge acceleration, electrocapillary effects, surface tension gradients, and double electric layer are discussed in the literature (Rounseley, 1985). However, attempts for clear demarcation of the contribution of each mechanism is under researched, which limits practical applications of EHD. We hope that the discussions presented in our review will serve to guide future researchers for performing much robust simulation of the coupled transport processes than hitherto reported.

3.2 Charge Transport

An analysis of the ion transport in corona wind can be carried out using the equations for the electric field strength, the fluid velocity and the concentration. Considering isotropic fluid free of surface forces

and magnetic fields, the relations include mass conservation relations and Navier-Stokes equations of fluid flow (equations (12) and (13)), Maxwell's relations for describing electrodynamics (equations (14), (15), (16)), and Ohm's law (equation (17)):

$$\nabla \cdot u = 0 \quad (12)$$

$$\rho(u \cdot \nabla)u = -\nabla P + F_E + \rho g + \mu \cdot \nabla^2 u \quad (13)$$

$$E = -\nabla V \quad (14)$$

$$\nabla \cdot E = \frac{\rho_c}{\epsilon_0} \quad (15)$$

$$\nabla \cdot j = 0 \quad (16)$$

$$j = \rho_c b E + \rho_c u \quad (17)$$

Note that equation (15) is the Poisson's equation (7). The electrically induced force F_E on a non-neutral particle in an isotropic continuum (Eq (13)) can be expressed as (Landau and Lifshitz, 1961):

$$F_E = \rho_c E - \frac{1}{2} \epsilon_0 \left[E \nabla \epsilon - \nabla \left(\rho \frac{\partial \epsilon}{\partial \rho} |E|^2 \right) \right] \quad (18)$$

where ρ_c represents the spatial density of charge (C/m^3), E is the strength of the electric field (V/m), ϵ_0 is dielectric constant, ϵ is the relative dielectric permittivity, and ρ is the air density (kg/m^3).

The first term on the R.H.S. of equation (18) is the Coulomb force exerted by the electric field upon the free charge (i.e. the electrophoretic component), the second term is related to dielectrophoretic force, and the third term, electrostriction force stems from the spatial inhomogeneity of the electric field. These latter two parts represents the polarization forces, which are created when pairs of charges transmit the electric force to the medium. Owsenek et al. (1995) suggested that the 2nd term is negligible in gas media. The 3rd term is effective in modulating the flow field only in presence of a biphasic interface (Nelson and Shaughnessy, 1986). It can be noted that the only electric force to consider in EHD is the spatial charge density ρ_c times the strength of electric field E . Therefore, the current across the electrodes is an outcome of the following co-occurring effects: (1) charge transport due to electric field and (2) charge transport due to advection of charged particles:

$$j = \epsilon_0 b E (\nabla \cdot E) + \rho_c u \quad (19)$$

The quantity $\rho_c u$ is the extent to which the current density is determined by the air moving under the influence of migrating ions. Since in gases electric wind velocity is much less than the ionic velocity (Robinson, 1961), in the partial case of negligible advection equation (19) simplifies to:

$$j = \epsilon_0 b E (\nabla \cdot E) \quad (20)$$

The set of equations (12)–(20) for wire-plate configuration was validated in simulation studies (Ould Ahmedou et al., 2009; Adamiak, 2013). A full theoretical solution of the equations for charge transport in any geometry is not yet available. On solving equation (20), one can obtain the relation between the current and applied voltage. By assuming an appropriate form for E at the discharge electrode, the i-V relationship can be reduced to equation (21) (Robinson, 1961):

$$i = g \epsilon_0 b V (V - V_{in}) \quad (21)$$

where, i (A) is the current, g (1/m) is the geometry factor, b ($\text{m}^2/\text{s V}$) is the ionic mobility, and V_{in} is the inception voltage (V) needed for inducing the discharge. This current-voltage relationship was experimentally verified by Lai and Lai (2002) for the pin-plate electrode. From their dataset it follows that $V_{in} = 5.0$ kV and a decrease in the gap from 2.54 to 1.27 cm is identical to switching the polarity from plus to minus. In either case, j in the discharge increased by 2.27-2.4 times. For a constant area of electrodes, the geometry factor (g) depends on the discharge gap (d). Subsequently, Eq. (21) may be re-expressed as:

$$i = \frac{k_0 \epsilon_0 b}{d} \cdot V(V - V_{in}) \quad (22)$$

where k_0 is the dimensionless coefficient, affected by the electrode curvature. For a pin-plate electrode, the data by Lai and Lai (2002) gives an estimate for $k_0 = 1.2$. Since space charge distribution becomes more uniform at increasing currents, the unipolar current is limited by saturation, reached at $k_0 = 2.0$ (Goldman et al., 1985). The ability of a negative corona to produce higher currents could be explained by higher mobility of negative ions ($b^- = 2.1 \times 10^{-4} \text{ m}^2/\text{Vs}$) as compared to positive ones ($b^+ = 1.43 \times 10^{-4} \text{ m}^2/\text{Vs}$).

It is important to note that equation (22) is valid only for the case of Coulomb force driving charge transfer, ignoring the component of forced air convection. However, the basic assumption of homogeneity of electric field should be carefully checked for different electrode geometries. Inhomogeneous electric field introduces additional dielectrophoretic force, which could play significant role in charge and mass transfer (Panasyuk et al., 1979). Depending on the sign, it could either accelerate or retard charge/mass transfer.

3.3 Mass Transport

Early research studies of EHD phenomenon considered ionic wind as a major reason for mass transport enhancement (Lai and Lai, 2002; Robinson, 1961). A pressure gradient created by electric field E on a unit volume of charged gas could be expressed as electric field force (Robinson, 1961):

$$\nabla p = \rho_c E \quad (23)$$

Furthermore, the equation for conservation of momentum allows estimation of the ionic wind velocity:

$$\frac{\rho u^2}{2} = \int_0^d \rho_c E dz \quad (24)$$

Assuming a uniform electric field in the gap between electrodes, Barthakur and Al-Kanani (1989) proposed the relationship between ionic wind velocity u_e and electric field strength:

$$u_e = E \sqrt{\frac{\epsilon_0}{\rho}} \quad (25)$$

The underlying assumption in equation (25) is that air density ρ is constant, independent of water vapour and electric charge density. However, this assumption requires further experimental verification (Kudra and Martynenko, 2015). A modified version of equation (25) emphasises the major effect of current density j (A/m^2) on the ionic wind velocity (Robinson, 1961):

$$u_e = \sqrt{\frac{jd}{\rho b}} = \sqrt{\frac{id}{\rho b A_p}} \quad (26)$$

with i being the total current (A), A_p , the total area of plate electrode (m^2), d , the gap between the electrodes (m).

Ionic wind velocity is usually in the order of several meters per second, creating aerodynamic effect in the boundary layer at the materials surface. For free surface convection problems it one can find an excellent correlation between electric wind and enhancement of mass/energy transfer (Sadek and Hurwitz, 1972). However, it is important to note that enhancement effect of ionic wind on mass transfer from the free surface gradually diminishes with receding of water-gas interface (Alemrajabi and Lai, 2005; Pogorzelski et al., 2013).

The effect of forced convection in EHD was thoroughly examined by Lai and Lai (2002) and Dalvand et al. (2014). It was concluded that forced convection changed the mechanism of mass transfer. To quantify the interaction between convective velocity fields and ionic wind, the dimensionless EHD number was proposed:

$$N_{EHD} = \frac{u_e}{u} \quad (27)$$

where u is velocity of the convective airflow, (m/s).

It is interesting to note that the effect of ionic wind on mass transfer has been found significant only under stagnant conditions or very low air velocities ($N_{EHD} > 1$). We can explain this suppression effect based on the domination of forced convection over the inertial forces of electric field (Lai and Lai, 2002). Under forced convection ($N_{EHD} < 1$) the mass transport turns out to be independent of the ionic wind, increasing with air velocity due to the direct effect on the boundary layer. One could typically link the convection from the surface, and diffusion to the surface, via the following boundary condition (28).

$$-D\partial c_x + h_m(c - c_\infty) = 0 \quad (28)$$

where D is the mass diffusion (m^2/s), $\Delta c = c - c_\infty$ represents the concentration gradient (the difference in water vapour concentration between the material and ambient air), and h_m is the mass transfer coefficient (m/s). Relative effect of different factors on the convective mass transfer under the same diffusion conditions could be compared by using the dimensionless Sherwood number (Sh). It is expressed as a ratio of total (convective) to diffusive mass transfer across the boundary:

$$Sh = \frac{\text{total mass transfer}}{\text{diffusion}} = \frac{h_m}{D/L} \quad (29)$$

Under conditions of constant diffusion and thickness of the boundary layer L , the Sherwood number is proportional to the mass transfer coefficient. Considering a uniform mass-transfer from a flat surface with area A_p , the mass-transfer coefficient could be determined as:

$$h_m = \frac{\dot{m}}{A_p \Delta c} \quad (30)$$

Via a careful consideration of the numerous research studies published, one can appreciate that forced convection is not complementary to EHD-driven mass transfer for at least two reasons, viz. (i) a reduction of the ionic wind at the surface and (ii) an increase in the overall energy consumption.

The density of the gaseous medium is another significant factor, affecting mass transfer in the presence of electric field (Nur et al., 2014; Liang et al., 2014; Robinson, 1961). We should recall that a decrease in the gas density would accelerate the mass and heat transfer (Robinson, 1961). In order to appreciate this idea, one can mentally visualise a thinning of the boundary layer under a low gas density scenario. The ability of the ionic wind to penetrate boundary layer could be quantified using the Reynolds number (Re):

$$Re = \frac{u_e L}{v} \quad (31)$$

where u_e is the ionic wind velocity (m/s), v is the air kinematic viscosity (m^2/s) and L is the characteristic thickness of the boundary layer (m).

Sherwood and Reynolds numbers have been successfully used in explaining the experimental observations of electrically-induced mass transport (Karami et al., 2012; Kamkari and Alemrajabi, 2010; Sadek and Hurwitz, 1972; Lai and Lai, 2002). Two important conclusions, coming from the research so far are:

1. The effect of ionic wind on the mass transfer, estimated from the linear relationship between Sherwood and EHD number, is suppressed by forced air convection and high air density is extremely low;
2. The direct effect of ionic wind is observed under laminar flow conditions.

These indicate the important role of boundary layers in electrically-induced mass transport. However, the mechanism of this enhancement is still unclear and we encourage further scientific explorations.

3.4 Heat Transport

In a first review by Thornton and Porter (1973), it was noted that electrically-induced changes in heat transport could not be explained by simple changes in fluid viscosity and thermal conductivity. The work of (Kronig and Schwarz, 1949) postulating the superposition of natural and electrically-induced convection allowed quantifying EHD effect on heat transport with dimensionless numbers.

Common approach for study of heat transfer is using the Nusselt number (Nu), which represents the ratio of convective to conductive heat transfer:

$$Nu = \frac{hL}{k} \quad (32)$$

where h is the convective heat transfer coefficient ($\text{W}/(\text{m}^2\text{K})$), L is the characteristic thickness of thermal boundary layer (m) and, k is the gas thermal conductivity ($\text{W}/\text{m.K}$). Similar to Sherwood number, the Nusselt number is proportional to the convective heat transfer coefficient, h .

When performing numerical experiments, one can accommodate the convective heat transfer from the heated plate via a Neumann boundary condition. Furthermore, one can simply estimate the local heat transfer coefficient from the temperature measurements at the surface and bulk of the phase:

$$h = \frac{q_w}{T_w - T_\infty} \quad (33)$$

where q_w is the power of heat source (W/m^2). Our recommendations are based on results of several past research works (Mahmoudi et al., 2011; Ould Ahmedou et al., 2009; Owesenek and Seyed-Yagoobi, 1997; Rashkovan et al., 2002). The interesting approach developed by Rashkovan et al. (2002) deserves a special mention here. They extended the widely used experimental approach to forced convection case via equation (34):

$$\frac{h_{forced}}{h_{free}} = \frac{(T_w - T_\infty)_{free}}{(T_w - T_\infty)_{forced}} \quad (34)$$

The increase in mass transfer coefficient (h) on application of strong electrical fields is an established science (Allen and Karayannist, 1995; Wolny and Kaniuk, 1996a; Mahmoudi et al., 2012). However, what is important is to note that some studies have reported a non-uniform local heat transfer coefficient with a periodic decrease due to the spacing in the multiple electrode configuration (Kasayapanand and Kiatsiriroat, 2005; Go et al., 2008).

By performing a careful analysis of the literature one can enlist two distinctive modes of enhanced heat transfer in EHD. The first mode is direct convective heat transfer enhancement due to ionic wind normal to the surface. Exposure of the surface to electric field, establishes a jet-like drag flow with both hydrodynamic and thermal boundary layers becoming thinner (Mahmoudi et al., 2011). Knowing this modus operandi, one can drive the enhancement even further, by increasing the strength of the applied electric field.

The fact that normal streams of charged particles emitted by multiple electrodes can produce longitudinal vortices has not received sufficient recognition in literature. This second mode of vortex induction depends on the electric field strength and the electrode arrangement (Mahmoudi et al., 2011). Among the two mechanisms, the normal ionic wind effect has been sufficiently investigated; in contrast, vortex induction effect has remained under researched. A poor understanding of the vortex properties could result in sub-optimal design of EHD systems.

As far as heat transfer applications are considered, EHD could be leveraged for modulation of nucleation in processes involving two-phase heat transfer; e.g. boiling and condensation. The mechanisms underlying heat transfer enhancement have been attributed to the local disturbances of the surface boundary layer and decrease in surface tension at the liquid/air interface (Laohalertdecha et al., 2007; Kwak, 2000). Nevertheless, we wish to highlight that the electrically induced enhancement in heat transfer is very sensitive to the geometry of electrode, i.e. gap and spacing between multiple discharge electrodes. Hence, the design of electrode system is critical to achieve uniform and predictable enhancement of two-phase heat transfer.

3.5 Correlations Between Transport Processes

For a long time, the scientific community has analysed transport processes assuming their relative independence. However, in practice this assumption is seldom valid. For example, water and gas diffusivities are strongly concentration dependent and generally increase with temperature. We wish to point at the significant similarity of mass diffusivity D , the thermal diffusivity $\alpha = \frac{k}{\rho c_p}$, and the momentum diffusivity (kinematic viscosity) $\nu = \frac{\mu}{\rho}$, all have the same dimension of L^2/T and occur in similar ways in the equations for energy, mass and momentum transfer. The ratios of diffusivities expressed in the form of dimensionless numbers indicate the relative ease of mass, momentum and energy transport (see appendix 7.5 for definitions of Schmidt, Prandtl, and Lewis numbers).

It is rare that transport processes are completely independent. For example, the coupling between heat and mass transport was discovered about 140 years ago. Accordingly, the effect of heat flux on mass transfer is known as thermodiffusion or ‘Soret effect’, while the effect of mass flux on heat transfer is known as ‘Dufour effect’ with due respect to the pioneers of these phenomena (Rahman and Saghir, 2014). It was Onsager (1949), who proposed to consider reciprocal relationships between forces and fluxes, which gave birth to irreversible thermodynamics. Significant correlations between electrically-induced transport processes require the development of theoretical approach to analysis of coupled phenomena. A number of not yet explained experimental observations, such as temperature discontinuity at the liquid-gas interface (Hashinga et al., 1995), distortion of the liquid surface just under discharge electrode (Wolny and Kaniuk, 1996b), as well as tangential vortices at the surface (Davidson and Shaughnessy, 1986), brought more attention to research of interfacial phenomena.

As opposed to the analysis of transport phenomena, a thermodynamic description of EHD systems would empower an engineer to obtain better insights from an energy conservation perspective. Although thermodynamics of charged interfaces is a mature science, very little has been done in describing EHD interfacial phenomena (Mahmoudi et al., 2012; Barthakur and Al-Kanani, 1989).

4 Pulsed Electric Fields

Application of Pulsed Electric Fields (PEF) is a nonthermal approach to food processing, involving electrical treatments of short time (from several nanoseconds to milliseconds) in the order of 100 V/cm to 80 kV/cm between two electrodes (high voltage and ground electrodes) normally in plate configuration, made of stainless steel, graphite, or titanium, separated by an insulating material (Barba et al., 2015; Puértolas et al., 2016); see Figure 9(b). PEF technology has the potential to be used for several applications due to its ability to induce electroporation phenomenon (cell electrical breakdown) in cells from different origin (e.g. animal, vegetal, yeast etc.), including, microbial inactivation, extraction of valuable compounds (especially vegetable and algae matters), reduction of food contaminants, osmotic dehydration, improvement of freezing and drying processes etc. (Barba et al., 2015; Carbonell-Capella et al., 2016). The electroporation of cell membranes of microbial cells results in cell leakage and loss of viability, thereby imparting the sterilization power to PEF. Details on the electroporation phenomenon will be provided later within this review.

A PEF treatment chamber essentially comprises of a waveform generator which produces electric pulses (typically squared or exponentially decaying) at a suitable voltage (<50 kV) and current (<1 kA), and a reactor holding the product to which the pulses are discharged (see Figure 9(a)). The treatment chamber in turn has a minimum of two electrodes, one of which is attached to the high voltage generator, while the other is grounded, and separated by a dielectric (e.g. PTFE). The difference of potential across the electrode separation results in the electric field, which is a function of the features of the electrical pulses, the configuration of the electrodes, and electrical properties of the product. The PEF chambers could belong to either of two classes; (1) static chambers are usually designed with parallel electrodes, and serve the needs for basic research, while (2) dynamic or continuous flow chambers, allow continuous processing of the product, such that industrial requirements can be met.

The efficacy of a PEF process is dictated by several factors, particularly the field strength, the specific energy delivered to the product, temperature and the total treatment time, besides the properties of the product, such as electrical conductivity (Knoerzer et al., 2012). The voltage, active residence time of the product, and the resistance of the treatment chamber, put together affect the total specific energy. When PEF is used for extraction purposes, there are several factors influencing the recovery yields. Some specific factors include the product size, pH, solvent type and concentration, temperature as well as the intrinsic properties of the matter such as structural arrangement of the cells, membrane characteristics and the electrical conductivity (Vorobiev and Lebovka, 2010; Puértolas et al., 2012). Moreover, the location of confinement within a cell (e.g. cytoplasm or vacuoles) of the molecules of interest, also rule the electro-permeabilization protocol (Soliva-Fortuny et al., 2009).

In order to optimise the number of process parameters that govern the PEF process for any give application, whether microbial inactivation or extraction, one would practically require some simplification and assumptions. Such simplifications would allow applying the physical laws for computer simulations and thus, deduce optimal designs with maximum efficiency. Therefore, we shall now discuss the physical laws governing the PEF processing.

4.1 Transport Phenomena in PEF

The physical processes such as heat, momentum, mass and charge transport are idiosyncratic to each PEF reactor's configuration. Therefore, it is necessary to take into consideration all the important parameters governing the reactor configuration and the physical processes, when attempting to computationally simulate a PEF process. An important parameter deciding the efficacy of PEF is the electric field (V/m) formed due to potential difference between the electrodes. As in the case of barrier discharges and coronas, this can be calculated using the standard Poisson equation (7) for charge conservation; however, some

modifications may be necessary if accounting for the electromagnetic fields is necessary (as with microwave or induction plasma).

$$\mathbf{E} = -\nabla \cdot \mathbf{V} \quad (35)$$

As a matter of fact, during the early years, mathematical models of PEF processes focused exclusively on predicting the uniformity of electric fields in the reactor (Qin et al., 1995). A uniform electric field is important for achieving a uniform treatment. In addition, even temperature distributions are also desired for uniform treatments, which is commonly established by operating in a turbulent regime. The fluid flow can be modelled using the standard Navier-Stokes equation (36) for incompressible Newtonian flow, and the equation (37) for continuity.

$$\rho \left[\underbrace{\frac{\partial \bar{u}}{\partial t} + (\bar{u} \cdot \nabla \bar{u})}_{\text{Inertial term}} \right] = \underbrace{-\nabla p}_{\text{pressure gradient}} + \underbrace{\nabla \cdot ((\mu + \mu_T) \cdot \nabla \bar{u})}_{\text{Viscous term}} + \rho g \quad (36)$$

$$\nabla \cdot \bar{u} = 0 \quad (37)$$

where \bar{u} is the average part of the turbulent flow velocity, p is the pressure and μ_T is the turbulent viscosity. The turbulence can be incorporated via standard $k-\epsilon$ or $k-\omega$ approaches (Joshi and Nandakumar, 2015). However, the standard $k-\epsilon$ closure is more favoured by researchers due to faster numerical convergence and low computer memory requirements. The equations to be solved for the turbulence parameters k and ϵ under the Reynolds Averaged Navier Stokes (RANS) approach are summarised below; equations (38)-(41) (Silva et al., 2015). RANS refers to an approach where the turbulent fluid velocity is approximated to the sum of mean velocity plus the small perturbations, and simplifying it to include a turbulent viscosity term (μ_T). In $k-\epsilon$ model we solve for two additional variables namely, the turbulent kinetic energy, k and the dissipation rate ϵ of this turbulent kinetic energy.

$$\rho \left(\frac{\partial k}{\partial t} + \bar{u} \nabla k \right) = \nabla \cdot \left(\left(\mu + \frac{\mu_T}{\sigma_k} \right) \nabla k \right) + \underbrace{P_k}_{\text{Production term}} - \rho \epsilon \quad (38)$$

$$P_k = \mu_T \left(\nabla \bar{u} : (\nabla \bar{u} + (\nabla \bar{u})^T) - \frac{2}{3} (\nabla \cdot \bar{u})^2 \right) - \frac{2}{3} \rho k \nabla \cdot \bar{u} \quad (39)$$

$$\mu_T = \frac{C_\mu k^2}{\epsilon} \quad (40)$$

$$\rho \left(\frac{\partial \epsilon}{\partial t} + \bar{u} \nabla (\epsilon) \right) = \nabla \cdot \left(\left(\mu + \frac{\mu_T}{\sigma_\epsilon} \right) \nabla \epsilon \right) + C_{\epsilon 1} \frac{\epsilon}{k} P_k - C_{\epsilon 2} \rho \frac{\epsilon^2}{k} \quad (41)$$

The standard $k-\epsilon$ model refers to a certain choice of the constants, σ_k (=1.0), σ_ϵ (=1.3), C_μ (=0.09), $C_{\epsilon 1}$ (=1.44), $C_{\epsilon 2}$ (=1.92) in the equations, which can be obtained from literature (Lauder and Spalding, 1974; Launder and Sharma, 1974). The operation ‘:’ symbolises a double dot product between the tensors; for e.g. $\mathbf{a} : \mathbf{b} = \sum_n \sum_m a_{mn} b_{nm}$. The equations possess the accuracy when the fluid is bounded by walls, as in the case of a PEF reactor. The key aim of solving the $k-\epsilon$ equations (or any other turbulence model) is to compute the value of this turbulent viscosity term, μ_T by applying a wall function (i.e. the $k-\epsilon$ relations, which allows to overcome the requirement of a finely resolved mesh at the boundaries). Unlike $k-\epsilon$ turbulence closure, in $k-\omega$ turbulence model, besides k , the parameter ω , specific kinetic energy dissipation rate is sought after. It is important to note that a Direct Numerical Simulation (DNS) involving the solution of Navier-Stokes solutions with a very fine mesh is another option, provided such computational hardware is available.

The equation governing heat transfer within a PEF reactor can be summarised as the sum of conduction and convection effects-

$$\rho C_p \left(\frac{\partial T}{\partial t} + \bar{u} \nabla T \right) = \underbrace{\varphi \sigma(x, y, z, T) E^2}_{\text{Energy Dissipation}} + \nabla \cdot \underbrace{((k_1 + k_T) \nabla T)}_{k_{eff}} \quad (42)$$

where, σ (S/m) is electrical conductivity, dependent on temperature and spatial location and the term φ accounts for the effective time-averaged potential, estimated as pulse repetition rate (f) times pulse width (ψ) for rectangular pulses. The terms $k_1 + k_T$ represent the effective thermal conductivity, in which k_T , the turbulent thermal conductivity is given by $k_T = C_p \mu_T / Pr_T$ (Pr_T being the turbulent Prandtl number). Note that the energy dissipation term signifies the heating effect of the electric field (by consolidating the pulses through φ).

To this end, the main user selling point of PEF technology has been the retention of food quality for several days while ensuring effective microbial kill, as compared to traditional heat processing methods. The rise in temperature of the fluid food during PEF processing deserves a special mention. To discuss this, it is worthwhile recalling that electric fields are ‘pulsed’ in PEF processing to avoid over heating and the occurrence of electrolysis, but not for ‘biocidal’ reasons. Broader insights into the ‘pulsing’ philosophy were recently highlighted by [Sastry \(2016\)](#). The energy dissipated by the electric pulses into the fluid food, Q (J/kg), partially translates to a rise in thermal energy by virtue of ohmic heating. The dissipated energy, Q , can be approximated from the applied field intensity, electrical conductivity of the food and the product flow rate, given by equation (43) ([Knoerzer et al., 2012](#))-

$$Q = \frac{\psi f}{\dot{m}} \iiint \sigma(x, y, z, T) \cdot E^2 dx dy dz \quad (43)$$

where, \dot{m} is the mass flow rate, f (Hz) is the frequency of the pulse, ψ (μ s) is the pulse width and x , y , z are the spatial coordinates within the treatment chamber.

[Buckow et al. \(2011\)](#), [Buckow et al. \(2010\)](#), and [Knoerzer et al. \(2012\)](#) employed a multi-physics modelling approach to describe the fluid flow coupled with the electric field distribution in a pilot-scale PEF reactor (see figure 10). These models allowed prediction of flow patterns and temperature rise in a model food (salt solution), orange juice and whole milk. With this model approach, they found the simulated PEF energy dissipated into the liquids (4-66 kJ/kg) as well as the process temperatures (25-80 °C), which were in close agreement with those found experimentally in the treatment chamber. The authors concluded the potential of computer simulations as a useful tool to optimize the design of PEF equipment, especially the geometry and dimensions of PEF insulator.

4.2 The Physics of Electroporation

Until now, much of the literature around PEF processing has highlighted the importance of electroporation phenomenon for inactivation of microbiological cells. However, scientists are increasingly exploring electroporation for mass transfer enhancement and improving extraction efficiencies in food and biotechnological industry. We will now steer the discussion towards thermodynamics of the electroporation phenomenon.

The mass transfer enhancement in PEF treated foods is supposedly regulated by the formation of pores at the nanoscale level in the cell membrane (see Figure 11) ([Weaver and Chizmadzhev, 1996](#)). Several research works have focused on image analysis to find direct pore formation after PEF. However, understanding the overall mechanism is far complicated as these pores are formed at a nanometer scale. This poses considerable difficulty when using optical microscopes. One may argue that advanced imaging methods such as electron microscopy can be employed for such studies. However, it is critical to note that

the electroporation process is extremely transient, and electron microscopy involves invasive preparation processes, thereby ruling out their practical usage (Sastry, 2016). Other notable findings in the context of electroporation are the formation of volcano-shaped pores in red blood cells on exposure to an electric field as observed by Chang and Reese (1990), and the formation of pores explained via field induced changes in the dynamic assembly of lipid and protein, as proposed by Spugnini et al. (2007). The most universally accepted theory is that the application of PEF induces the formation of hydrophobic pores spontaneously and randomly mainly due to changes in the phospholipid molecules of the cell membranes. In its present state of the science, it is crucial to point out that the exact mechanism of pore formation at a molecular level is yet to be thoroughly understood (Golberg and Rubinsky, 2013). Comprehensive details on physics of electroporation, beginning from historical milestones, can be found in the recent review by Saulis (2010).

In order to induce the development of hydrophobic pores, it is necessary to overcome the activation energy barrier ($\Delta W_p(r)$) (Equation (44)) for the formation of a single pore of radius (r) which is based on classical surface chemistry (Weaver and Chizmadzhev, 1996).

$$\Delta W_p(r) = 2\gamma\pi r - \pi r^2 \hat{W} \quad (44)$$

where the constant γ is the energy per edge length of the pore and \hat{W} is the energy per area of a flat, pore-free membrane. If the radius (r) of the hydrophobic pore is higher than the critical radius r_t (0.3 to 0.5 nm) (Glaser et al., 1988), it overcomes the energy barrier and turns into a hydrophilic pore. The formation of a hydrophilic pore favours the entrance of water molecules in the intermembrane space, thus creating a nano-hydrophilic environment and the subsequent reorientation of nearby lipids to form more stable structures (Golberg and Rubinsky, 2013).

The electroporation phenomenon (formation of pores) in the cell membrane depends on the local transmembrane potential $\Delta\varphi_m$, as it affects the mobility of small molecules and ions through the cell membrane. It is necessary to take into account that the ions are not able to cross through the small pores because of the high energy barrier (Levine, 2013). In the presence of transmembrane potential $\Delta\varphi_m$ the energy for hydrophilic pore formation can be described by Equation (45) (Weaver and Chizmadzhev, 1996):

$$\Delta W_p(r, U) = 2\gamma\pi r - \pi r^2 \hat{W} - 0.5C_{LW}\pi r^2 U^2 \quad (45)$$

where U is the spatially averaged transmembrane voltage ($\Delta\varphi_m$) and C_{LW} is the change in specific capacitance attributed to the replacement of lipid molecules with water.

For cells with a spherical shape, the application of PEF results in a time varying transmembrane potential ($u_m(t)$), with a rise time τ given by equation (46) (Tsong, 2012)-

$$u_m(t) = \alpha f d_c E \cos \theta \left(1 - e^{-\frac{t}{\tau}}\right) + \Delta u_p \quad (46)$$

Herein, $\alpha=0.75$ is a constant (in general case the value of α is a function of the cell shape; for example, it equals unity when the cell could be approximated to a rectangle). The parameter f is contingent on the electrical and geometrical properties of a cell; d_c is the cellular diameter ($d_c \approx 20 \times 10^{-6}$ – 100×10^{-6} m for plant cells (Kotnik et al., 1998)); θ is the angle in radians between the field lines and a reference point taken on the membrane surface and Δu_p (V) is the physiological potential of the cell.

The rise time (τ) can be assessed using equation (47) proposed by (Kinoshita et al., 2012)-

$$\tau = 0.5d_c f C_m \left(\frac{1}{\sigma_c} + \frac{1}{2\sigma_e}\right) \quad (47)$$

where C_m is the specific membrane capacitance (which approximations vary; c.f. $C_m \approx 3.5\text{-}3.9 \mu\text{F}/\text{cm}^2$ (Lebedeva, 1987), $C_m \approx 0.1\text{-}3 \mu\text{F}/\text{cm}^2$ (Rogov et al., 1981), $C_m \approx 0.95 \mu\text{F}/\text{cm}^2$ (DeBruin and Krassowska, 1999), $C_m \approx 0.2\text{-}0.4 \mu\text{F}/\text{cm}^2$ (Angersbach et al., 1999)), σ_c is the electrical conductivity of the cell (the different estimations give $\sigma_c \approx 0.1\text{-}1 \text{ S/m}$ (Rogov et al., 1981), $\sigma_c \approx 0.5 \text{ S/m}$ (DeBruin and Krassowska, 1999), $\sigma_c \approx 0.05\text{-}0.5 \text{ S/m}$ (Angersbach et al., 1999)).

The value of f can be estimated using the description provided by Kotnik et al. (1998):

$$f = \frac{3\sigma_e(3d_m d_c^2 \sigma_c + (3d_m^2 d_c - d_m^3)(\sigma_m - \sigma_c))}{2d_c^3(\sigma_m + 2\sigma_e)(\sigma_m + 0.5\sigma_c) - 2(d_c - d_m)^3(\sigma_e - \sigma_m)(\sigma_c - \sigma_m)} \quad (48)$$

where σ_e is the electrical conductivity of intracellular compartments ($\approx 10^{-3}\text{-}10^{-4} \text{ S/m}$ (Angersbach et al., 1999)), σ_m is the electrical conductivity of the membrane (again, various approximations exist; c.f. $\sigma_m \approx 10^{-4}\text{-}10^{-6} \text{ S/m}$ (Kotnik et al., 1998), $\sigma_m \approx 10^{-10}\text{-}10^{-6} \text{ S/m}$ (Angersbach et al., 1999)) and d_m is thickness of the membrane ($\approx 5\text{-}10 \text{ nm}$ (Kotnik et al., 1998)). It should be noted that when transmembrane potential increases it can promote the formation of a ‘super-pore’ that can expand uncontrollably, thus eliminating completely cell membrane structure (Weaver and Chizmadzhev, 1996).

4.3 PEF Assisted Extraction of Intracellular Compounds

Several empirical equations have been proposed to describe the solid–liquid extraction of intracellular compounds (IC) after applying PEF. The most commonly used equation for describing the extraction yields post-PEF treatments is a first-order rate equation; c.f. Vorobiev and Lebovka (2006), and Spigno et al. (2007)-

$$\text{IC}_t^{\text{EY}} = \text{IC}_{\max}^{\text{EY}}(1 - e^{-kt}) \quad (49)$$

where IC_t^{EY} is the extraction yield of intracellular compounds at time t ; $\text{IC}_{\max}^{\text{EY}}$ is the intracellular compound extraction yield at equilibrium ($t = \infty$); and k is the rate constant that differs according to the extraction parameters. It may be recalled that the variable k is a function of the diffusion coefficient of the extracted compounds, the total surface area, the volume of solvent and the size and geometry of solid particles. The first order equation has been successfully employed for describing the extraction of polyphenols from Borago leaves (Segovia et al., 2015), and betanin from red beet (Luengo et al., 2016). Besides the first-order equation, a stretched exponential empirical model has also been shown to fit the PEF assisted extraction data (see appendix 7.6). Note that the conventional approaches (zero and first order kinetics) are usually based on steady state assumption, and therefore, cannot completely explain the PEF assisted time-varying extraction yields of intracellular compounds from different food sources. Notably, a multiscale physics based model coupling the electroporation phenomenon with the classical models of diffusion process is absent in literature.

4.4 Radical Formation

Some previous studies have mentioned about the potential ability of PEF to induce water molecule polarization, thus facilitating its dissociation into ions at high field strength (Boussetta et al., 2014) with the subsequent potential formation of free radicals. Although the potential of PEF to form radical species is a fact, there is a lack of studies in the available literature evaluating this phenomenon. For instance, some studies have evaluated the formation of free radicals after PEF treatment by using electron spin resonance (ESR) spectroscopy (Zhao et al., 2011; Zhang et al., 2011b). In one of these works, it was found that electric field strength had a significant effect on the concentration of H_2O_2 . These authors found the appearance of trace concentrations of H_2O_2 (0.177×10^{-6} and $2.035 \times 10^{-6} \text{ mol/L}$, respectively) after

applying PEF at 30 kV/cm and 35 kV/cm, respectively, thus indicating the ability of PEF to induce radical formation.

The effects of PEF on the oxidation of oleic acid and subsequent formation of secondary radicals have been evaluated by [Zhao et al. \(2011\)](#). The authors found an increase in the peroxide value of the oleic acid induced by PEF, although the extent of increase was clearly influenced according to the electric field strength and also by storage time. Additionally, the presence of hydrogen radicals in PEF-treated oleic acid was observed via ESR, thus concluding the potential role of PEF as an initiator of free-radical reaction.

The generation of reactive species (radicals) after applying PEF can be seen in a positive or negative way depending on the application that we intend to give to this technology. For instance, apart from cell electroporation phenomena, the inactivation of micro-organisms in food systems is attributed to the formation of highly reactive free radicals from chemical species when PEF is applied ([Sitzmann, 1995](#)). On the other hand, PEF can modify antioxidant compounds and their antioxidant properties due to radical formation.

For example, the formation of free radicals ($\cdot\text{OH}$) after PEF has been associated with the conversion of vitamin C isomer from enol-form to keto-form ([Zhang et al., 2015c](#)). These authors confirmed the possible mechanism by determining fluorescence intensity, which was increased after PEF treatment, thus indicating the conversion of vitamin C isomer induced by hydroxyl radicals. On a related note, other previous studies have also demonstrated the conversion of vitamin C isomer from enol-form to keto-form at basic conditions (pH 9.3–9.5) induced by hydroxyl ion ($\cdot\text{OH}$) ([Wu et al., 2003](#)). It should be noted that although vitamin C structure could modify after PEF treatments, this technology does not appear to significantly decrease its content and could be a useful tool to slow down the oxidation process. On the other hand, PEF radicals could induce the degradation of some polyphenols (eg. anthocyanin). [Zhang et al. \(2008\)](#) evaluated the effects of PEF (1.2–3.0 kV/cm) on purified cyanindin-3-glucoside from red raspberry and demonstrated the formation of chalcone after the treatment, which is considered the first step for degradation of anthocyanins together with opening of the pyrilium ring ([Hrazdina, 1971](#)). A possible explanation for this fact could be an increase in the concentration of H_2O_2 or hydroxyl radical, which was shown to enhance the anthocyanin degradation of litchi fruit ([Ruenroengklin et al., 2009](#)).

Previous studies have also investigated the influence of PEF treatments on the structure of amino acids, proteins and polysaccharides, mainly related to the weak bonds such as hydrogen bonds, disulfide bonds and hydrophobic bonds ([Perez and Pilosof, 2004; Han et al., 2012; Sui et al., 2011](#)), which can be partially explained by H_2O_2 or free radical formation after PEF; however, further research dealing with this topic is needed for a complete understanding of the observations.

5 Ultrasound Processing

Ultrasound (US) is predominantly a non-conventional food processing technology with vast majority of applications under exploration confined to high power, low frequency ultrasound energy. There have been several explorations for assessing the benefits of power ultrasound applications in food processing. A summary of these applications is provided in figure 12. These applications have been reviewed time and again by many authors ([Chemat et al., 2011; Awad et al., 2012; Deora et al., 2013; Kentish and Feng, 2014; Tao and Sun, 2015; Ashokkumar, 2015; Musielak et al., 2016; Chemat et al., 2017](#)). We will therefore, refrain from reviewing these applications.

5.1 Principles and applications of ultrasound to food systems

The applications of US to food systems are based on certain physical and chemical effects associated with sound fields. The major physical effects that occur during US applications to liquid media are ‘cavitation’

and ‘streaming’ (Leighton, 2007), which promote localised momentum transfer. As a consequence of these localised dynamics, heat and mass transfer enhancements at a macroscopic scale can be realised. These phenomena are of great importance in food processing. Ultrasound assisted extraction is example of an intensified process, wherein the high shear forces generated by sonic waves promote extraction by enhancing mass transfer (Chemat et al., 2017). In this case, two major effects are promoted by cavitation phenomena: implosion of cavitation bubbles generating macro-turbulence with a fast moving stream of liquid through the cavity, and inter-particle collisions, which all act in the way of accelerating diffusion. In addition, there is erosion and surface peeling caused by microstreaming as well as particle breakdown.

When ultrasound is applied to liquids, even minor amounts of gas bubbles present in the media have the potential to grow into cavities under the influence of negative cycles of sonic fields. These cavities tend to undergo nonlinear oscillations under the influence of the waves, which could be either stable or transient as decided by their lifetime. While the stable cavitation bubbles hover around their mean radius between sonic cycles, the transient ones explode in a single cycle, releasing a large quantity of localised energy. When the ultrasound frequency is very high, the time scales available for the growth of cavities are very small, such that they seldom reach their collapse phase (Vaidya et al., 2016). This is the reason, as to why low frequency ultrasound is preferred over high frequency for applications involving modulation of transport phenomena and/or requiring localised high pressure-temperature conditions, such as those typical to most food processing operations stated earlier. That said, for some scenarios, the transient cavitation must be avoided; e.g. for accelerating the demixing of phases containing sensitive molecules and polymers intended for reuse, mostly encountered in biotechnological applications (Trujillo et al., 2014; Raghavarao et al., 2002; Srinivas et al., 2000). Note that the counter-process of demixing is emulsification. The ultrasound induced cavitation, and the resulting hydrodynamic effects have long been employed for effective emulsification of immiscible phases in food processing. Emulsification via sonication is commonly illustrated as a two step process involving an initial droplet formation that can be visualised as a Rayleigh-Taylor instability mechanism and a break up process. The initial phase of droplet creation is governed by the ratio of the densities and viscosities of the immiscible liquids. An often ignored fact is that emulsification by ultrasound occurs only in the presence of dissolved gas such as air, N₂, O₂, H₂ or Ar (or any other inert gas) and at a certain value of an external pressure.

The heating effect in liquids subjected to ultrasound is a direct consequence of the dissipation of mechanical energy into the medium. Note that the acoustic streaming phenomenon results from the acoustic radiation force, and it becomes more pronounced when the applied power increases. Furthermore, the acoustic radiation force is a function of the compressibility and density of the matrix through which the sound waves propagate.

Yet another phenomenon associated with ultrasound is the ‘sponge effect’, which essentially describes the alternative compressions and expansions that are generated by the waves propagating in the medium (Miano et al., 2016). The sponge effect has been exploited for decreasing the overall drying times of foods, where US has been speculated to cause the diffusion of the liquid from inner part of the food matrix to the surface in response to the compressions and rarefactions. The contributions of these mechanical effects is spectacular considering that some of the forces involved are higher than the surface tension, thus driving the movement of water molecules inside the material’s capillaries. Due to these changes, microscopic channels are often formed, promoting the exchange of matter across the phases. These effects are very important in food engineering applications governed by the transport phenomena, as they help to bring down the external and internal resistances to transport (Tao et al., 2016; scar Rodrguez et al., 2014).

There are also chemical effects of ultrasound in aqueous phase, and these are studied under the broad field of ‘sonochemistry’. The most notable chemical effect of ultrasound is its ability to form radicals under suitable conditions. The chemical effects due to sonication are attributed to the indirect impact of cavitation phenomena. When cavitation occurs, microbubbles are formed in liquid media. During cavitation very high localised temperature is reached, which can produce significant changes

in the chemical composition. In addition, there also occurs generation of radical species and chemical components from gas molecules, such as singlet oxygen, and therefore, an overall increase in the reactivity of the system. Cavitation bubbles are short lived and eventually collapse resulting in chemical effects within the bulk medium, besides the physical effects. Acoustic factors, viz. frequency and intensity of the ultrasonic wave dictate the cavitation intensity and associated effects. With an increase in frequency there is a decrease in rarefaction phase, thus requiring more power, so that the equivalent amount of cavitation in a system can be achieved (Mason and Peters, 2002). External factors such as dissolved gases or small gas bubbles in the liquid may act as nuclei for cavitation, and therefore reduce cavitation threshold.

The cavitation phenomenon and the chemical effects of ultrasound (more details to follow in section 5.4) are also responsible for the inactivation of a range of micro-organisms in liquid media and liquid foods. Several studies have shown the ability of ultrasound to inactivate spoilage and pathogenic microorganisms (Mohammadi et al., 2014; Khanal et al., 2014; Khandpur and Gogate, 2016). Microbial inactivation by ultrasound induced cavitation is attributed to the free radicals and shock waves that are produced (Gao et al., 2014). Bactericidal effects involving cell membranes has generally been attributed either to pore formation or mechanical disruption of the cell wall or membrane (Rokhina et al., 2009). The use of sonication produces mechanical forces which result in the breaking and shearing of the cell walls in micro-organisms. The localized hotspots and free radicals within the bulk medium produced by ultrasound induce some thinning of cell wall membranes (Kim et al., 2014; Joyce et al., 2011). Electron microscopic analysis has shown that sonication inflicts both internal and external damage on *Escherichia coli*, *Saccharomyces cerevisiae* and *Lactobacillus acidophilus* (Cameron et al., 2009, 2008). Most benefits of microbial inactivation are seen with combined treatments such as thermosonication, manosonication or use of UV irradiation which couple heat, pressure and light with sonication during treatment processes Chemat et al. (2011). High intensity, low frequency (10-1000 W/cm² or 20-100 kHz) ultrasound is most often quoted as being able to generate sufficient acoustic cavitation to be of benefit in food processes. In addition, ultrasound is known to cause changes to the ultra-structures within cells, inactivate enzymes, and cause bacterial cell acidification, thereby decreasing functional stability of the cells (see figure 13).

5.2 Thermodynamics in ultrasound processing

At their heart, US systems transform electrical power into vibrational/mechanical energy, which in practical applications is transferred into a sonicated media. During ultrasonication, the distribution of the energy is asymmetric, with some amount lost through direct conversion into heat, while a larger proportion utilized to promote cavitation. During US processing, a fraction of the cavitation energy is responsible for inducing chemical, physical, or biological effects, while the remaining fraction is reflected, and involved in sound re-emission (harmonics and sub-harmonics).

When applying US to foods, it is necessary to take into account the amount of energy that is reflected back to the transducer. If not accounted for, such energy loss would result in loss of accuracy in measurement of output power. For liquid samples, almost all mechanical energy generates heat. When ultrasonic power is increased, the ultrasonic yield increases. Near the cavitation power threshold, the yield is mostly increased and afterwards it remains nearly constant (Legay et al., 2012).

Another factor that should be taken into consideration is the energy necessary to transfer mechanical forces at specific vibration amplitudes, which is reflected by power (P) measured in watts (W). The power transfer labelled for any ultrasonic transducer is usually higher the power that actually is transmitted into a food matrix during any practical application. This is a direct consequence of the power losses encountered. Therefore, for most practical applications and also for research studies, the actual power transmitted into a system should be calculated using the widely accepted calorimetric method, as follows. Ultrasound should be applied to the medium and the increase in temperature over time should be recorded (heating cycle). Subsequently, the transducer should be switched off and the rate of cooling resulting from

convective heat losses across the walls of reactor should be noted. The power can then be calculated from the resulting graph (see figure 14) by applying equation (50)-

$$P = mC_p \left[\left(\frac{\partial T}{\partial t} \right)_{heating} - \left(\frac{\partial T}{\partial t} \right)_{cooling} \right] \quad (50)$$

where, m , C_p , t , T correspond to the mass of the sample, the specific heat capacity of medium (kJ/kg/K), time (s), and temperature (K), respectively. Note that the frequency of ultrasound, the viscosity of the medium, and the medium's relaxation time dictate the absorption of ultrasound, and therefore the extent of heating. Other factors could also include thermal conduction and molecular effects.

The US energy and intensity are two other important parameters for practical applications. US energy is typically expressed as the energy input (W) per volume (L) of the processed material (W/L), while US intensity measures the energy available per unit volume of liquid. The ultrasound energy input can be calculated from the product of power and time of exposure. The treatment time in turn is directly related to the flow rate through the acoustic device. A generic qualitative relationship between flow rate and energy for several applications of ultrasound of importance to food and bio-processing was given by [Patist and Bates \(2008\)](#), as shown in figure 15.

There is a direct relationship between ultrasound intensity and amplitude given by equation (51)-

$$I_{us} = \frac{P}{A_{tr}} \quad (51)$$

where, I_{us} is the ultrasonic intensity (power output per surface area of the sonotrode, W/m²) and A_{tr} is the surface area of the transducer (m²). Density (ρ), bulk modulus (B), the specific acoustic impedance ($Z = \rho c$) and the attenuation, are other useful parameters to characterize the acoustic behaviour of a simple homogeneous liquid. The speed of sound in a given matrix can be estimated from the following equation-

$$c = \sqrt{\frac{B}{\rho}} \quad (52)$$

Note that equation (52) is basis for many non-destructive testing applications of high frequency, low power ultrasound as applied to food systems.

For design of efficient ultrasonic reactors, it is desirable to obtain a good approximation of the cavitation intensities represented by the peak temperature and pressure reached at the collapse of micro-bubbles. Until a decade ago, a simplification in bubble dynamics simulations was introduced by assuming uniform pressure and temperature inside the bubble. This is referred to as 'polytropic approximation', which results in simpler equations for pressure and temperature of gas inside the bubble, which can then directly be linked to the bubble radius. However, this approximation was realized to have serious drawbacks such as a bad representation of the thermal behaviour and inability to capture spatial non-uniformity of bubble temperature. These are important for many sonochemical applications, where well controlled thermal or reaction conditions are highly desired.

5.3 Transport Phenomena in ultrasound processing

While thermodynamic considerations in isolation, help us to get a picture of the overall energy change, they do not allow us to obtain the rate of transport. Therefore, the rates of changes also need consideration for a detailed understanding of the ultrasound processes. Unlike the incompressible Navier-Stokes equations describing the momentum transport for the technologies described so far, the propagation of ultrasonic

waves in a liquid medium should be described by compressible Navier-Stokes equation, given by equation (53) (assuming isothermal conditions) (Brenner et al., 2002)-

$$\rho(\partial_t u + u \cdot \nabla u) = -\nabla p + \mu \nabla^2 u + \zeta \nabla \nabla \cdot u \quad (53)$$

$$\partial_t \rho + \nabla \cdot (\rho u) = 0 \quad (54)$$

where u is the fluid velocity, ρ the density, p the pressure, μ the shear viscosity, and ζ the bulk viscosity of the liquid. In equation (53) the term on LHS corresponds to the inertial forces. The first term on RHS corresponds to pressure forces, and the remaining terms correspond to viscous forces. Note that equation (54) is the corresponding continuity equation. Using this formulation and coupling with an analysis of the pressure inside a cavitating bubble, the equations for mass, momentum and energy conservation for a single bubble were deduced by Kim et al. (2007) as follows (in the respective order)-

$$u_g(r, t) = \frac{1}{\gamma P_g} \left[(\gamma - 1) k_g \partial T_{br} - \frac{1}{3} r \frac{dP_g}{dt} \right] \quad (55)$$

$$\frac{dP_b}{dt} = \frac{3}{R_b} \left[(\gamma - 1) k_g (\partial T_{br})_{r=R_b} - \gamma P_b U_b \right] \quad (56)$$

$$\frac{\gamma}{\gamma - 1} \frac{P_b}{T_b} (\partial T_{bt} + u_g \partial T_{br}) - \frac{dP_b}{dt} = \frac{1}{r^2} \partial (r^2 k_g \partial T_{br})_r \quad (57)$$

where, u_g is the gas velocity, P_g is the pressure in the gas assumed to be spatially uniform, P_b is pressure inside bubble, γ is specific heat ratio of the gas in bubble, k_g the thermal conductivity of the gas, T_b the temperature inside the gas bubble, r the radius from the bubble centre, R_b , radius of the bubble, and U_b is the bubble wall velocity. The simultaneous solutions to equations (55)-(57) will yield the gas velocity and temperature profiles inside the bubble.

Note that insights into the dynamics of a single cavitation bubble becomes relatively less important when the role of ultrasound induced hydrodynamics in an ultrasound reactor also dominates the overall outcome of the process; e.g. ultrasonic emulsification. Therefore, for hydrodynamics at scales of a ultrasonic reactor, the propagation of acoustic waves are studied by solving the Helmholtz wave equation (Ajmal et al., 2016)-

$$\nabla \left(\frac{1}{\rho} \nabla p \right) - \frac{\omega^2}{\rho c^2} \cdot p = 0 \quad (58)$$

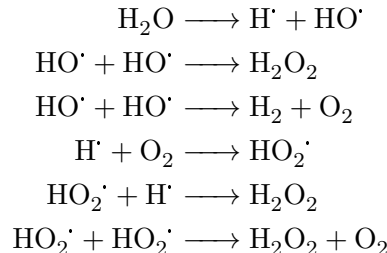
where ρ is the density of the medium [kg/m³], p is the acoustic pressure [Pa], c is the speed of sound in the medium [m/s], $\omega = 2\pi f$ is the angular frequency [rad/s], and f is the frequency [Hz]. The acoustic pressure, p can be approximated by a cosine function $p = p_a \cos(\omega t)$ with p_a being the maximum acoustic pressure and t , the time (s). For experimental determination of acoustic pressure in a ultrasound reactor, one can install a hydrophone capable of sampling acoustic signals at a sufficiently high frequency, together with an oscilloscope (Wei and Weavers, 2016).

5.4 Radical chemistry in ultrasound processing

It is well known that during sonication, radicals are produced via a cascade effect of the cavitation induced changes in the medium through which sound passes. Therefore, a slightly deeper dive into the changes during cavitation is worthwhile at this point. The mechanical and chemical effects of the collapsing

cavitation bubble are believed to occur in distinct stages (Luo et al., 2014), which we shall briefly outline here. At the very beginning (few microseconds) of the collapse (implosion) of the cavitation bubble, the motion of bubble walls reaches the speed of sound. The presence of gas in the bubble results in a moving bubble wall, thereby resulting in propagation of shock waves. Consequently, adiabatic heating is triggered, resulting in an increase in the temperature. The temperature within a short-lived cavity reaches several thousand kelvin (5000-10,000 K) and so does the local pressure, shooting up to 50 MPa (Merouani et al., 2014). Note that these conditions are just sufficient for ionisation, causing production of short-lived radicals within the cavity. In fact, with a careful consideration, one will be convinced that these conditions in the bubble are sufficient for the development of a nano/micro-scale plasma. Indeed, this cavitation induced plasma contributes toward light emission (called ‘sonoluminescence’) and this has been experimentally verified (Flannigan and Suslick, 2005). Thus, it becomes clear that ultrasound field in liquids can yield short-lifetime reactive radicals such as H[•] and HO[•] at the moment of bubble collapse.

As radicals are expelled from the collapsing bubble (owing to the micro-scale fluid dynamics) they also undergo chemical reactions with less volatile species found within the bulk medium itself. In the case of aqueous systems the formation of radicals occurs through aqueous vapour entering the ultrasonically induced cavitation bubbles within the bulk medium. As a result of the high temperatures and pressures found within cavitation bubbles radicals are formed via the homologous fission of water molecules. The extent of radical production in an aqueous phase is a function of frequency of applied ultrasound. Primary radicals formed may then induce secondary reactions, convert to other radicals, initiate a radical chain, or react with other substrates present in the medium. The key reactions responsible for sonolysis of water and radical formation are summarized below (Merouani et al., 2014)-



Note that in these reactions, radical species such as H[•], O[•], OH[•] and HO₂[•] are formed through bond dissociation. In water the cleavage of the H-O bond to form H and HO[•] radicals has a bond dissociation energy requirement of 460 kJ/mol. In the case of the hydrogen peroxide the bond energy requirement to form OH radicals from HO-OH dissociation has a far lower energy requirement than water dissociation, namely 180 kJ/mol. Therefore, the existence of OH radicals from the dissociation of water, and also subsequent dissociation of hydrogen peroxide, would be the most likely source of oxidative species with hydrogen peroxide easily contributing to their formation. The formation of O radicals, from either the dissociation of water or from O₂ itself, has the highest energy requirement namely 497 kJ/mol and so would be a less likely. Therefore, under ultrasonic conditions within aqueous media it would be expected that HO[•] radicals would be preferentially formed. By correlating the production of OH radicals to the temperature and pressure achieved in the bubble, Merouani et al. (2014) have also concluded that OH radical is the main oxidant developed in an O₂ bubble. Further details regarding some important research developments concerned with hydroxyl radical production in ultrasound field is provided in Appendix 7.7.

In the context of food science research, very little work has been undertaken for the identification and analysis of the actual free radicals produced by sonication during the processing of various food materials. Much literature states ‘free radical effect’, ‘deactivation by free radicals’ and so on, but there is clearly no ironclad evidence or clear mechanistic insight for the involvement or identification of the radicals. However, most references suggest a strong role of hydroxyl radical species responsible for the

observed food chemistry. Next, we will provide some examples to emphasise the role of radicals formed during sonication on food quality. Very little work in this area has been undertaken since the very early paper by Vercet et al. (1998) where it was investigated the application of manothermosonation (MTS), a combined treatment of elevate temperature and US (20 kHz frequency, moderate pressure). Vercet et al. (1998) suggested that one of the inactivation mechanisms by MTS on enzymes was the interaction between free radicals (produced by water sonolysis) and amino acid residues. Zhang et al. (2015b) provided a direct experimental evidence for the formation of 1-hydroxylethyl radicals when sonicating red wine. Their analysis was performed using electron paramagnetic resonance spin trapping with DMPO, wherein free HO[·] and 1-hydroxylethyl free radicals were detected in DMPO aqueous solution ultrasound-processed red wine, respectively. Note that the latter is produced upon oxidation of ethanol via the HO[·] generated from sonication of aqueous phase. Karaseva et al. (2009) studied the inactivation of *Aspergillus niger* glucose oxidase using 27 kHz sonication at a range of pHs and temperatures in the presence of HO[·] radical acceptors. Their work confirmed that free radicals play an important part in the enzyme inactivation process and that the use of mannitol reduces deactivation of the enzyme and could be used as a preventative measure by the food industry.

6 Final Remarks

Application of strong external fields for driving food processes has remained a major research area in food and allied biosciences. Typical examples of externally applied fields include electromagnetic fields, pressure fields, acoustic fields etc. Sound field by itself is a form of pressure field, developed from electromagnetic fields applied to transducers. In this review we discussed the fundamentals and typical traits of some emerging electromagnetic field based applications for foods, e.g. cold plasma, electrohydrodynamic (EHD) processing, and pulsed electric fields. We also discussed the applications of ultrasonic fields. In all the cases, we noted that the addition of these external fields served the purpose of enhancing the process either in terms of improving the food safety and quality, or by promoting the transport phenomena. For example, in EHD, an ionic air stream is employed to considerably alter the boundary layer, and intensify the convective heat transfer between the moisture carrying medium and the drying product for low primary airflow velocities. Similarly, pulsed electric field and ultrasound also promote extraction from solid food matrices, promote drying of foods etc. In addition, PEF, ultrasound, and cold plasma are also important as these fields result in direct or indirect physical and chemical effects resulting in inactivation of pathogenic micro-organisms and spoilage causing enzymes.

In general, the mode of action of the discussed technologies overlap to distinct degrees. For example, in many studies it has been either confirmed or hypothesised that hydroxyl radicals or hydrogen peroxide form in the aqueous phase with PEF, US and cold plasma, which cause the observed effects. The considerable complexity of the physics and chemistry of these processes underlines the fact that a complete understanding of the fundamental interactions between the external fields and food components will remain elusive until next few years. The on-going efforts to develop new diagnostic methods capable of explaining the physical and chemical interactions between the fields and food materials is sure to drive forward the science; technological developments shall then follow. The concepts and thoughts shared within this review are expected to provide a holistic introduction to new researchers involved in developing innovative processes for food applications based on these technologies.

7 Appendices

7.1 Quasineutrality of plasma

By definition, a plasma has approximately an equal number of positive (q) and negative charges (e), such that the sum of charge over the entire plasma is nearly equal to zero (i.e. $qn_i \approx en_e$, where n is the number density), a property which is referred to as *quasineutrality*.

7.2 Knudsen Number

The average distance that a particle will travel before it collides with another particle (molecule or ion or electron) is called the mean free path. The non-dimensional *Knudsen Number* (K_n) is defined as $K_n = \lambda/l$, with λ being the mean free path of the electrons and l , the characteristic length scale. Thus, for the validity of the continuum model, the mean free path of the electrons should be much smaller than the characteristic length scale of the gas plasma reactor ($K_n \ll 1$).

The mean free path for a homogeneous, single-species, neutral ideal gas is given by the equation (59),

$$\lambda = \frac{1}{n_g \sigma} \quad (59)$$

where n_g is the neutral gas density and σ is the cross-section for a momentum-exchange collision. A cross section (σ) represents an effective surface area of interaction between colliding partners.

In the context of most atmospheric pressure dielectric barrier discharge plasma the continuity is a valid assumption, for such plasmas are weakly ionised with near ambient temperatures and the mean free path is about 0.1 μm, which is much smaller than typical reactor dimensions.

7.3 Gas heating in plasma

The thermal energy equation for the gas is given by

$$\rho C_p \frac{\partial T(x, y, z, t)}{\partial t} + \underbrace{\rho C_p (u \cdot \nabla T(x, y, z, t))}_{\text{only in gas domain}} = \nabla \cdot (k \nabla T(x, y, z, t)) + \underbrace{Q_p}_{\text{From plasma}} \quad (60)$$

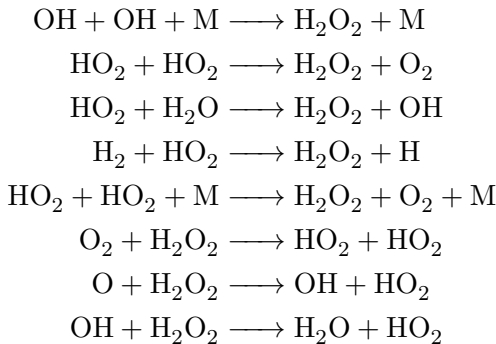
where, ρ is the gas density, C_p is the heat capacity, T the temperature, k the thermal conductivity, u the fluid velocity, and Q_p is heat from plasma, which is given by-

$$Q_p = \sum_s q_s \Phi_s(x, y, z, t) \cdot E + \sum_j \Delta \varepsilon_j R_j + 3 \frac{m_s}{M_g} K_{el} k_b (T_e - T_g) \quad (61)$$

Here, the heat liberated for reaction j is given by $\Delta \varepsilon_j$, R_j the rate for inelastic collision losses, K_{el} the rate for elastic collision losses, T_g the gas temperature, while the thermodynamic parameters are obtained from literature. The convective temperature gradient term in equation (60) is valid only in the gas, and will not be valid in the solid dielectric region in a barrier discharge or jet. Prediction of the global gas temperature via computer simulation could be useful in scenarios where it is challenging to measure the temperature.

7.4 Reactions leading to formation of hydrogen peroxide

A partial list of reactions leading to the formation of hydrogen peroxide in atmospheric plasma are summarised as follows-



7.5 Dimensionless Numbers of Transport Processes

Schmidt number (Sc) reflects the coupling of momentum and mass transport:

$$Sc = \frac{\nu}{D} \quad (62)$$

Prandtl number (Pr): reflects the coupling of momentum and heat transport:

$$Pr = \frac{\nu}{\alpha} = \frac{c_v \mu}{k} \quad (63)$$

Lewis number (Le) reflects the coupling of mass and heat transport:

$$Le = \frac{\alpha}{D} = \frac{k}{\rho c_p D} \quad (64)$$

7.6 The Stretched Exponential Model

The stretched exponential function (equation 65) has been employed to explain the yields of polyphenols and proteins from mango and papaya peels assisted by PEF, observing that the extraction behaviour of these compounds may be fitted well using this approach.

$$C = C_{max} \left[1 - \exp \left(-\frac{t}{\tau} \right)^\beta \right] \quad (65)$$

where C is the concentration (of protein or phenolics), C_{max} is the maximal value of C at long time of extraction, t is time of extraction and τ is a parameter of the model.

The stretching parameter β characterizes the broadness of the distribution of the extraction times. The case $\beta=1$ corresponds to the single extraction time and larger the deviation of β from 1 is, the broader the distribution of the extraction times ([Gradshteyn and Ryzhik, 1979](#)). The mean extraction time $\langle \tau \rangle$ is calculated as

$$\langle \tau \rangle = (\tau \beta^{-1}) \Gamma(\beta^{-1}) \quad (66)$$

where Γ is the Euler gamma function. The stretching parameter, β and the mean relaxation time, $\langle \tau \rangle$ tend to vary according to the food matrix ([Parniakov et al., 2015](#)).

7.7 Radical production during ultrasound application

Radical production in water is dependent upon frequency of sonication and many studies have been undertaken identifying which frequency produces the highest levels of radicals and hence greatest oxidative effects. For many years' studies revolved around the common frequency of 20 kHz; c.f. Yusof et al. (2016), Henglein (1995). However, more recently, with the expansion of more readily available equipment and a range of alternate frequencies, a wider range of ultrasonic frequencies have been studied: 359 kHz (Ouerhani et al., 2015), 204-362 kHz (Pfleiger et al., 2015), 382 kHz, 584 kHz, 862 kHz, 998 kHz (Milne et al., 2013), 515 kHz (Price, 2010). The consensus appears that higher frequencies produce higher levels of radicals as determined by various methods of detection, namely via the use of hydroxyterephthalic acid (Barreto et al., 1994), potassium iodide (Kimura, 1996) and luminol (Maddox et al., 1998), salicylic acid (Milne et al., 2013) dosimeters as examples. This can be attributed to the shorter rarefaction and compression cycles experienced at these higher frequencies resulting in cavitation collapse occurring at far shorter bubble life spans, thus releasing more radicals into the bulk medium. However, this may not always be true, as can be seen in figure 16.

The production of hydrogen peroxide and hydroxyl radicals clearly depends on the ultrasonic frequency employed. Pétrier and Francony (1997) reported that 200 kHz gave a high yield of 0.6 mM of hydrogen peroxide after 2 hours sonication which exceeded the levels obtained when using other frequencies namely 20, 500 or 850 kHz 28. Milne et al. (2013) examined OH radical formation at ultrasonic frequencies of 20 kHz, 382 kHz, 584 kHz, 862 kHz and 998 kHz utilising the salicylic acid dosimeter. They determined at similar ultrasonic powers (W) 862 kHz is around 10% more efficient at generating hydroxyl radicals than 382 kHz however these are still much more effective than the other frequencies. Comeskey et al. (2012) also employed a range of ultrasonic frequencies to determine levels of hydrogen peroxide formed in sonicated aqueous systems. Employing the decolourisation of several dyes using a range of ultrasonic frequencies namely 20, 40, 380, 512, 850, 1,000 and 1,176 kHz they found the highest amounts of H_2O_2 as well as the greatest effect on decolourisation at 850 kHz with 380 and 512 kHz also exhibiting some oxidative effects however not to the same extent.

Anbar and Pecht (1964) originally investigated the formation of hydrogen peroxide using labelled water H_2O^{18} in the presence of hydrogen peroxide $\text{H}_2\text{O}_2^{16,16}$ in a solvent saturated either with argon or with labelled molecular oxygen $\text{O}_2^{18,18}$ (Anbar and Pecht, 1964). Under an argon atmosphere the formation of pure $\text{H}_2\text{O}_2^{18,18}$ supported the splitting of water. However, experiments conducted with H_2O^{18} saturated with $\text{O}_2^{16,16}$, or water H_2O^{16} saturated with $\text{O}_2^{18,18}$ led to the formation of both to $\text{H}_2\text{O}_2^{18,18}$ and $\text{H}_2\text{O}_2^{16,18}$. Therefore, in a medium saturated with O_2 three possible sources of H_2O_2 can be found: (i) water, (ii) molecular oxygen and (iii) oxygen atoms. Fischer et al. (1986) took this further by taking into account the stability of intermediates in various cavitation bubble zones. They suggested that the formation of H_2O_2 occurred in the low temperature interfacial zone between bubble and bulk solution mainly through the recombination of hydroxyl radicals. However, the reaction between atomic oxygen and H_2O occurs mainly in the high temperature zone inside the bubble and should produce only HO^\cdot .

Makino et al. (1983) confirmed the production of radicals in an aqueous medium by using ESR when they observed the stable spin adducts HO-DMPO and H-DMPO obtained from DMPO (5,5-dimethyl-1-pyrroline N-oxide) in sonicated water saturated with argon. Moreover, the formation of HO^\cdot in sonicated (20-60 kHz) water was also established by observing the formation of hydroxyterephthalate ions when terephthalic acid (TA) reacts with HO^\cdot Mason et al. (1994). The authors found the highest response radical formation at 60 kHz and they found a direct relationship between power input and TA concentration. The same method was used to compare the formation of hydroxyl radicals in cavitating water under batch and continuous flow conditions Juretic et al. (2015). At the same acoustic energy input for batch reactions the efficiency of radical production depended upon reactor volume and for the flow system or the flow

rate.

About two decades ago, Hua and Hoffmann (1997) examined the effect of dissolved gases (Kr, Ar, He, O₂) on the production of H₂O₂, HO· at US frequencies of 20–500 kHz. Using KI and terephthalic acid dosimeters the highest rate constants to produce H₂O₂ were observed at pH 7.0, 2.94 μM/min and for HO· at pH 11.0, 0.39 μM/min with Kr-saturated solutions at 500 kHz. Lowest levels were noted when He-saturated solutions were sonicated at 20 kHz with rate constants for H₂O₂ (0.051 μM/min) and HO· (0.031 μM/min). This fact can be explained by modifications in bubble dynamics and thermodynamics as the resonant bubble radius decreases from 177 μm at 20 kHz to 7 μm at 500 kHz. In 2011, Rooze et al. (2011) again reviewed the effect of dissolved gases type on radical formation employing 20, 41 and 62 kHz frequency in aqueous solutions. A range of dissolved gases were explored viz. CO₂, Ar, He, O₂, air, and radical formation was monitored using potassium iodide and luminol visualisations. They determined that ultrasonic power and frequency had significant effects with Potassium iodide oxidation at 20 kHz being most efficient under argon, and at 41 and 62 kHz under air also indicating that the saturation gas also plays a part in radical formation.

Acknowledgements

Authors are thankful to the anonymous reviewer whose suggestions contributed to considerable improvement of this work.

References

- Adamiak, K. (2013). Numerical models in simulating wire-plate electrostatic precipitators : A review of ion convection electric field. *Journal of Electrostatics*, 71:673–680.
- Ajmal, M., Rusli, S., and Fieg, G. (2016). Modeling and experimental validation of hydrodynamics in an ultrasonic batch reactor. *Ultrasonics Sonochemistry*, 28:218 – 229.
- Alemrajabi, A. and Lai, F. C. (2005). Ehd-enhanced drying of partially wetted glass beads. *Drying Technology*, 23:597–609.
- Alemrajabi, A. A., Rezaee, F., Mirhosseini, M., and Esehaghbeygi, A. (2012). Comparative evaluation of the effects of electrohydrodynamic, oven, and ambient air on carrot cylindrical slices during drying process. *Drying Technology*, 30(1):88–96.
- Allen, P. H. G. and Karayiannist, T. G. (1995). Electrohydrodynamic enhancement of heat transfer and fluid flow. *Heat Recovery Systems and CHP*, 15:389–423.
- Anbar, M. and Pecht, I. (1964). On the sonochemical formation of hydrogen peroxide in water. *The Journal of Physical Chemistry*, 68:352–355.
- Angersbach, A., Heinz, V., and Knorr, D. (1999). Electrophysiological model of intact and processed plant tissues: Cell disintegration criteria. *Biotechnology Progress*, 15:753–762.
- Ardelyan, N., Bychkov, V., Kochetov, I., and Kosmachevskii, K. (2013). Kinetic model of pulsed discharge in humid air. *Plasma Science, IEEE Transactions on*, 41:3240–3244.
- Asakawa, Y. (1976). Promotion and retardation of heat transfer by electric fields. *Nature*, 261:220–221.
- Ashokkumar, M. (2015). Applications of ultrasound in food and bioprocessing. *Ultrasonics Sonochemistry*, 25:17 – 23.

- Ashokkumar, M., Sunartio, D., Kentish, S., Mawson, R., Simons, L., Vilkhu, K., and Versteeg, C. K. (2008). Modification of food ingredients by ultrasound to improve functionality: A preliminary study on a model system. *Innovative Food Science & Emerging Technologies*, 9:155 – 160.
- Atungulu, G., Atungulu, E., and Nishiyama, Y. (2005a). Electrode configuration and treatment timing effects of electric fields on fruit putrefaction and molding post harvest. *Journal of food engineering*, 70:506–511.
- Atungulu, G., Atungulu, E., Okada, R., and Nishiyama, Y. (2005b). Efficacy of high voltage treatment on tomato storage. *Journal of Food Technology*, 3:209–215.
- Atungulu, G., Nishiyama, Y., and Koide, S. (2003). Use of an electric field to extend the shelf life of apples. *Biosystems engineering*, 85:41–49.
- Atungulu, G., Nishiyama, Y., and Koide, S. (2004a). Electrode configuration and polarity effects on physicochemical properties of electric field treated apples post harvest. *Biosystems engineering*, 87:313–323.
- Atungulu, G., Nishiyama, Y., and Koide, S. (2004b). Respiration and climacteric patterns of apples treated with continuous and intermittent direct current electric field. *Journal of food engineering*, 63:1–8.
- Atungulu, G. G. (2007). High electric field technology in post harvest drying. *Fresh Produce*, 1:23–31.
- Awad, T. S., Moharram, H. A., Shaltout, O. E., Asker, D., and Youssef, M. M. (2012). Applications of ultrasound in analysis, processing and quality control of food: A review. *Food Research International*, 48(2):410–427.
- Bablon, G., Bellamy, W., Bourbigot, M.-M., Daniel, F., Dore, M., Erb, F., Gordon, G., Langlais, B., Laplanche, A., Legube, B., Martin, G., Masschlein, W., Pacey, G., Reckhow, D., and Ventresque, C. (1991). Fundamental aspects. In G., L., D.A., R., and D.R., B., editors, *Ozone in water treatment: Application and engineering*, pages 11–132. Lewis Publishers, Inc., Chelsea, Mich., U.S.A.
- Bai, Y., Bai, Y., Li, X., Yang, S., and Shi, H. (2011a). Thin layer electrohydrodynamic (ehd) drying and mathematical modeling of fish. *International Journal of Applied Electromagnetics and Mechanics*, 36:217–228.
- Bai, Y., Hu, Y., and Li, X. (2010). The tofu's characteristics of electrohydrodynamic drying with wire electrode. In *Power and Energy Engineering Conference (APPEEC), 2010 Asia-Pacific*, pages 1–4. IEEE.
- Bai, Y., Qu, M., Luan, Z., Li, X., and Yang, Y. (2013). Electrohydrodynamic drying of sea cucumber (*Stichopus japonicus*). *LWT - Food Science and Technology*, 54:570 – 576.
- Bai, Y., Sun, Y., Li, Z., and Kang, D. (2011b). Study the optimum parameters of high voltage electrostatic field thawing. *Procedia Engineering*, 16:679–684.
- Bai, Y.-X., Yang, G.-J., Hu, Y.-C., and Qu, M. (2012). Physical and sensory properties of electrohydrodynamic (EHD) dried scallop muscle. *Journal of Aquatic Food Product Technology*, 21:238–247.
- Bailey, A. G. (1998). The science and technology of electrostatic powder spraying, transport and coating. *Journal of Electrostatics*, 45:85–120.

- Bajgai, T. and Hashinaga, F. (2001a). High electric field drying of japanese radish. *Drying Technology*, 19:2291–2302.
- Bajgai, T. R. and Hashinaga, F. (2001b). Drying of spinach with a high electric field. *Drying Technology*, 19:2331–2341.
- Bajgai, T. R., Hashinaga, F., Isobe, S., Raghavan, G. V., and Ngadi, M. O. (2006a). Application of high electric field (hef) on the shelf-life extension of emblic fruit (*phyllanthus emblica l.*). *Journal of Food Engineering*, 74:308–313.
- Bajgai, T. R., Raghavan, G. V., Hashinaga, F., and Ngadi, M. O. (2006b). Electrohydrodynamic dryinga concise overview. *Drying Technology*, 24:905–910.
- Barba, F. J., Parniakov, O., Pereira, S. A., Wiktor, A., Grimi, N., Boussetta, N., Saraiva, J. A., Raso, J., Martin-Belloso, O., Witrowa-Rajchert, D., Lebovka, N., and Vorobiev, E. (2015). Current applications and new opportunities for the use of pulsed electric fields in food science and industry. *Food Research International*, 77:773–798.
- Bárdos, L. and Baránková, H. (2010). Cold atmospheric plasma: Sources, processes, and applications. *Thin Solid Films*, 518:6705 – 6713.
- Barni, R., Esena, P., and Riccardi, C. (2005a). Chemical kinetics simulation for atmospheric pressure air plasmas in a streamer regime. *Journal of Applied Physics*, 97.
- Barni, R., Esena, P., and Riccardi, C. (2005b). Chemical kinetics simulations of an atmospheric pressure plasma device in air. *Surface and Coatings Technology*, 200:924–927.
- Barreto, J. C., Smith, G. S., Strobel, N. H. P., McQuillin, P. A., and Miller, T. A. (1994). Terephthalic acid: A dosimeter for the detection of hydroxyl radicals in vitro. *Life Sciences*, 56:PL89–PL96.
- Barthakur, N. (1990). Electrohydrodynamic from NaCl Solutions Enhancement of Evaporation. *Desalination*, 78:455–465.
- Barthakur, N. N. and Al-Kanani, T. (1989). Impact of air ions of both polarity on evaporation of certain organic and inorganic liquids. *International Journal of Biometeorology*, 33:136–141.
- Basiry, M. and Esehaghbeygi, A. (2010). Electrohydrodynamic (EHD) drying of rapeseed (*Brassica napus L.*). *Journal of Electrostatics*, 68:360–363.
- Benilov, M. S. and Naidis, G. V. (2003). Modelling of low-current discharges in atmospheric-pressure air taking account of non-equilibrium effects. *Journal of Physics D: Applied Physics*, 36:1834.
- Bhoj, A. N. (2006). *Multiscale Simulation of Atmospheric Pressure Pulsed Discharges Used in Polymer Surface Functionalization*. PhD thesis, University of Michigan.
- Bird, R. B., Stewart, W., and Lightfoot, E. N. (2007). *Transport Phenomena*. John Wiley and Sons Ltd.
- Bittencourt, J. A. (2004). *Fundamentals of Plasma Physics*. Springer-Verlag GmbH.
- Boussetta, N., Soichi, E., Lanoiselé, J. L., and Vorobiev, E. (2014). Valorization of oilseed residues: Extraction of polyphenols from flaxseed hulls by pulsed electric fields. *Industrial Crops and Products*, 52:347–353.

- Brenner, M. P., Hilgenfeldt, S., and Lohse, D. (2002). Single-bubble sonoluminescence. *Rev. Mod. Phys.*, 74:425–484.
- Buckow, R., Baumann, P., Schroeder, S., and Knoerzer, K. (2011). Effect of dimensions and geometry of co-field and co-linear pulsed electric field treatment chambers on electric field strength and energy utilisation. *Journal of Food Engineering*, 105:545 – 556.
- Buckow, R., Schroeder, S., Berres, P., Baumann, P., and Knoerzer, K. (2010). Simulation and evaluation of pilot-scale pulsed electric field (PEF) processing. *Journal of Food Engineering*, 101:67 – 77.
- Cameron, M., McMaster, L. D., and Britz, T. J. (2008). Electron microscopic analysis of dairy microbes inactivated by ultrasound. *Ultrasonics Sonochemistry*, 15:960–964.
- Cameron, M., McMaster, L. D., and Britz, T. J. (2009). Impact of ultrasound on dairy spoilage microbes and milk components. *Dairy Science & Technology*, 89:83–98.
- Cammack, R., Joannou, C., Cui, X.-Y., Martinez, C. T., Maraj, S. R., and Hughes, M. N. (1999). Nitrite and nitrosyl compounds in food preservation. *Biochimica et Biophysica Acta (BBA) - Bioenergetics*, 1411:475 – 488.
- Cao, W., Nishiyama, Y., and Koide, S. (2004). Electrohydrodynamic drying characteristics of wheat using high voltage electrostatic field. *Journal of Food Engineering*, 62:209 – 213.
- Carbonell-Capella, J. M., Parniakov, O., Barba, F. J., Grimi, N., Bals, O., Lebovka, N., and Vorobiev, E. (2016). “ice” juice from apples obtained by pressing at subzero temperatures of apples pretreated by pulsed electric fields. *Innovative Food Science & Emerging Technologies*, 33:187 – 194.
- Carpenter, K. and Bahadur, V. (2015). Electrofreezing of water droplets under electrowetting fields. *Langmuir*, 31:2243–2248.
- Chang, D. and Reese, T. S. (1990). Changes in membrane structure induced by electroporation as revealed by rapid-freezing electron microscopy. *Biophysical journal*, 58(1):1.
- Chemat, F., Khan, M. K., et al. (2011). Applications of ultrasound in food technology: processing, preservation and extraction. *Ultrasonics sonochemistry*, 18:813–835.
- Chemat, F., Rombaut, N., Sicaire, A.-G., Meullemiestre, A., Fabiano-Tixier, A.-S., and Abert-Vian, M. (2017). Ultrasound assisted extraction of food and natural products. mechanisms, techniques, combinations, protocols and applications. A review. *Ultrasonics Sonochemistry*, 34:540 – 560.
- Chen, C., Liu, D. X., Liu, Z. C., Yang, A. J., Chen, H. L., Shama, G., and Kong, M. G. (2014). A model of plasma-biofilm and plasma-tissue interactions at ambient pressure. *Plasma Chem Plasma Process*, 34:403–441.
- Chen, G. and Mujumdar, A. S. (2002). Application of electrical fields in dewatering and drying. *Developments in Chemical Engineering and Mineral Processing*, 10:429–441.
- Chen, Y. H. and Barthakur, N. N. (1991). Potato slab dehydration by air ions from corona discharge. *International Journal of Biometeorology*, 35:67–70.
- Comeskey, D., Larparadsudthi, O. A., Mason, T. J., and Paniwnyk, L. (2012). The use of a range of ultrasound frequencies to reduce colouration caused by dyes. *Water Science and Technology*, 66:2251–2257.

- Dalvand, M., Mohtasebi, S., and Rafiee, S. (2013). Study on effective structural parameters on drying rate of kiwi fruits in a solar ehd dryer. *International Journal of Multidisciplinary Sciences and Engineering*, 3:66–70.
- Dalvand, M. J., Mohtasebi, S. S., and Rafiee, S. (2014). Modeling of electrohydrodynamic drying process using response surface methodology. *Food science & nutrition*, 2:200–9.
- Dalvi-Isfahan, M., Hamdami, N., and Le-Bail, A. (2016). Effect of freezing under electrostatic field on the quality of lamb meat. *Innovative Food Science & Emerging Technologies*, 37:68–73.
- Davidson, J. H. and Shaughnessy, E. J. (1986). Turbulence generation by electric body forces. *Experiments in Fluids*, 4:17–26.
- DeBruin, K. and Krassowska, W. (1999). Modeling electroporation in a single cell. II. Effects of ionic concentrations. *Biophysical journal*, 77:1225–1233.
- Deng, L., Pan, X., Chen, L., Shen, L., and Sheng, J. (2013). Effects of preharvest nitric oxide treatment on ethylene biosynthesis and soluble sugars metabolism in golden delicious apples. *Postharvest Biology and Technology*, 84:9 – 15.
- Deora, N., Misra, N., Deswal, A., Mishra, H., Cullen, P., and Tiwari, B. (2013). Ultrasound for improved crystallisation in food processing. *Food Engineering Reviews*, 5:36–44.
- Dinani, S. T., Hamdami, N., Shahedi, M., and Havet, M. (2014). Mathematical modeling of hot air/electrohydrodynamic (ehd) drying kinetics of mushroom slices. *Energy Conversion and Management*, 86:70 – 80.
- Ding, C., Lu, J., and Song, Z. (2015). Electrohydrodynamic drying of carrot slices. *PLOS ONE*, 10:e0124077.
- Ding, C., Lu, J., Song, Z., and Bao, S. (2014). The drying efficiency of electrohydrodynamic (ehd) systems based on the drying characteristics of cooked beef and mathematical modeling. *International Journal of Applied Electromagnetics and Mechanics*, 46:455–461.
- Dujko, S., Markosyan, A. H., White, R. D., and Ebert, U. (2013). High-order fluid model for streamer discharges: I. derivation of model and transport data. *Journal of Physics D: Applied Physics*, 46:475202.
- Dutta, B., Raghavan, G., Dev, S., Lilap, P., Murugesan, R., Anekella, K., and Kaushal, T. (2012). A comparative study on the effects of microwave and high electric field pretreatments on drying kinetics and quality of mushrooms. *Drying Technology*, 30:891–897.
- Ellis, H., McDaniel, E., Albritton, D., Viehland, L., Lin, S., and Mason, E. (1978). Transport properties of gaseous ions over a wide energy range. part ii. *Atomic Data and Nuclear Data Tables*, 22:179 – 217.
- Ellis, H., Pai, R., McDaniel, E., Mason, E., and Viehland, L. (1976). Transport properties of gaseous ions over a wide energy range. *Atomic Data and Nuclear Data Tables*, 17:177 – 210.
- Ellis, H., Thackston, M., McDaniel, E., and Mason, E. (1984). Transport properties of gaseous ions over a wide energy range. part {III}. *Atomic Data and Nuclear Data Tables*, 31:113 – 151.
- Esehaghbeygi, A. (2012). Effect of electrohydrodynamic and batch drying on rice fissuring. *Drying Technology*, 30:1644–1648.

- Esehaghbeygi, A. and Basiry, M. (2011). Electrohydrodynamic (EHD) drying of tomato slices (*lycopersicon esculentum*). *Journal of Food Engineering*, 104:628–631.
- Esehaghbeygi, A., Pirnazari, K., and Sadeghi, M. (2014). Quality assessment of electrohydrodynamic and microwave dehydrated banana slices. *LWT - Food Science and Technology*, 55:565 – 571.
- Fischer, C., Hart, E., and Henglein, A. (1986). Ultrasonic Irradiation of water in the presence of $^{18}\text{O}_2$: isotope Exchange and Isotopic Distribution of H_2O_2 . *Journal of Physical Chemistry*, 90:1954–1956.
- Flannigan, D. J. and Suslick, K. S. (2005). Plasma formation and temperature measurement during single-bubble cavitation. *Nature*, 434:52–55.
- Fridman, A. (2008). *Plasma chemistry*. Cambridge University Press.
- Gao, S., Hemar, Y., Ashokkumar, M., Paturel, S., and Lewis, G. D. (2014). Inactivation of bacteria and yeast using high-frequency ultrasound treatment. *Water Research*, 60:93 – 104.
- Glaser, R. W., Leikin, S. L., Chernomordik, L. V., Pastushenko, V. F., and Sokirko, A. I. (1988). Reversible electrical breakdown of lipid bilayers: formation and evolution of pores. *Biochimica et Biophysica Acta (BBA) - Biomembranes*, 940:275–287.
- Go, D. B., Maturana, R. A., Fisher, T. S., and Garimella, S. V. (2008). Enhancement of external forced convection by ionic wind. *International Journal of Heat and Mass Transfer*, 51:6047–6053.
- Gogolides, E. and Sawin, H. H. (1992). Continuum modeling of radio-frequency glow discharges. 1. Theory and results for electropositive and electronegative gases. *Journal of Applied Physics*, 72:3971–3987.
- Golberg, A. and Rubinsky, B. (2013). Chapter 12 - mass transfer phenomena in electroporation. In Becker, S. M. and Kuznetsov, A. V., editors, *Transport in Biological Media*, pages 455–492. Elsevier, Boston.
- Goldman, M., Goldman, A., and Sigmond, R. (1985). The corona discharge, its properties and specific uses. *Pure and Applied Chemistry*, 57:1353–1362.
- Gradshteyn, I. S. and Ryzhik, I. M. (1979). *Table of integrals, series and products, corrected and enlarged edition*. Academic Press.
- Hagelaar, G. and Pitchford, L. (2005). Solving the boltzmann equation to obtain electron transport coefficients and rate coefficients for fluid models. *Plasma Sources Science and Technology*, 14:722.
- Hamaguchi, S. (2013). Chemically reactive species in liquids generated by atmospheric-pressure plasmas and their roles in plasma medicine. *AIP Conference Proceedings*, 1545:214–222.
- Han, Z., Zeng, X. A., Fu, N., Yu, S. J., Chen, X. D., and Kennedy, J. F. (2012). Effects of pulsed electric field treatments on some properties of tapioca starch. *Carbohydrate Polymers*, 89:1012–1017.
- Hashinaga, F., Bajgai, T. R., Isobe, S., and Barthakur, N. N. (1999). Electrohydrodynamic (EHD) drying of apple slices. *Drying Technology*, 17:479–495.
- Hashinga, F., Kharel, G. P., and Shintani, R. (1995). Effect of ordinary frequency high electric fields on evaporation and drying. *Food Science and Technology International, Tokyo*, 1:77–81.
- He, X., Jia, G., Tatsumi, E., and Liu, H. (2016). Effect of corona wind, current, electric field and energy consumption on the reduction of the thawing time during the high-voltage electrostatic-field (HVEF) treatment process. *Innovative Food Science & Emerging Technologies*, 34:135–140.

- He, X., Liu, R., Nirasawa, S., Zheng, D., and Liu, H. (2013). Effect of high voltage electrostatic field treatment on thawing characteristics and post-thawing quality of frozen pork tenderloin meat. *Journal of Food Engineering*, 115:245–250.
- Henglein, A. (1995). Chemical effects of continuous and pulsed ultrasound in aqueous solutions. *Ultrasonics sonochemistry*, 2:115–121.
- Hrazdina, G. (1971). Reactions of the anthocyanidin-3,5-diglucosides: Formation of 3,5-di-(α - β -d-glucosyl)-7-hydroxy coumarin. *Phytochemistry*, 10:1125–1130.
- Hsieh, C.-W. and Ko, W.-C. (2008). Effect of high-voltage electrostatic field on quality of carrot juice during refrigeration. *LWT-Food Science and Technology*, 41:1752–1757.
- Hsieh, C.-W., Lai, C.-H., Ho, W.-J., Huang, S.-C., and Ko, W.-C. (2010). Effect of thawing and cold storage on frozen chicken thigh meat quality by high-voltage electrostatic field. *Journal of food science*, 75:M193–M197.
- Hsieh, C.-W., Lai, C.-H., Lee, C.-H., and Ko, W.-C. (2011). Effects of high-voltage electrostatic fields on the quality of tilapia meat during refrigeration. *Journal of food science*, 76:M312–M317.
- Hua, I. and Hoffmann, M. R. (1997). Optimization of ultrasonic irradiation as an advanced oxidation technology. *Environmental Science & Technology*, 31:2237–2243.
- Isobe, S., Barthakur, N., Yoshino, T., Okushima, L., and Sase, S. (1999). Electrohydrodynamic drying characteristic of agar gel. *Food Science Technology Research*, 5:132–136.
- Joshi, J. and Nandakumar, K. (2015). Computational modeling of multiphase reactors. *Annual Review of Chemical & Biomolecular Engineering*, 6:347–378.
- Joyce, E., Al-Hashimi, A., and Mason, T. (2011). Assessing the effect of different ultrasonic frequencies on bacterial viability using flow cytometry. *Journal of applied microbiology*, 110:862–870.
- Jung, S., Kim, H. J., Park, S., Yong, H. I., Choe, J. H., Jeon, H.-J., Choe, W., and Jo, C. (2015). The use of atmospheric pressure plasma-treated water as a source of nitrite for emulsion-type sausage. *Meat Science*, 108:132 – 137.
- Juretic, H., Montalbo-Lomboy, M., van Leeuwen, J. H., Cooper, W. J., and Grewell, D. (2015). Hydroxyl radical formation in batch and continuous flow ultrasonic systems. *Ultrasonics sonochemistry*, 22:600–6.
- Kamgang-Youbi, G., Herry, J.-M., Meylheuc, T., Brisset, J.-L., Bellon-Fontaine, M.-N., Doubla, A., and Naitali, M. (2009). Microbial inactivation using plasma-activated water obtained by gliding electric discharges. *Letters in applied microbiology*, 48:13–18.
- Kamkari, B. and Alemrajabi, A. A. (2010). Investigation of Electrohydrodynamically-Enhanced Convective Heat and Mass Transfer from Water Surface. *Heat Transfer Engineering*, 31:138–146.
- Karami, R., Ayazi, M., Samiee, L., Mobarake, M. D., and Goodarzvand-Chegini, F. (2012). An experimental study of the effect of high electric field on mass transfer enhancement. *Journal of Petroleum Science and Technology*, 2:40–49.
- Karaseva, E. I., Tarun, E. I., and Metelitsa, D. I. (2009). An ultrasonic inactivation of *Aspergillus niger* glucose oxidase in aqueous solutions. *Applied Biochemistry and Microbiology*, 45:9–16.

- Kasayapanand, N. and Kiatsiriroat, T. (2005). Ehd enhanced heat transfer in wavy channel. *International Communications in Heat and Mass Transfer*, 32:809–821.
- Kentish, S. and Feng, H. (2014). Applications of power ultrasound in food processing. *Annual review of food science and technology*, 5:263–284.
- Khadre, M. A., Yousef, A. E., and Kim, J. G. (2001). Microbiological aspects of ozone applications in food: A review. *Journal of food science*, 66:1242–1252.
- Khanal, S. N., Anand, S., and Muthukumarappan, K. (2014). Evaluation of high-intensity ultrasonication for the inactivation of endospores of 3 bacillus species in nonfat milk. *Journal of dairy science*, 97:5952–5963.
- Khandpur, P. and Gogate, P. R. (2016). Evaluation of ultrasound based sterilization approaches in terms of shelf life and quality parameters of fruit and vegetable juices. *Ultrasonics Sonochemistry*, 29:337–353.
- Kharel, G. P., Hashinaga, F., and Shintani, R. (1996). Effect of high electric fields on some fruits and vegetables. *journal of the japanese society for cold preservation of food*, 22:17–22.
- Kim, K. Y., Byun, K.-T., and Kwak, H.-Y. (2007). Temperature and pressure fields due to collapsing bubble under ultrasound. *Chemical Engineering Journal*, 132:125 – 135.
- Kim, T. G., Kim, S.-H., and Cho, K.-S. (2014). Effects of ultrasonic pretreatment on quantity and composition of bacterial dna recovered from granular activated carbon used for drinking water treatment. *Journal of Environmental Science and Health, Part A*, 49:609–616.
- Kimura, T. (1996). Standardization of ultrasonic power for sonochemical reaction. *Ultrasonics Sonochemistry*, 3:S157–S161.
- Kinosita, K., Hibino, M., Itoh, H., Shigemori, M., Hirano, K., Kirino, Y., and Hayakawa, T. (2012). Events of membrane electroporation visualized on a time scale from microsecond to seconds. In Chang, D., Chassy, B. M., Saunders, J. A., and Sowers, A. E., editors, *Guide to Electroporation and Electrofusion*, pages 29–46. Academic Press, New York.
- Knoerzer, K., Baumann, P., and Buckow, R. (2012). An iterative modelling approach for improving the performance of a pulsed electric field (PEF) treatment chamber. *Computers & Chemical Engineering*, 37:48 – 63.
- Ko, W.-C., Shi, H.-Z., Chang, C.-K., Huang, Y.-H., Chen, Y.-A., and Hsieh, C.-W. (2016a). Effect of adjustable parallel high voltage on biochemical indicators and actomyosin ca^{2+} -atpase from tilapia (*Orechromis niloticus*). *LWT-Food Science and Technology*, 69:417–423.
- Ko, W.-C., Yang, S.-Y., Chang, C.-K., and Hsieh, C.-W. (2016b). Effects of adjustable parallel high voltage electrostatic field on the freshness of tilapia (*Orechromis niloticus*) during refrigeration. *LWT-Food Science and Technology*, 66:151–157.
- Kodama, S., Thawatchaipracha, B., and Sekiguchi, H. (2014). Enhancement of essential oil extraction for steam distillation by dbd surface treatment. *Plasma Processes and Polymers*, 11:126–132.
- Kossyi, I. A., Kostinsky, A. Y., Matveyev, A. A., and Silakov, V. P. (1992). Kinetic scheme of the non-equilibrium discharge in nitrogen-oxygen mixtures. *Plasma Sources Science and Technology*, 1:207.

- Kotnik, T., Miklavčič, D., and Slivnik, T. (1998). Time course of transmembrane voltage induced by time-varying electric fields - A method for theoretical analysis and its application. *Bioelectrochemistry and Bioenergetics*, 45:3–16.
- Koubaa, M., Roselló-Soto, E., Žlabur, J. Š., Jambrak, A. R., Brnčić, M., Grimi, N., Boussetta, N., and Barba, F. J. (2015). Current and new insights in the sustainable and green recovery of nutritionally valuable compounds from stevia rebaudiana bertoni. *J. Agric. Food Chem.*, 63:6835–6846.
- Kronig, R. and Schwarz, N. (1949). on the Theory of Heat Transfer From a Wire in an Electric Field. *Appl. Sci. Res.*, AI(1):35–46.
- Kudra, T. and Martynenko, A. (2015). Energy aspects in electrohydrodynamic drying. *Drying Technology*, 33:1534–1540.
- Kulacki, F. A. (1982). Electrohydrodynamic enhancement of convective heat and mass transfer. In Mujumdar, A. S. and Mashelkar, R. A., editors, *Advances in transport processes*, chapter Electrohydrodynamic enhancement of convective heat and mass transfer. Wiley Eastern Ltd., NY.
- Kwak, Si-Doek Oh, H.-Y. (2000). A study of bubble behavior and boiling heat transfer enhancement under electric field. *Heat Transfer Engineering*, 21:33–45.
- Lai, F. C. and Lai, K.-W. (2002). EHD-enhanced drying with wire electrode. *Drying Technology*, 20(7):1393–1405.
- Landau, L. and Lifshitz, E. M. (1961). *Electrodynamics of Continuous Media*, volume 8. Pergamon, New York.
- Laohalertdecha, S., Naphon, P., and Wongwises, S. (2007). A review of electrohydrodynamic enhancement of heat transfer. *Renewable and Sustainable Energy Reviews*, 11:858–876.
- Launder, B. and Sharma, B. (1974). Application of the energy-dissipation model of turbulence to the calculation of flow near a spinning disc. *Letters in heat and mass transfer*, 1:131–137.
- Launder, B. E. and Spalding, D. (1974). The numerical computation of turbulent flows. *Computer methods in applied mechanics and engineering*, 3:269–289.
- Lebedeva, V. E. (1987). Electric breakdown of bilayer lipid membranes at short times of voltage effect. *Biologicheskiye Membrany*, 4(9):994–998.
- Legay, M., Simony, B., Boldo, P., Gondrexon, N., Person, S. L., and Bontemps, A. (2012). Improvement of heat transfer by means of ultrasound: Application to a double-tube heat exchanger. *Ultrasonics Sonochemistry*, 19:1194–1200.
- Leighton, T. G. (2007). What is ultrasound? *Progress in Biophysics and Molecular Biology*, 93:3 – 83.
- Levine, H. (2013). The physics of. *Journal of Biological Physics*, 29(4):1–6.
- Li, F.-D., Li, L.-T., Sun, J.-F., and Tatsumi, E. (2005). Electrohydrodynamic (EHD) drying characteristic of okara cake. *Drying Technology*, 23:565–580.
- Li, L., Li, F., and Tatsumi, E. (2000). Effects of high voltage electrostatic field on evaporation of distilled water and okara drying. *Biosystem Studies*, 3:43–52.

- Liang, C. P., Chang, C. H., Liang, C. C., Hung, K. Y., and Hsieh, C. W. (2014). In vitro Antioxidant activities, free Radical Scavenging Capacity, and Tyrosinase inhibitory of Flavonoid compounds and Ferulic Acid from *Spiranthes sinensis* (Pers.) Ames. *Molecules*, 19:4681–4694.
- Lieberman, M. A. and Lichtenberg, A. J. (2005). *Principles of plasma discharges and materials processing*. John Wiley & Sons.
- Luengo, E., Martínez, J. M., Álvarez, I., and Raso, J. (2016). Effects of millisecond and microsecond pulsed electric fields on red beet cell disintegration and extraction of betanines. *Industrial Crops and Products*, 84:28–33.
- Luo, J., Fang, Z., and Smith, R. L. (2014). Ultrasound-enhanced conversion of biomass to biofuels. *Progress in Energy and Combustion Science*, 41:56–93.
- Ma, R., Wang, G., Tian, Y., Wang, K., Zhang, J., and Fang, J. (2015). Non-thermal plasma-activated water inactivation of food-borne pathogen on fresh produce. *Journal of Hazardous Materials*, 300:643–651.
- Maddox, L., Reeves, M., Wood, K., Roberts, K., Studer, J., Wetzel, J., Smith, J. T., Whittington, K., Alls, J. L., Parker, J. E., Holwitt, E., Kiel, J., and Wright, J. R. (1998). Acoustic Wave Dosimetry Based on Diazotized Luminol Solutions. *Microchemical Journal*, 58:209–217.
- Mahmoudi, S. R., Adamiak, K., and Castle, G. (2012). On the thermodynamic description of electrohydrodynamic flows. In *Proceedings of the 2012 Electrostatics Joint Conference*, pages 1–12.
- Mahmoudi, S. R., Adamiak, K., and Castle, G. S. P. (2011). Electrohydrodynamic single-phase convection heat transfer enhancement techniques: direct ionic wind and vortex induction. In *Proceedings ESA Annual Meeting*, Cleveland, Ohio.
- Makino, K., Mossoba, M., and Riesz, P. (1983). Chemical effects of ultrasound on aqueous solutions. Formation of hydroxyl radicals and hydrogen atoms. *The Journal of physical chemistry*, 87:1369–1377.
- Martynenko, A. and Kudra, T. (2016). Electrically-induced transport phenomena in ehd drying—a review. *Trends in Food Science & Technology*, 54:63–73.
- Martynenko, A. and Zheng, W. (2016). Electrohydrodynamic drying of apple slices: Energy and quality aspects. *Journal of Food Engineering*, 168:215 – 222.
- Mason, T. and Peters, D. (2002). *Practical sonochemistry: uses and applications of ultrasound*. Horwood, Chichester.
- Mason, T. J., Lorimer, J. P., Bates, D. M., and Zhao, Y. (1994). Dosimetry in sonochemistry: the use of aqueous terephthalate ion as a fluorescence monitor. *Ultrasonics - Sonochemistry*, 1:S91–S95.
- Merouani, S., Hamdaoui, O., Rezgui, Y., and Guemini, M. (2014). Theoretical estimation of the temperature and pressure within collapsing acoustical bubbles. *Ultrasonics Sonochemistry*, 21:53–59.
- Miano, A. C., Ibarz, A., and Augusto, P. E. D. (2016). Mechanisms for improving mass transfer in food with ultrasound technology: Describing the phenomena in two model cases. *Ultrasonics Sonochemistry*, 29:413 – 419.
- Milne, L., Stewart, I., and Bremner, D. H. (2013). Comparison of hydroxyl radical formation in aqueous solutions at different ultrasound frequencies and powers using the salicylic acid dosimeter. *Ultrasonics Sonochemistry*, 20:984–989.

- Misra, N. (2015). The contribution of non-thermal and advanced oxidation technologies towards dissipation of pesticide residues. *Trends in Food Science & Technology*, 45:229 – 244.
- Misra, N., Han, L., Tiwari, B., Bourke, P., and Cullen, P. (2014a). Nonthermal plasma technology for decontamination of foods. In Boziaris, I., editor, *Novel Food Preservation and Microbial Assessment Techniques*, chapter 6, pages 155–183. CRC Press.
- Misra, N., Kaur, S., Tiwari, B. K., Kaur, A., Singh, N., and Cullen, P. (2015a). Atmospheric pressure cold plasma (ACP) treatment of wheat flour. *Food Hydrocolloids*, 44:115 – 121.
- Misra, N., Keener, K., Bourke, P., and Cullen, P. (2015b). Generation of in-package cold plasma and efficacy assessment using methylene blue. *Plasma Chemistry and Plasma Processing*, 35:1043–1056.
- Misra, N., Pankaj, S., Frias, J., Keener, K., and Cullen, P. (2015c). The effects of nonthermal plasma on chemical quality of strawberries. *Postharvest Biology and Technology*, 110:197–202.
- Misra, N., Sullivan, C., Pankaj, S., Alvarez-Jubete, L., Cama, R., Jacoby, F., and Cullen, P. (2014b). Enhancement of oil spreadability of biscuit surface by nonthermal barrier discharge plasma. *Innovative Food Science & Emerging Technologies*, 26:456 – 461.
- Misra, N., Tiwari, B., Raghavarao, K., and Cullen, P. (2011). Nonthermal plasma inactivation of food-borne pathogens. *Food Engineering Reviews*, 3:159–170.
- Mohammadi, V., Ghasemi-Varnamkhasti, M., Ebrahimi, R., and Abbasvali, M. (2014). Ultrasonic techniques for the milk production industry. *Measurement*, 58:93–102.
- Moiseev, T., Misra, N. N., Patil, S., Cullen, P. J., Bourke, P., Keener, K. M., and Mosnier, J. P. (2014). Post-discharge gas composition of a large-gap dbd in humid air by uvvis absorption spectroscopy. *Plasma Sources Science and Technology*, 23:065033.
- Mousakhani-Ganjeh, A., Hamdami, N., and Soltanizadeh, N. (2015). Impact of high voltage electric field thawing on the quality of frozen tuna fish (*thunnus albacares*). *Journal of Food Engineering*, 156:39–44.
- Mozetič, M., Primc, G., Vesel, A., Zaplotnik, R., Modic, M., Junkar, I., Recek, N., Klanjšek-Gunde, M., Guhy, L., Sunkara, M. K., Assensio, M. C., Milošević, S., Lehocký, M., Sedlarík, V., Gorjanc, M., Kutasi, K., and Stana-Kleinschek, K. (2015). Application of extremely non-equilibrium plasmas in the processing of nano and biomedical materials. *Plasma Sources Science and Technology*, 24:015026.
- Musielak, G., Mierzwa, D., and Kroehnke, J. (2016). Food drying enhancement by ultrasound a review. *Trends in Food Science & Technology*, 56:126 – 141.
- Nelson, D. A. and Shaughnessy, E. J. (1986). Electric Field Effects on Natural Convection in Enclosures. *Journal of Heat Transfer*, 108(4):749–754.
- Norberg, S. A. (2015). *Modeling Atmospheric Pressure Plasma Jets: Plasma Dynamics, Interaction with Dielectric Surfaces, Liquid Layers, and Cells*. PhD thesis, Department of Mechanical Engineering, University of Michigan at Ann Arbor.
- Norberg, S. A., Johnsen, E., and Kushner, M. J. (2015). Formation of reactive oxygen and nitrogen species by repetitive negatively pulsed helium atmospheric pressure plasma jets propagating into humid air. *Plasma Sources Science and Technology*, 24:035026.
- Nur, M., Bonifaci, N., and Denat, A. (2014). Ionic wind phenomenon and charge carrier mobility in very high density argon corona discharge plasma. *Journal of Physics: Conference Series*, 495.

- O'Donnell, C., Tiwari, B. K., Cullen, P., and Rice, R. G. (2012). *Ozone in food processing*. John Wiley & Sons.
- Onsager, L. (1949). Statistical hydrodynamics. *Convegno Internazionale di Meccanica Statistica Firenze*, 6:279–287.
- Orlowska, M., Havet, M., and Le-Bail, A. (2009). Controlled ice nucleation under high voltage dc electrostatic field conditions. *Food research international*, 42:879–884.
- Ouerhani, T., Pflieger, R., Messaoud, W. B., and Nikitenko, S. I. (2015). Spectroscopy of sonoluminescence and sonochemistry in water saturated with N₂-Ar mixtures. *The Journal of Physical Chemistry B*, 119:15885–15891.
- Ould Ahmedou, S. A., Rouaud, O., and Havet, M. (2009). Assessment of the electrohydrodynamic drying process. *Food and Bioprocess Technology*, 2:240–247.
- Owsenek, B. and Seyed-Yagoobi, J. (1997). Theoretical and experimental study of electrohydrodynamic heat transfer enhancement through wire-plate corona discharge. *Journal of Heat Transfer*, 119:604–610.
- Owsenek, B. L., Seyed-Yagoobi, J., and Page, R. H. (1995). Experimental investigation of corona wind heat transfer enhancement with a heated horizontal flat plate. *Journal of Heat Transfer*, 117:309–314.
- Pal, P., Kaur, P., Singh, N., Kaur, A. P., Misra, N., Tiwari, B. K., Cullen, P. J., and Virdi, A. S. (2015). Effect of nonthermal plasma on physico-chemical, amino acid composition, pasting and protein characteristics of short and long grain rice flour. *Food Research International*, pages –.
- Palanimuthu, V., Rajkumar, P., Orsat, V., Gariépy, Y., and Raghavan, G. (2009). Improving cranberry shelf-life using high voltage electric field treatment. *Journal of food engineering*, 90:365–371.
- Panasyuk, A. L., Panchenko, M. S., Starov, V. M., and Churaev, N. V. (1979). Influence of inhomogeneous electric and magnetic fields on internal mass transfer in capillary-porous bodies. *Journal of Engineering Physics*, 35(1):827–832.
- Parniakov, O., Roselló-Soto, E., Barba, F. J., Grimi, N., Lebovka, N., and Vorobiev, E. (2015). New approaches for the effective valorization of papaya seeds: Extraction of proteins, phenolic compounds, carbohydrates, and isothiocyanates assisted by pulsed electric energy. *Food Research International*, 77:711–717.
- Patil, S., Moiseev, T., Misra, N., Cullen, P., Mosnier, J., Keener, K., and Bourke, P. (2014). Influence of high voltage atmospheric cold plasma process parameters and role of relative humidity on inactivation of bacillus atropphaeus spores inside a sealed package. *Journal of Hospital Infection*, 88:162–169.
- Patist, A. and Bates, D. (2008). Ultrasonic innovations in the food industry: From the laboratory to commercial production. *Innovative Food Science & Emerging Technologies*, 9:147 – 154.
- Perez, O. E. and Pilosof, A. M. R. (2004). Pulsed electric fields effects on the molecular structure and gelation of beta-lactoglobulin concentrate and egg white. *Food Research International*, 37:102–110.
- Pétrier, C. and Francony, a. (1997). Ultrasonic waste-water treatment: incidence of ultrasonic frequency on the rate of phenol and carbon tetrachloride degradation. *Ultrasonics sonochemistry*, 4:295–300.
- Pflieger, R., Chave, T., Vite, G., Jouve, L., and Nikitenko, S. I. (2015). Ultrasonics Sonochemistry Effect of operational conditions on sonoluminescence and kinetics of H₂O₂ formation during the sonolysis of water in the presence of Ar / O₂ gas mixture. *Ultrasonics - Sonochemistry*, 26:169–175.

Pitchford, L. C., Alves, L. L., Bartschat, K., Biagi, S. F., Bordage, M.-C., Bray, I., Brion, C. E., Brunger, M. J., Campbell, L., Chachereau, A., Chaudhury, B., Christophorou, L. G., Carbone, E., Dyatko, N. A., Franck, C. M., Fursa, D. V., Gangwar, R. K., Guerra, V., Haefliger, P., Hagelaar, G. J. M., Hoesl, A., Itikawa, Y., Kochetov, I. V., McEachran, R. P., Morgan, W. L., Napartovich, A. P., Puech, V., Rabie, M., Sharma, L., Srivastava, R., Stauffer, A. D., Tennyson, J., de Urquijo, J., van Dijk, J., Viehland, L. A., Zammit, M. C., Zatsarinny, O., and Pancheshnyi, S. (2017). Lxcat: an open-access, web-based platform for data needed for modeling low temperature plasmas. *Plasma Processes and Polymers*, 14:1600098–n/a.

Pogorzelski, M., Zander, Z., Zander, L., and Wrotniak, M. (2013). Drying kinetics of plant material using the electrohydrodynamic (EHD) method. *Chemical Engineering and Equipment*, 44(6):552–553.

Price, G. J. (2010). Sonochemistry and sonoluminescence in aqueous systems. In *20th International Congress on Acoustics 2010, ICA 2010 - Incorporating Proceedings of the 2010 Annual Conference of the Australian Acoustical Society*, volume 1, pages 582–587.

Prochownick, L. and Spaeth, F. (1890). Über die keimtötende wirkung des galvanischen stroms. *Deutsche Medizinische Wochenschrift*, 26:564–565.

Puértolas, E., Koubaa, M., and Barba, F. J. (2016). An overview of the impact of electrotechnologies for the recovery of oil and high-value compounds from vegetable oil industry: Energy and economic cost implications. *Food Research International*, 80:19–26.

Puértolas, E., Luengo, E., Álvarez, I., and Raso, J. (2012). Improving mass transfer to soften tissues by pulsed electric fields: Fundamentals and applications. *Annual Review of Food Science and Technology*, 3:263–282.

Qin, B., Zhang, Q., Barbosa-Cánovas, G. V., Swanson, B. G., and Pedrow, P. D. (1995). Pulsed electric field treatment chamber design for liquid food pasteurization using a finite element method. *Transactions of the ASAE*, 38:557–565.

Raghavarao, K., Doddamane, S. N., Sampangi, C., and Todd, P. W. (2002). Field-assisted extraction of cells, particles and macromolecules. *Trends in Biotechnology*, 20:72 – 78.

Rahman, M. and Saghir, M. (2014). Thermodiffusion or soret effect: Historical review. *International Journal of Heat and Mass Transfer*, 73:693 – 705.

Rashkovan, A., Sher, E., and Kalman, H. (2002). Experimental optimization of an electric blower by corona wind. *Applied Thermal Engineering*, 22:1587–1599.

Rastogi, N., Raghavarao, K., Balasubramaniam, V., Niranjan, K., and Knorr, D. (2007). Opportunities and challenges in high pressure processing of foods. *Critical Reviews in Food Science and Nutrition*, 47:69–112.

Robinson, M. (1961). Movement of air in the electric wind of the corona discharge. *American Institute of Electrical Engineers, Part I: Communication and Electronics, Transactions of the*, 80:143–150.

Rogov, I. A., Adamenko, V. Y., Nekrutman, S. V., Ilyasov, S. G., Krasnikov, V. V., Kopylov, Y. A., Turev, E. P., Zhukov, N. N., and Vigderman, V. S. (1981). Electrophysical, optical and acoustical properties of foods. In *Legkaya et Pischewaya promyshlennost [in Russian]*. Moscow, Moscow.

Rokhina, E. V., Lens, P., and Virkutyte, J. (2009). Low-frequency ultrasound in biotechnology: state of the art. *Trends in Biotechnology*, 27:298–306.

- Rooze, J., Rebrov, E. V., Schouten, J. C., and Keurentjes, J. T. F. (2011). Effect of resonance frequency, power input, and saturation gas type on the oxidation efficiency of an ultrasound horn. *Ultrasonics Sonochemistry*, 18:209–215.
- Rounseley, R. R. (1985). Drying in the presence of an electrostatic field. *Tappi journal*, 68:108–112.
- Ruenroengklin, N., Yang, B., Lin, H., Chen, F., and Jiang, Y. (2009). Degradation of anthocyanin from litchi fruit pericarp by H₂O₂ and hydroxyl radical. *Food Chemistry*, 116:995–998.
- Russell, A. (1982). *The destruction of bacterial spores*. Academic Press London, New York.
- Sadek, S. E. and Hurwitz, M. (1972). Influence of Electric Fields on Convective Heat and Mass Transfer From a Horizontal Surface Under Forced Convection. *Journal of Heat Transfer, Transactions ASME*, 94 Ser C:144–148.
- Sakiyama, Y., Graves, D. B., Chang, H.-W., Shimizu, T., and Morfill, G. E. (2012). Plasma chemistry model of surface microdischarge in humid air and dynamics of reactive neutral species. *Journal of Physics D: Applied Physics*, 45:425201.
- Sastray, S. K. (2016). Toward a Philosophy and Theory of Volumetric Nonthermal Processing. *Journal of Food Science*, 81:E1431–E1446.
- Saulis, G. (2010). Electroporation of cell membranes: The fundamental effects of pulsed electric fields in food processing. *Food Eng. Rev.*, 2:52–73.
- scar Rodrguez, Santacatalina, J. V., Simal, S., Garcia-Perez, J. V., Femenia, A., and Rossell, C. (2014). Influence of power ultrasound application on drying kinetics of apple and its antioxidant and microstructural properties. *Journal of Food Engineering*, 129:21 – 29.
- Schutze, A., Jeong, J., Babayan, S., Park, J., Selwyn, G. S., and Hicks, R. F. (1998). The atmospheric-pressure plasma jet: a review and comparison to other plasma sources. *Plasma Science, IEEE Transactions on*, 26:1685–1694.
- Segat, A., Misra, N., Cullen, P., and Innocente, N. (2015). Atmospheric pressure cold plasma (acp) treatment of whey protein isolate model solution. *Innovative Food Science & Emerging Technologies*, 29:247 – 254.
- Segovia, F. J., Luengo, E., Corral-Pérez, J. J., Raso, J., and Almajano, M. P. (2015). Improvements in the aqueous extraction of polyphenols from borage (*Borago officinalis L.*) leaves by pulsed electric fields: Pulsed electric fields (PEF) applications. *Industrial Crops and Products*, 65:390–396.
- Setlow, B. and Setlow, P. (1993). Binding of small, acid-soluble spore proteins to dna plays a significant role in the resistance of bacillus subtilis spores to hydrogen peroxide. *Applied and environmental microbiology*, 59(10):3418–3423.
- Shivashankara, K., Isobe, S., Al-Haq, M. I., Takenaka, M., and Shiina, T. (2004). Fruit antioxidant activity, ascorbic acid, total phenol, quercetin, and carotene of irwin mango fruits stored at low temperature after high electric field pretreatment. *Journal of Agricultural and Food Chemistry*, 52:1281–1286.
- Silva, R., Garcia, F. A., Faia, P. M., and Rasteiro, M. G. (2015). Evaluating the performance of the mixture model coupled with high and low reynolds turbulence closures in the numerical description of concentrated solid-liquid flows of settling particles. *The Journal of Computational Multiphase Flows*, 7:241–257.

- Singh, A., Orsat, V., and Raghavan, V. (2012). A comprehensive review on electrohydrodynamic drying and high-voltage electric field in the context of food and bioprocessing. *Drying Technology*, 30:1812–1820.
- Singh, A., Orsat, V., and Raghavan, V. (2013). Soybean hydrophobic protein response to external electric field: a molecular modeling approach. *Biomolecules*, 3:168–179.
- Sitzmann, W. (1995). High-voltage techniques for food preservation. In Gould, G. W., editor, *New Methods of Food Preservation.*, chapter High-voltage pulse techniques for food preservation, pages 236–252. Springer US, Boston.
- Smirnov, B. M. (2008). *Physics of ionized gases*. John Wiley & Sons.
- Soliva-Fortuny, R., Balasa, A., Knorr, D., and Martín-Belloso, O. (2009). Effects of pulsed electric fields on bioactive compounds in foods: a review. *Trends in Food Science & Technology*, 20:544–556.
- Song, J., Fan, L., Hildebrand, P. D., and Forney, C. F. (2000). Biological effects of corona discharge on onions in a commercial storage facility. *HortTechnology*, 10:608–612.
- Spignoli, G., Tramelli, L., and De Faveri, D. M. (2007). Effects of extraction time, temperature and solvent on concentration and antioxidant activity of grape marc phenolics. *Journal of Food Engineering*, 81:200–208.
- Spugnini, E. P., Arancia, G., Porrello, A., Colone, M., Formisano, G., Stringaro, A., Citro, G., and Molinari, A. (2007). Ultrastructural modifications of cell membranes induced by electroporation on melanoma xenografts. *Microscopy research and technique*, 70:1041–1050.
- Srinivas, N., Barhate, R., Raghavarao, K., and Todd, P. (2000). Acoustic field assisted enhanced demixing of aqueous two-phase systems. *Biochimica et Biophysica Acta (BBA) - General Subjects*, 1524:38 – 44.
- Sui, Q., Roginski, H., Williams, R. P. W., Versteeg, C., and Wan, J. (2011). Effect of pulsed electric field and thermal treatment on the physicochemical and functional properties of whey protein isolate. *International Dairy Journal*, 21:206–213.
- Tao, S., Kaihua, L., Cheng, Z., Ping, Y., Shichang, Z., and Ruzheng, P. (2008). Experimental study on repetitive unipolar nanosecond-pulse dielectric barrier discharge in air at atmospheric pressure. *Journal of Physics D: Applied Physics*, 41:215203.
- Tao, Y. and Sun, D.-W. (2015). Enhancement of food processes by ultrasound: a review. *Critical reviews in food science and nutrition*, 55:570–594.
- Tao, Y., Wang, P., Wang, Y., Kadam, S. U., Han, Y., Wang, J., and Zhou, J. (2016). Power ultrasound as a pretreatment to convective drying of mulberry (*morus alba l.*) leaves: Impact on drying kinetics and selected quality properties. *Ultrasonics Sonochemistry*, 31:310 – 318.
- Thornton, J. D. and Porter, J. E. (1973). Electrically augmented heat and mass transfer. *Symp Electrochem Eng Lond*, pages 3–38.
- Tian, W. and Kushner, M. J. (2014). Atmospheric pressure dielectric barrier discharges interacting with liquid covered tissue. *Journal of Physics D: Applied Physics*, 47:165201.
- Tian, Y., Ma, R., Zhang, Q., Feng, H., Liang, Y., Zhang, J., and Fang, J. (2014). Assessment of the physicochemical properties and biological effects of water activated by non-thermal plasma above and beneath the water surface. *Plasma Processes and Polymers*, 12:439–449.

- Trujillo, F. J., Juliano, P., Barbosa-Cnovas, G., and Knoerzer, K. (2014). Separation of suspensions and emulsions via ultrasonic standing waves a review. *Ultrasonics Sonochemistry*, 21:2151 – 2164.
- Tsong, T. Y. (2012). Time Sequence of Molecular Events in Electroporation. In Chand, D. C., Chassy, B. M., Saunders, J. A., and Sowers, A. E., editors, *Guide to Electroporation and Electrofusion*, pages 47–61. Academic Press, New York.
- Vaidya, H. A., Özgür Ertunc, Lichtenegger, T., Delgado, A., and Skupin, A. (2016). The penetration of acoustic cavitation bubbles into micrometer-scale cavities. *Ultrasonics*, 67:190 – 198.
- Vanga, S. K., Singh, A., Kalkan, F., Gariepy, Y., Orsat, V., and Raghavan, V. (2015a). Effect of thermal and high electric fields on secondary structure of peanut protein. *International Journal of Food Properties*, 19:1259–1271.
- Vanga, S. K., Singh, A., and Raghavan, V. (2015b). Effect of thermal and electric field treatment on the conformation of ara h 6 peanut protein allergen. *Innovative Food Science & Emerging Technologies*, 30:79 – 88.
- Vercet, A., Lopez, P., and Burgos, J. (1998). Free radical production by manothermosonication. *Ultrasonics*, 36:615–618.
- Viehland, L. and Mason, E. (1995). Transport properties of gaseous ions over a wide energy range, {IV}. *Atomic Data and Nuclear Data Tables*, 60:37 – 95.
- Vorobiev, E. and Lebovka, N. (2010). Enhanced extraction from solid foods and biosuspensions by pulsed electrical energy. *Food Engineering Reviews*, 2:95–108.
- Vorobiev, E. and Lebovka, N. I. (2006). chapter Extraction of Intercellular Components by Pulsed Electric Fields, pages 153–193. Springer US, Boston, MA.
- Weaver, J. C. and Chizmadzhev, Y. (1996). Theory of electroporation: A review. *Bioelectrochemistry and Bioenergetics*, 41:135–160.
- Weber, A. Z., Borup, R. L., Darling, R. M., Das, P. K., Dursch, T. J., Gu, W., Harvey, D., Kusoglu, A., Litster, S., Mench, M. M., Mukundan, R., Owejan, J., Pharoah, J., Secanell, M., and Zenyuka, I. (2014). A critical review of modeling transport phenomena in polymer-electrolyte fuel cells. *Journal of The Electrochemical Society*, 161:F1254–F1299.
- Wei, S., Xiaobin, X., Hong, Z., and Chuanxiang, X. (2008). Effects of dipole polarization of water molecules on ice formation under an electrostatic field. *Cryobiology*, 56:93–99.
- Wei, Z. and Weavers, L. K. (2016). Combining {COMSOL} modeling with acoustic pressure maps to design sono-reactors. *Ultrasonics Sonochemistry*, 31:490 – 498.
- Wolny, A. and Kaniuk, R. (1996a). The effect of electric field on heat and mass transfer. *Drying Technology*, 14:195–216.
- Wolny, A. and Kaniuk, R. (1996b). The effect of electric field on heat and mass transfer. *Drying technology*, 14:195–216.
- Wu, X., Diao, Y., Sun, C., Yang, J., Wang, Y., and Sun, S. (2003). Fluorimetric determination of ascorbic acid with o-phenylenediamine. *Talanta*, 59:95–99.

- Xanthakis, E., Havet, M., Chevallier, S., Abadie, J., and Le-Bail, A. (2013). Effect of static electric field on ice crystal size reduction during freezing of pork meat. *Innovative Food Science & Emerging Technologies*, 20:115–120.
- Xue, X., Barthakur, N., and Alli, I. (1999). Electrohydrodynamically-dried whey protein: An electrophoretic and differential calorimetric analysis. *Drying technology*, 17:467–478.
- Yong, H. I., Kim, H.-J., Park, S., Kim, K., Choe, W., Yoo, S. J., and Jo, C. (2015). Pathogen inactivation and quality changes in sliced cheddar cheese treated using flexible thin-layer dielectric barrier discharge plasma. *Food Research International*, 69:57 – 63.
- Yusof, N. S. M., Babgi, B., Alghamdi, Y., Aksu, M., Madhavan, J., and Ashokkumar, M. (2016). Physical and chemical effects of acoustic cavitation in selected ultrasonic cleaning applications. *Ultrasonics Sonochemistry*, 29:568 – 576.
- Zhang, H. and Hashinaga, F. (1997). Effect of high electric field on the quality of satsuma mandarin fruits. *Journal of Society of High Technology in Agriculture (Japan)*.
- Zhang, H. Q., Barbosa-Canoval, G. V., Balasubramaniam, V. B., Dunne, C. P., Farkas, D. F., and Yuan, J. T., editors (2011a). *Nonthermal processing technologies for food*. John Wiley & Sons.
- Zhang, M., Chen, H., Mujumdar, A. S., Zhong, Q., and Sun, J. (2015a). Recent developments in high-quality drying with energy-saving characteristic for fresh foods. *Drying Technology*, 33:1590–1600.
- Zhang, Q. A., Shen, Y., Fan, X. H., Martin, J. F. G., Wang, X., and Song, Y. (2015b). Free radical generation induced by ultrasound in red wine and model wine: An EPR spin-trapping study. *Ultrasonics Sonochemistry*, 27:96–101.
- Zhang, S., Yang, R., Zhao, W., Liang, Q., and Zhang, Z. (2011b). The first esr observation of radical species generated under pulsed electric fields processing. *LWT-Food Science and Technology*, 44:1233–1235.
- Zhang, Y., Hu, X. S., Chen, F., Wu, J. H., Liao, X. J., and Wang, Z. F. (2008). Stability and colour characteristics of PEF-treated cyanidin-3-glucoside during storage. *Food Chemistry*, 106:669–676.
- Zhang, Z.-H., Zeng, X.-A., Brennan, C., Brennan, M., Han, Z., and Xiong, X.-Y. (2015c). Effects of Pulsed Electric Fields (PEF) on Vitamin C and Its Antioxidant Properties. *International Journal of Molecular Sciences*, 16:24159–24173.
- Zhao, W., Yang, R., Shi, X., Pan, K., Zhang, S., Zhang, W., and Hua, X. (2011). Oxidation of oleic acid under pulsed electric field processing. *Food Research International*, 44:1463–1467.
- Zhu, X. M. and Kong, M. G. (2005). Electron kinetic effects in atmospheric dielectric-barrier glow discharges. *Journal of Applied Physics*, 97:083301.
- Zhu, Z., He, J., Liu, G., Barba, F. J., Koubaa, M., Ding, L., Bals, O., Grimi, N., and Vorobiev, E. (2016). Recent insights for the green recovery of inulin from plant food materials using non-conventional extraction technologies: A review. *Innovative Food Science & Emerging Technologies*.

Nomenclature

AOP	Advanced Oxidation Process	e	Elementary charge, C
CFD	Computational Fluid Dynamics	f	Frequency, Hz
DMPO	5,5-dimethyl-1-pyrroline N-oxide	F_E	Electric force, N
EHD	Electrohydrodynamic	f_s	Distribution function
HT	Heat Transfer	g	Geometry factor, (1/m)
NO_x	Nitrogen oxides	h	Convective HT coefficient, W/(m ² K)
PEF	Pulsed Electric Field	h_m	Mass transfer coefficient
PTFE	polytetrafluoroethylene	I	Identity tensor
RHS	Right Hand Side	i	Current, A
∇	Nabla	I_{col}	Collision operator
∇^2	Laplacian	I_{us}	Ultrasound intensity, W/m ²
∂	partial differential	j	Current density, A/m ²
α'	Semi-vertical cone angle	k	Thermal conductivity, W/mK
\approx	Approximately	k_0	Dimensionless geometry factor
Δc	Concentration gradient	k_g	Thermal conductivity
$\Delta \varphi_m$	Transmembrane potential	K_n	Knudsen number
\dot{m}	Mass flow rate, kg/s	k_T	Turbulent thermal conductivity
ϵ	Relative dielectric permittivity	k_{ijk}	Reaction rate
ϵ_0	Permitivity of free space, F/m	L	Boundary layer thickness, m
γ	Energy per edge length	m_1	Mass of particle 1, kg
\hat{W}	Energy per area	m_2	Mass of particle 2, kg
\bar{u}	Average velocity	P	Power, W
μ	Dynamic viscosity, Pa.s	p	Pressure, Pa
μ_s	Mobility	P_b	Pressure inside bubble, Pa
μ_T	Turbulent viscosity	P_g	Pressure of gas, Pa
Φ_s	Species Flux	Pr_T	Turbulent Prandtl Number
ψ	Pulse width (μ s)	Q	Energy dissipated by field, J/kg
ρ	Density of air, kg/m ³	q_s	Species charge
σ	Electrical conductivity (S/m)	q_w	Power of heat source, W/m ²
\mathbf{g}	Gravitational acceleration, m/s ²	r	Pore radius, m
\mathbf{m}	Electron mass, kg	r_t	Critical pore radius, m
γ	Specific heat ratio	T	Temperature, K
μ	Micrometer, 10^{-6}	t	Time, s
ε	Mean e^- energy	T_e	Electron temperature, K
ζ	Bulk viscosity, Pa.s	T_g	Gas temperature, K
A_p	Electrode plate area, m ²	U	Space average voltage, V
a_s	species acceleration	u	Fluid velocity, m/s
A_{tr}	Transducer surface area, m ²	u_g	Gas velocity, m/s
B	Bulk modulus	V	Voltage, V
b	Ionic mobility, m ² /(Vs)	v	Velocity, m/s
C_p	Specific heat capacity, kJ/kg/K	V_b	Breakdown Voltage, V
D	Mass diffusion, m ² /s	V_{in}	Initiation voltage, V
d	Distance between electrodes	Z	Impedance
D_e	e^- Diffusion coefficient	C_{LW}	Specific capacitance
E	Electric Field, V/m	L	Boundary layer thickness, m

List of Figures

1	Photograph of a DBD discharge comprising of doughnut shaped electrodes with dielectric barriers in between, and operating in air at 35 kV applied voltage and 1 kHz frequency. (a) At 2 mm gap with a 2 mm thick PTFE barrier, a homogeneous glow regime can be observed. (b) At 8 mm gap with a 2 mm thick glass barrier, a filamentary regime can be observed. The filaments are perpendicular to the electrodes and randomly distributed. From Tao et al. (2008). (Colour online)	56
2	Modelled time profile of (a) charged and (b) neutral species in a DBD streamer (10^{-9} - 10^{-3} s). From Barni et al. (2005b). (Colour online)	57
3	Evolution of the concentrations of major species (intermediates and products) in a microwave plasma discharge of a 4:1 N ₂ /O ₂ mixture obtained via simulation. From Kossyi et al. (1992). (Colour online)	58
4	The time evolution of RNS densities in the liquid exposed to plasma, obtained via simulations. The changes in the overall liquid chemistry, although appears very minor, it results in spectacularly different results in different biological systems. From Hamaguchi (2013). (Colour online)	59
5	The evolution of ROS (left) and RNS (right) densities in a 200 μm water layer exposed to the afterglow of a DBD. While the transient species, HO _{2aq} (hydroperoxyl radical), mainly forms at the top of the water layer by H _{aq} combining with dissolved O _{2aq} and quenched well-before it can diffuse further, O _{3aq} is a long lived species in the water mostly originate from the diffusion of O ₃ from the gas phase. The reaction of incoming NO and NO ₂ from the gas phase with the increasing OH density results in the formation of HNO ₂ , HNO ₃ and HOONO. The figure depicts the time-evolution of ONOO _{aq} ⁻ (peroxynitrite) and NO _{3aq} ⁻ (nitrates) in the liquid. One should note that the density of ONOO _{aq} ⁻ is higher at the surface because it forms via reaction of NO with OH and HO ₂ (Tian and Kushner, 2014). (Colour online)	60
6	Ionic discharge from multiple pin-to-plate electrode. The bright spots are in the vicinity of the pin electrodes.	61
7	An exemplary needle-plane corona discharge, showing current density distribution. From Goldman et al. (1985), with permission. (Colour online)	62
8	EHD experimental set-up: 1-desktop computer, 2-high voltage power supply, 3-multiple-pin electrode, 4-grounded plate-type electrode, 5-drying chamber, 6-digital balance, 7-air blower. From Martynenko and Zheng (2016), with permission. (Colour online)	63
9	A schematic of (a) the experimental set-up for PEF processing, and (b) zoomed in cross section of the PEF chamber (Koubaa et al., 2015; Zhu et al., 2016) (Colour online)	64
10	3D CFD simulations of a PEF chamber with sodium chloride solution. (A) The PEF chamber having co-linear electrodes and the treatment zones (zoomed section). (B) Electric field distribution in the reactor, and the treatment zones. The average field strength was ~ 17 kV/cm. (C) The spatial temperature profile of the treatment chamber with large differential between solid and fluid regions. The temperature rises in first and second chamber were in the order of ~ 7.5 and ~ 10.5 °C, with the difference resulting from an increase in σ with rising temperature, whereby higher conversion of electrical into thermal energy occurs. From Knoerzer et al. (2012), with permission. (Colour online)	65
11	Pore formation in plant cell membrane after pulsed electric fields (PEF). From Zhu et al. (2016), with permission. (Colour online)	66
12	A pictorial summary of applications of ultrasound in food processing and the mechanism of action. (Colour online)	67

13	A pictorial summary of the mechanisms underlying anti-microbiological action of ultrasound waves. (Colour online)	68
14	Calorimetric procedure for experimental determination of input power during ultrasound application. (Colour online)	69
15	Generalized relationship between flow rate (L/h) and energy for several ultrasonic applications. From Patist and Bates (2008), with permission. (Colour online)	70
16	'OH radical yield generated in water upon sonication at different ultrasonic frequencies (0.90 W/cm ²). Note that the 'OH radical yield increases when the frequency is increased from 20 kHz to 358 kHz, but the amount decreases when the frequency is further increased to 1062 kHz. This decrease was explained on the basis of shorter acoustic cycles at higher frequencies, thereby restricting the amount of water vapour that can evaporate into the bubble during the expansion phase. Hence, a decrease in the amount of radicals generated. From Ashokkumar et al. (2008), with permission. (Colour online)	71

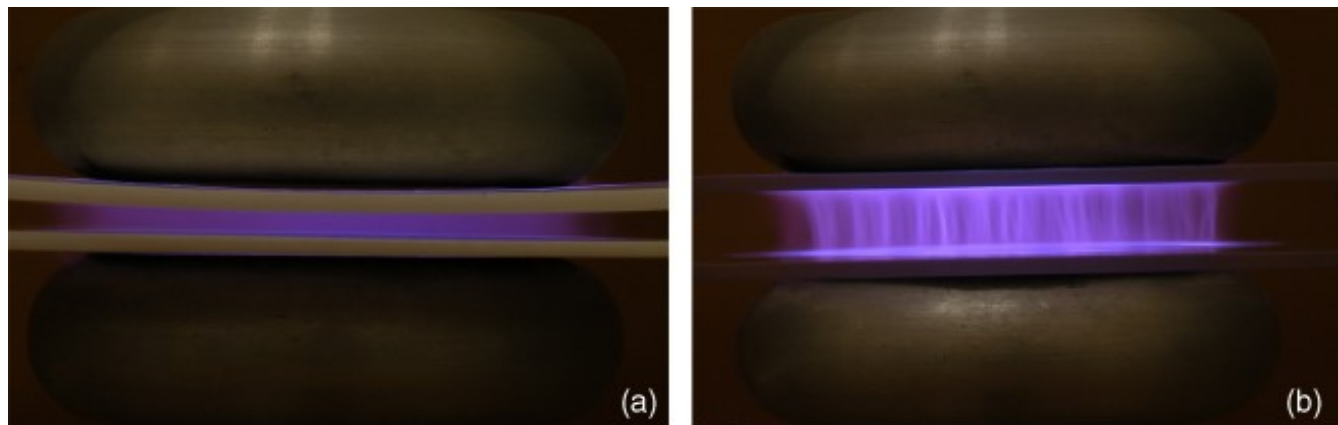


Figure 1

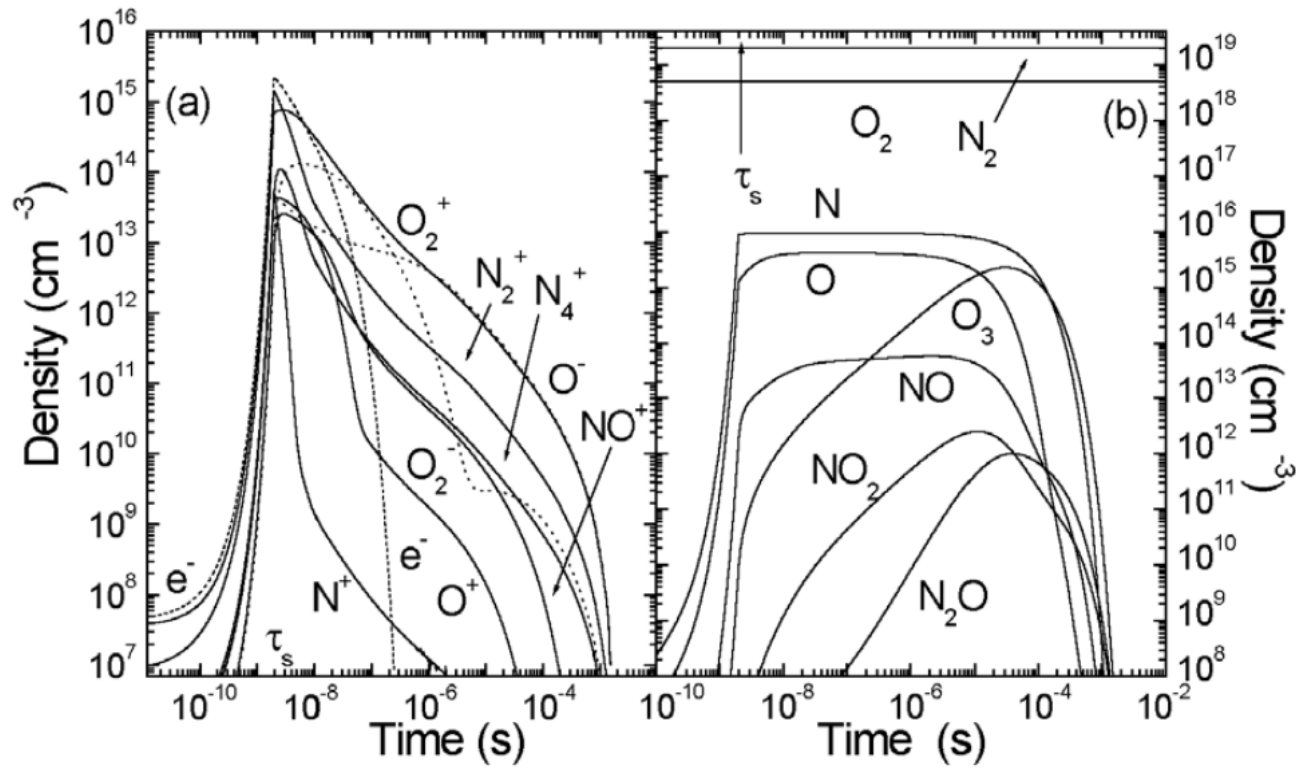


Figure 2

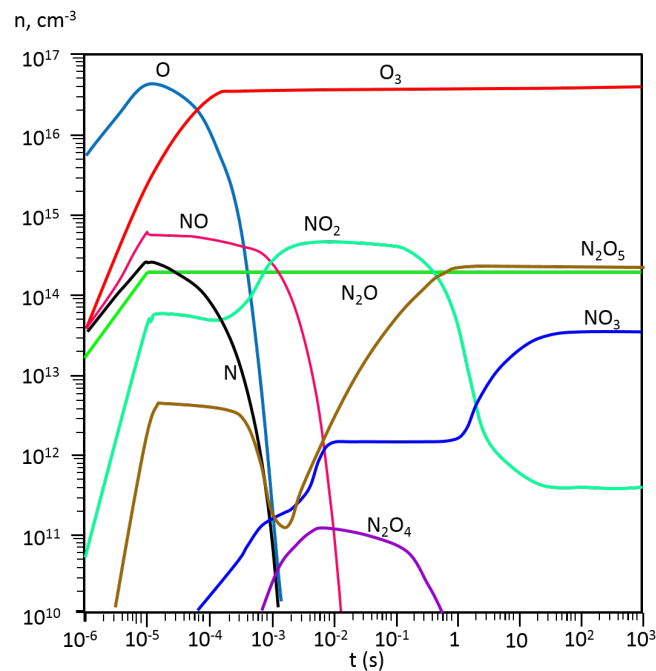


Figure 3

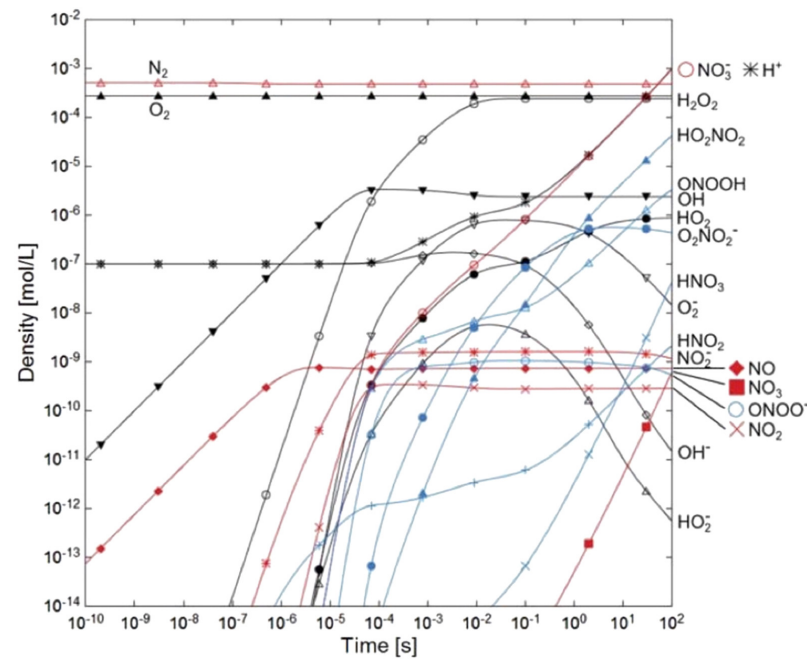


Figure 4

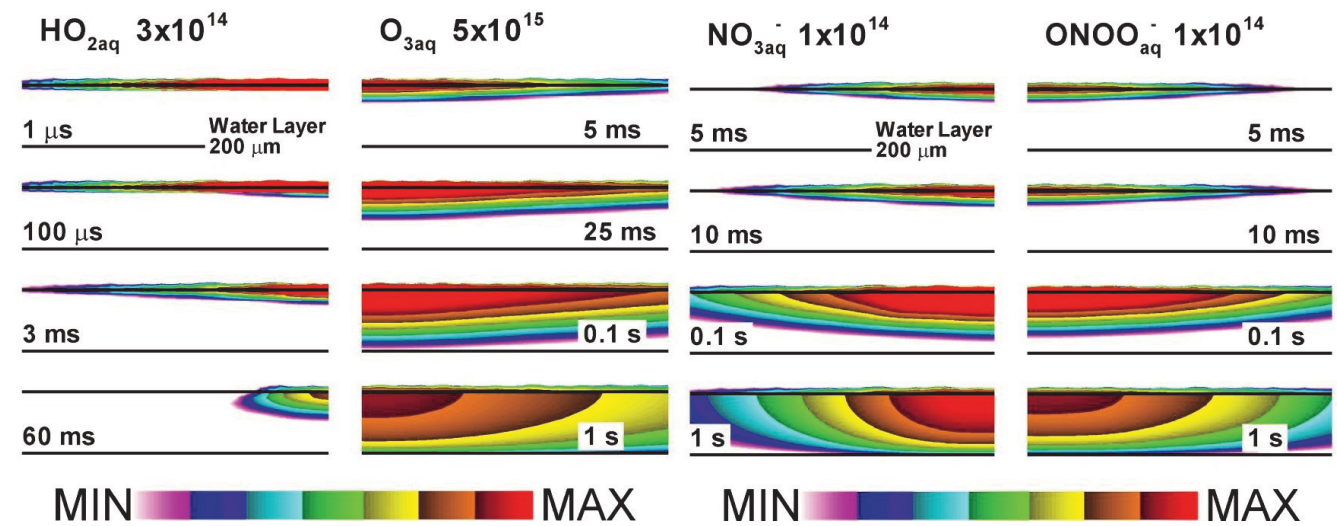


Figure 5

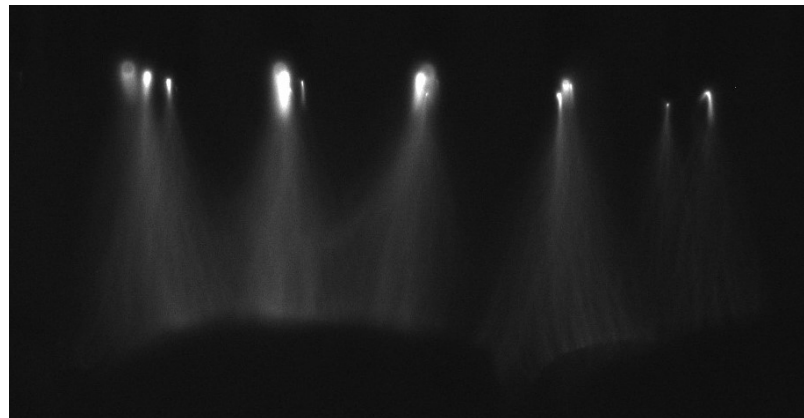


Figure 6

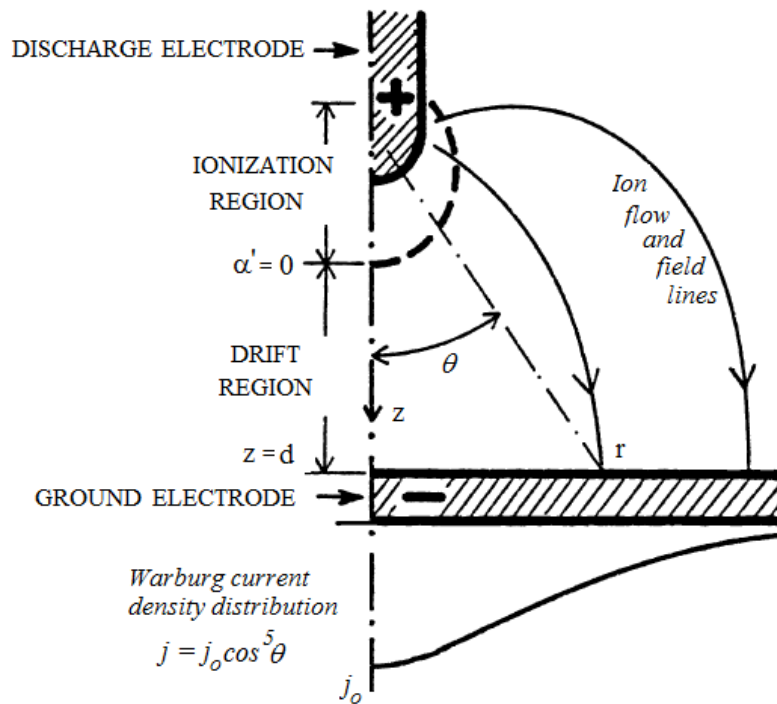


Figure 7

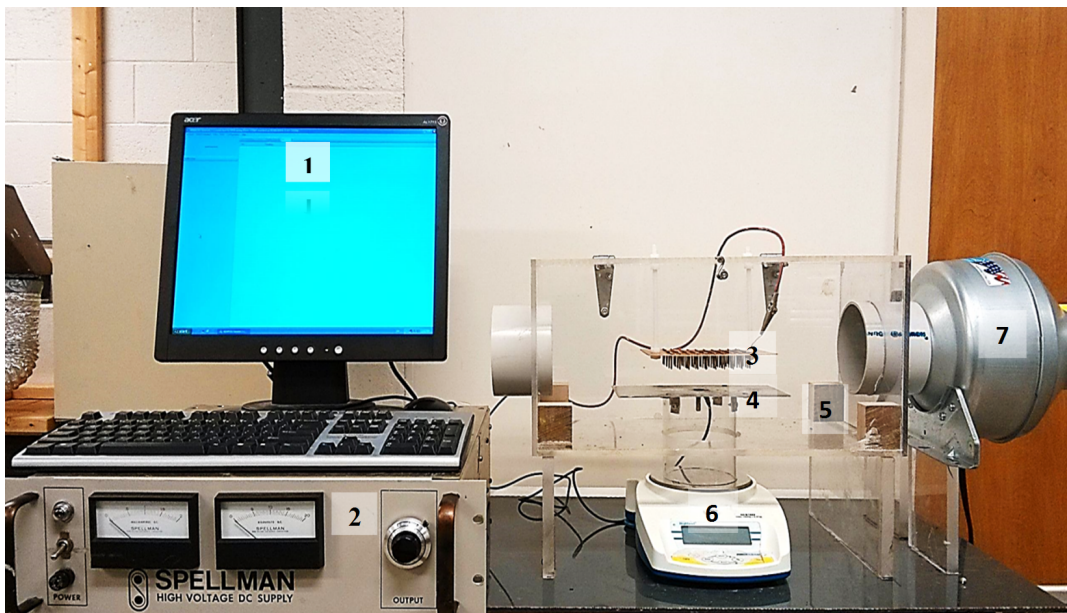


Figure 8

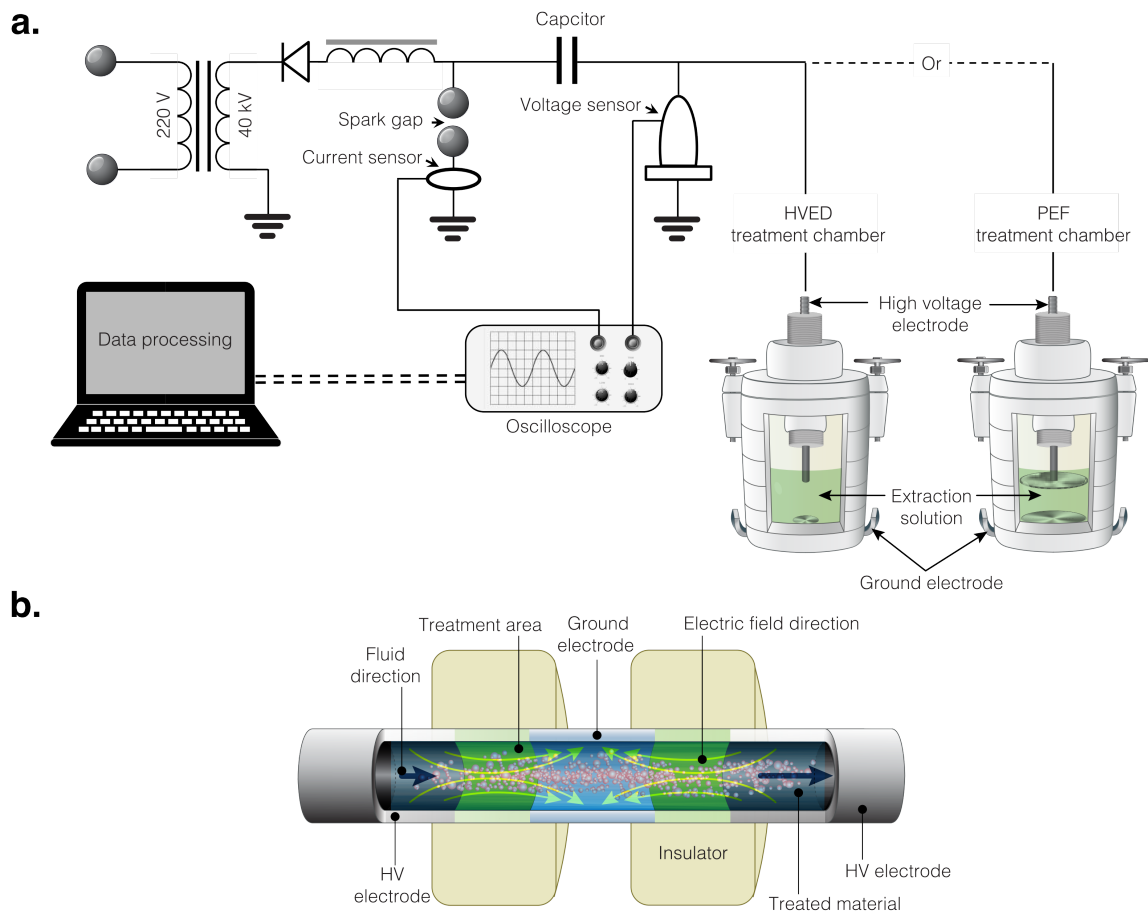


Figure 9

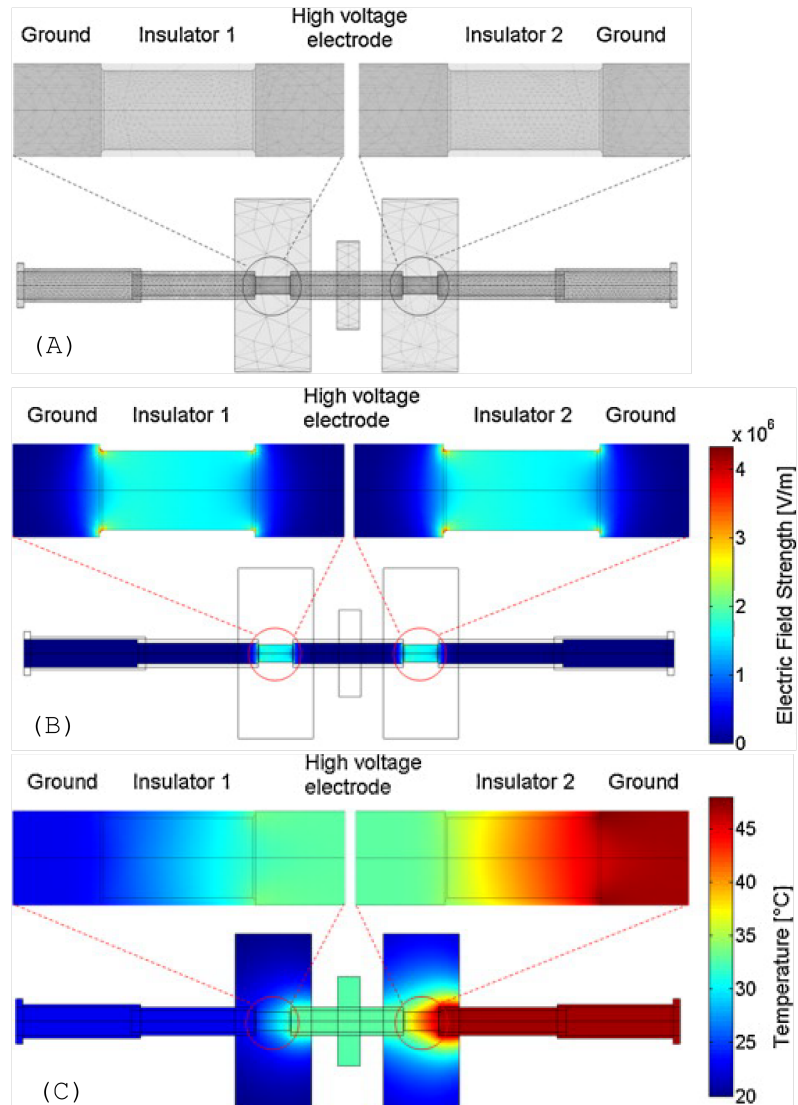


Figure 10



Figure 11

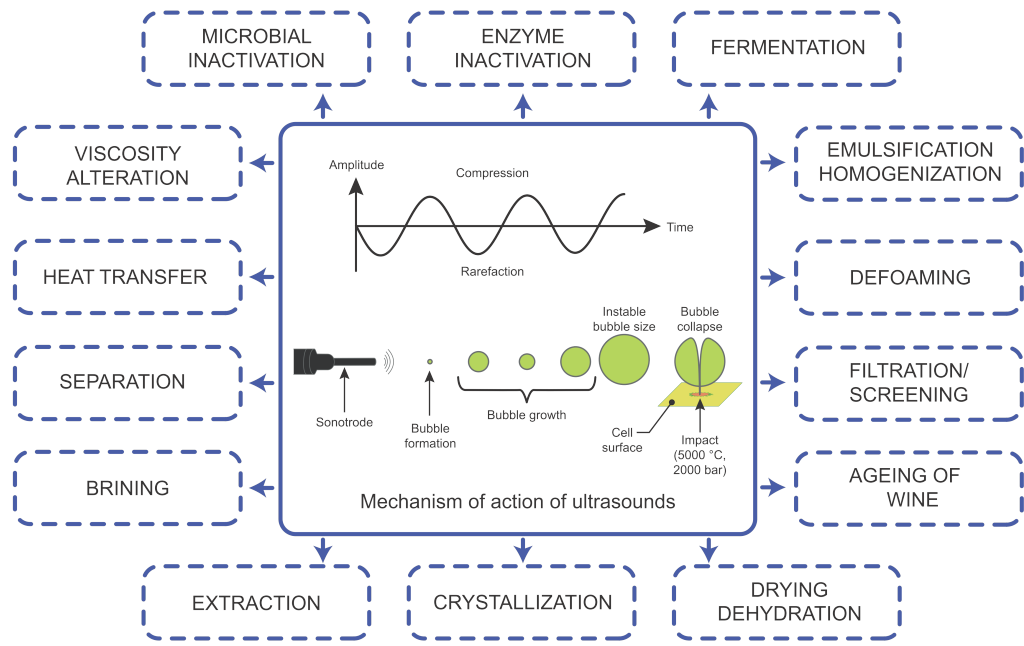


Figure 12

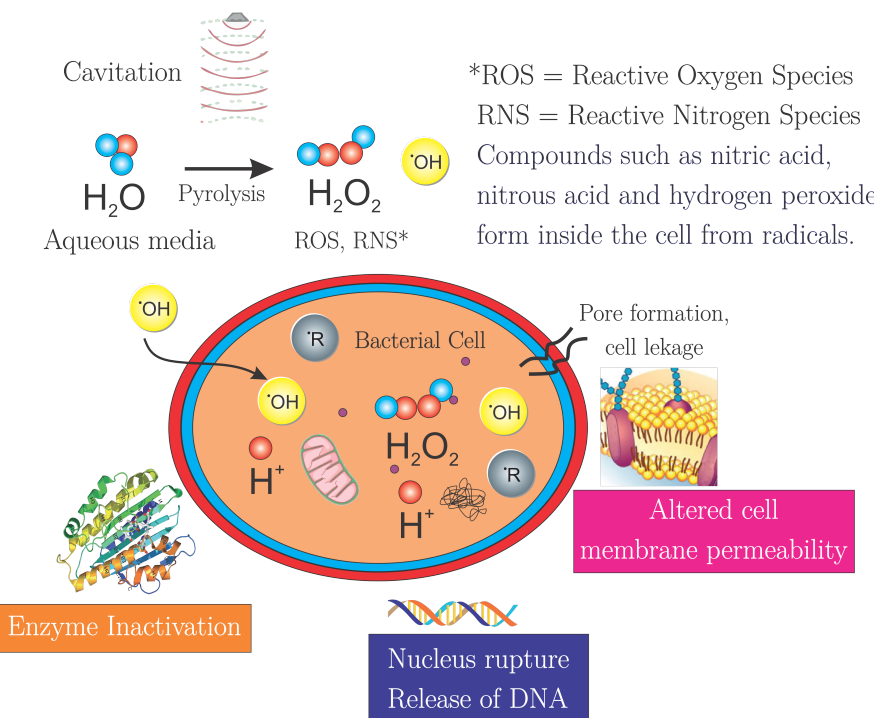


Figure 13

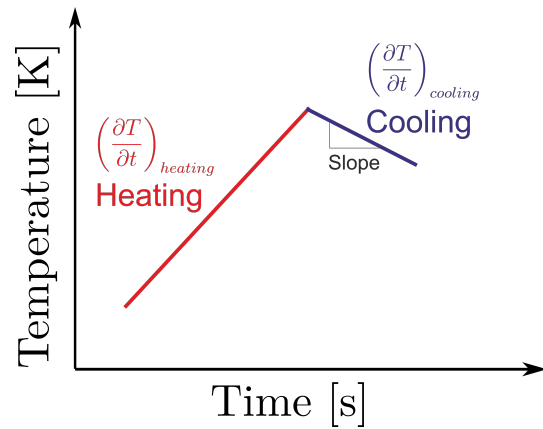


Figure 14

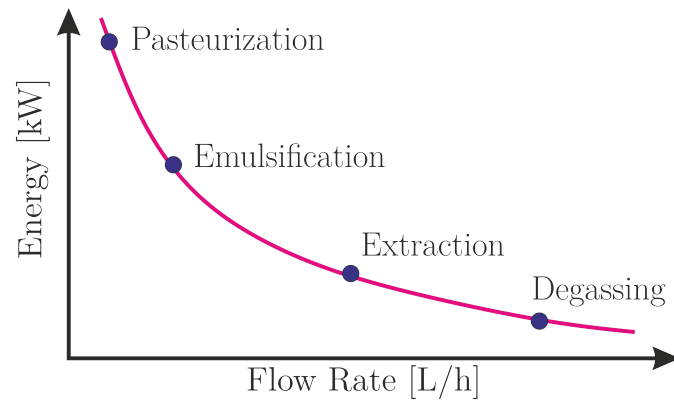


Figure 15

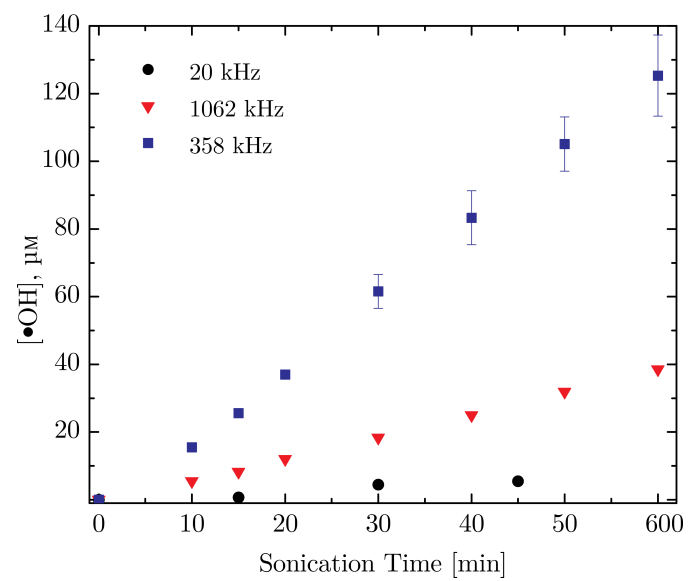


Figure 16